

Effects of Permafrost and Seasonally Frozen Ground  
on the Seismic Response of  
Transportation Infrastructure Sites

Final Report

Prepared for  
Alaska University Transportation Center &  
State of Alaska Department of Transportation & Public Facilities

Zhaohui Joey Yang  
Utpal Dutta  
Gang Xu

School of Engineering  
University of Alaska Anchorage  
Anchorage, Alaska

Kenan Hazirbaba  
Institute of Northern Engineering  
University of Alaska Fairbanks  
Fairbanks, Alaska

Report # FHWA-AK-RD-XX-XX  
February 2010

## Table of Contents

Table of Contents .....	ii
List of Figures .....	v
List of Tables .....	xi
Acknowledgement .....	xii
Abstract .....	xiii
<b>Summary of Findings</b> .....	1
<b>CHAPTER 1 – INTRODUCTION</b> .....	2
1.1 Background .....	2
1.2 Objective of Research .....	4
1.3 Scope of Study .....	4
<b>CHAPTER 2 - METHODOLOGY OF SITE RESPONSE ANALYSIS</b> .....	5
2.1 Introduction .....	5
2.2 Site Response Analysis Model .....	5
2.2.1 Equivalent Linear Analysis .....	6
2.2.2 Nonlinear Analysis .....	8
2.2.3 Discussion on Analysis Method .....	8
2.3 Identification of Seismic Hazard and De-aggregation of Seismic Hazard .....	8
2.3.1 Identification of Seismic Hazard .....	9
2.3.2 De-aggregation of Seismic Hazard .....	9
2.4 Generation of Hazard-Consistent Ground Motions .....	9
2.4.1 Time Histories Selection Criteria .....	10
2.4.2 Time Histories Scaling .....	10
2.5 Demonstration of the Effectiveness of Analysis Method .....	11

CHAPTER 3 - EFFECTS OF SEASONALLY FROZEN SOIL ON THE SEISMIC SITE RESPONSE .....	13
3.1 Introduction.....	13
3.2 General Geology of the Selected Seasonally Frozen Soil Site .....	13
3.3 Identification of the Seismic Hazard at the C-OM Site.....	13
3.4 De-aggregation of Seismic Hazard at the C-OM Site .....	15
3.5 Time Histories Selection and Scaling .....	19
3.6 The Soil Profile with Seasonally Frozen Soil.....	27
3.7 Analyses Results .....	29
3.7.1 Acceleration Time Histories and Peak Shear Strain.....	29
3.7.2 RS of Computed Surface Motions .....	30
3.7.3 Transfer Function Comparison.....	34
3.7.4 Effects of Seasonally Frozen Soil Depth on Spectral Acceleration .....	38
3.8 Sensitivity of Results on Shear Wave Velocity of Frozen Soil.....	42
3.9 Discussion of Results.....	45
CHAPTER 4 - EFFECTS OF PERMAFROST ON THE SEISMIC SITE RESPONSE ....	47
4.1 Introduction.....	47
4.2 General Geology and Soil Profile of the Selected Permafrost Site.....	47
4.2.1 General Geology .....	47
4.2.2 Soil Profile .....	48
4.3 Identification of the Seismic Hazard at the GC Site .....	49
4.4 De-aggregation of Seismic Hazard at the GC Site.....	50
4.5 Time Histories Selection and Scaling .....	52
4.5.1 Time Histories Selection.....	52
4.5.2 Time History Scaling .....	55

4.6 Discussion on the representativeness of selected input motions .....	58
4.7 Analysis Results.....	61
4.7.1 Time History of Acceleration and Peak Shear Strain.....	61
4.7.2 Site Response for Different Permafrost Table .....	63
4.7.3 Effects of Permafrost Table Variation on Site Response.....	68
4.7.4 Effects of Permafrost with Variation in Bedrock Table .....	69
4.7.5 Discussion on Role of Permafrost .....	71
4.7.5 Sensitivity of Results to Permafrost Shear Wave Velocity.....	72
4.8 Average Response Spectra for Similar Sites .....	74
CHAPTER 6 – CONCLUSIONS AND SUGGESTED RESEARCH.....	78
6.1 Conclusions .....	78
6.2 Suggested Research.....	79
REFERENCES .....	80

## List of Figures

Figure 1.1 Thickness of the active layer and vertical distribution of permafrost in Alaska and western Canada based (Davis, 2001) .....	2
Figure 2.1 One-dimensional idealization of a horizontally-layered soil deposit over a uniform Half-Space.....	6
Figure 2.2 Modulus vs. shear strain for unfrozen and frozen soils .....	7
Figure 2.3 Damping ratio vs. shear strain for unfrozen and frozen soils .....	7
Figure 2.4 A hypothetical soil deposit consisting of frozen soil over bedrock.....	11
Figure 2.5 Comparison between RS of bedrock and surface motions of the hypothetical soil site.....	12
Figure 3.1 A geological cross section at C-OM site based on Combellick (1999).....	14
Figure 3.2 Comparison of bedrock motion RS for three levels of seismic hazard.....	15
Figure 3.3 De-aggregation of the AASHTO Design Earthquake level seismic hazard (7.5% PE in 75 yrs) at C-OM site for PGA .....	16
Figure 3.4 De-aggregation of the AASHTO Design Earthquake level seismic hazard (7.5% PE in 75 yrs) at C-OM site for $S_s$ .....	17
Figure 3.5 De-aggregation of the AASHTO Design Earthquake level seismic hazard (7.5% PE in 75 yrs) at C-OM site for $S_1$ .....	17
Figure 3.6 Plots of acceleration vs. time for the five time histories selected from the Kik-Net database.....	20
Figure 3.7 Comparison of the RS of IWTH23 ground motion time histories with target bedrock RS for the C-OM site corresponding to (a) MCE, (b) AASHTO Design Earthquake and (c) IBC Design Earthquake levels of seismic hazard.....	22

Figure 3.8 Comparison of the RS of MYGH11 ground motion time histories with target bedrock RS for the C-OM site corresponding to (a) MCE, (b) AASHTO Design Earthquake and (c) IBC Design Earthquake levels of seismic hazard.....	23
Figure 3.9 Comparison of the RS of NIGH01 ground motion time histories with target bedrock RS for the C-OM site corresponding to (a) MCE, (b) AASHTO Design Earthquake and (c) IBC Design Earthquake levels of seismic hazard.....	24
Figure 3.10 Comparison of the RS of SMNH01 ground motion time histories with target bedrock RS for the C-OM site corresponding to (a) MCE, (b) AASHTO Design Earthquake and (c) IBC Design Earthquake levels of seismic hazard.....	25
Figure 3.11 Comparison of the RS of KOCH05 ground motion time histories with target bedrock RS for the C-OM site corresponding to (a) MCE, (b) AASHTO Design Earthquake and (c) IBC Design Earthquake levels of seismic hazard.....	26
Figure 3.12 Shear wave velocities of different sedimentary units in Anchorage, Alaska (Combellick, 1999) .....	27
Figure 3.13 A soil profile for the C-OM site .....	28
Figure 3.14 Input motion NIGH01 and computed surface motion for the C-OM site.....	29
Figure 3.15 Plot of peak shear strain vs. depth for five selected input motions scaled to MCE level hazard. ....	30
Figure 3.16 Computed surface motions RS and their average RS for the soil profile without seasonally frozen soil (IBC Design Earthquake level hazard).....	31
Figure 3.17 Computed surface motions RS and their average RS for the soil profile with 5 ft of seasonally frozen soil (IBC Design Earthquake level hazard).....	31
Figure 3.18 Computed surface motions RS and their average RS for the soil profile with 10 ft of seasonally frozen soil (IBC Design Earthquake level hazard) .....	32
Figure 3.19 Comparison of the average RS for soil profiles with 0, 5 or 10 ft (0, 1.5 or 3 m) of seasonally frozen soil (IBC Design Earthquake level hazard).....	32

Figure 3.20 Comparison of the average RS for soil profiles with 0, 5 and 10 ft (0, 1.5 and 3 m) of seasonally frozen soil (AASHTO Design Earthquake level hazard).....	33
Figure 3.21 Comparison of the average RS for soil profiles with 0, 5 and 10 ft (0, 1.5 and 3 m) of seasonally frozen soil (MCE level hazard).....	34
Figure 3.22 Transfer functions for the five computed surface motions and their average for the soil profile without seasonally frozen soil (IBC Design Earthquake level hazard).	35
Figure 3.23 Transfer functions of the five computed surface motions and their average for the soil profile with 5 ft of seasonally frozen (IBC Design Earthquake level hazard)..	35
Figure 3.24 Transfer functions of the five computed surface motions and their average for the soil profile with 10 ft of seasonally frozen soil (IBC Design Earthquake level hazard).....	36
Figure 3.25 Comparison of the average transfer functions for soil profiles with 0, 5 and 10 ft (0, 1.5 and 3 m) of seasonally frozen soil (IBC Design Earthquake level hazard) .....	36
Figure 3.26 Comparison of average transfer functions with 0, 5 and 10 ft (0, 1.5 and 3 m) seasonally frozen soil corresponding to AASHTO Design Earthquake level hazard (7.5% PE in 75 years) .....	37
Figure 3.27 Comparison of the average transfer functions for soil profiles with 0, 5 and 10 ft (0, 1.5 and 3 m) of seasonally frozen soil (MCE level hazard).....	37
Figure 3.28 Variation of (a) PGA, (b) $S_s$ and (c) $S_1$ with seasonally frozen soil depth for IBC Design Earthquake level hazard.....	41
Figure 3.29 Variation of (a) PGA, (b) $S_s$ and (c) $S_1$ with seasonally frozen soil depth for AASHTO Design Earthquake level hazard (7.5% PE in 75 years).....	40
Figure 3.30 Variation of (a) PGA, (b) $S_s$ and (c) $S_1$ with seasonally frozen soil depth for MCE level hazard (2% PE in 50 years) .....	39
Figure 3.31 Variation of PGA with frozen soil depth and shear wave velocity $V_s$ for input motion MYGH11 .....	42

Figure 3.32 Variation of $S_s$ with frozen soil depth and shear wave velocity $V_s$ for input motion MYGH11 .....	43
Figure 3.33 Variation of $S_1$ with frozen soil depth and shear wave velocity $V_s$ for input motion MYGH11 .....	43
Figure 3.34 Variation of PGA with frozen soil depth and shear wave velocity $V_s$ for input motion NIGH01 .....	44
Figure 3.35 Variation of $S_s$ with frozen soil depth and shear wave velocity $V_s$ for input motion NIGH01 .....	44
Figure 3.36 Variation of $S_1$ with frozen soil depth and shear wave velocity $V_s$ for input motion NIGH01 .....	45
Figure 4.1 A geological cross-section of Fairbanks area (Péwé, 1982).....	48
Figure 4.2 Soil profiles with varying permafrost table .....	49
Figure 4.3 De-aggregation of the AASHTO Design Earthquake level seismic hazard (7.5% PE in 75 yrs) of the GC site for PGA.....	50
Figure 4.4 De-aggregation of the AASHTO Design Earthquake level seismic hazard (7.5% PE in 75 yrs) of the GC site for $S_s$ .....	51
Figure 4.5 De-aggregation of the AASHTO Design Earthquake level seismic hazard (7.5% PE in 75 yrs) of the GC site for $S_1$ .....	51
Figure 4.6 Earthquake ground motions selected for the GC site .....	54
Figure 4.7 Earthquake ground motions selected for the GC site (cont'd).....	55
Figure 4.8 Comparison of the RS of scaled input motions with target bedrock RS for the GC site (AASHTO Design Earthquake level hazard) .....	57
Figure 4.9 Comparison of the RS of scaled input motions with target bedrock RS for the GC site (AASHTO Design Earthquake level hazard) (cont'd).....	58

Figure 4.10 Comparison of the average RS of the ten input motion time histories with bedrock RS of the GC site (IBC Design Earthquake level hazard) .....	59
Figure 4.11 Comparison of the average RS of the ten input motion time histories with bedrock RS of the GC site (AASHTO Design Earthquake level hazard).....	59
Figure 4.12 Comparison of the average RS of the ten input motion time histories with bedrock RS of the GC site (MCE level hazard).....	60
Figure 4.13 Comparison of the average RS of selected input motions with the target RS of the GC site for AASHTO Design Earthquake level hazard.....	61
Figure 4.14 Comparison between the input time series (Denali) and computed time series at the surface and within permafrost.....	62
Figure 4.15 Peak shear strain vs. depth for ten input motions scaled to MCE level hazard for a soil profile with permafrost table at -20 m and bedrock table at -66 m. ....	63
Figure 4.16 RS of the surface motions and their average for the soil profile with permafrost table at 0 ft (0 m) (AASHTO Design Earthquake level).....	64
Figure 4.17 RS of the surface motions and their average for the soil profile with permafrost table at -16 ft (-5 m) (AASHTO Design Earthquake level).....	64
Figure 4.18 RS of the surface motions and their average for the soil profile with permafrost table at -33 ft (-10 m) (AASHTO Design Earthquake level).....	65
Figure 4.19 RS of the surface motions and their average for the soil profile with permafrost table at - 50 ft (-15 m) (AASHTO Design Earthquake level) .....	65
Figure 4.20 RS of the surface motions and their average for the soil profile with permafrost table at -66 ft (-20 m) (AASHTO Design Earthquake level).....	66
Figure 4.21 RS of the surface motions and their average for the soil profile with permafrost table at -82 ft (-25 m) (AASHTO Design Earthquake level).....	66
Figure 4.22 RS of the surface motions and their average for the soil profile with permafrost table at -100 ft (-30 m) (AASHTO Design Earthquake level) .....	67

Figure 4.23 RS of the surface motions and their average for the soil profile with permafrost table at -130 ft (-40 m) (AASHTO Design Earthquake level) .....	67
Figure 4.24 RS of the surface motions and their average for the soil profile with permafrost table at -160 ft (-50 m) or no permafrost (AASHTO Design Earthquake level).....	68
Figure 4.25 Comparison of the average RS with varying permafrost table for input motions scaled to AASHTO Design Earthquake level hazard for the GC site.....	69
Figure 4.26 Soil profiles with varying bedrock table.....	70
Figure 4.27 Average RS of surface motions for soil profiles with varying bedrock table for AASHTO level hazard .....	71
Figure 4.28 Transfer functions of (a) the top unfrozen layer and (b) underlying permafrost for soil profiles with permafrost table varying from 0 to -115 ft (-35 m).....	72
Figure 4.29 Variation of RS with permafrost shear wave velocity for input motions Denali (a) and Hector Mine (b) scaled to AASHTO Design Earthquake level hazard.....	73
Figure 4.30 Average surface displacement, velocity and acceleration RS for the GC Site-Worst Case Scenario at MCE level hazard (2% PE in 50 years) .....	75
Figure 4.32 Average surface displacement, velocity and acceleration RS for the GC Site-Worst Case Scenario at IBC Design Earthquake level hazard.....	77

## List of Tables

Table 3.1 Bedrock motion parameters at the C-OM Site.....	14
Table 3.2 Summary of major seismic sources for the AASHTO Design Earthquake level hazard (7.5% PE in 75 yrs) of the C-OM site .....	18
Table 3.3 Source parameters of the events and recording site conditions of ground motion time histories selected from Kik-net database .....	19
Table 3.4 Scaling factor ( $F_k$ ) applied to the selected earthquake ground motion time histories for generating hazard-consistent input motions at the C-OM site for three levels of seismic hazard .....	21
Table 4.1 Ground motion parameters at the GC Site .....	49
Table 4.2 Summary of major sources of seismic hazard for the GC site.....	52
Table 4.3 Selected ground motion time histories and their source parameters.....	53
Table 4.4 Scaling factor ( $F_k$ ) applied to the selected earthquake ground motions for generating hazard-consistent input motions at the GC site.....	56

## **Acknowledgement**

The research was performed under AUTC Project #107017 by the Earthquake Engineering Group, Department of Civil Engineering, University of Alaska Anchorage, and Department of Civil Engineering, University of Alaska Fairbanks. This project was jointly funded by Alaska University Transportation Center and State of Alaska Department of Transportation & Public Facilities.

Dr. Zhaohui Yang, Associate Professor of Civil Engineering, University of Alaska Anchorage, was the principal investigator (PI). Co-PI's of this project include Dr. Utpal Dutta, Associate Professor of Civil Engineering, University of Alaska Anchorage and Dr. Kenan Hazirbaba, Assistant Professor of Civil Engineering, University of Alaska Fairbanks. Mr. Gang Xu, former graduate student of University of Alaska Anchorage, now Staff Engineer of State of Alaska Department of Transportation & Public Facilities, worked as Research Assistant in this project. Mr. Elmer E. Marx, Bridge Engineer at the Bridge Section and Mr. Clint Adler, Chief, Research Development & Technology Transfer, State of Alaska Department of Transportation & Public Facilities, and Mr. Billy G. Connor, Director of Alaska University Transportation Center, among others, have provided invaluable technical advices.

## Abstract

The state of Alaska is located in one of the most seismically active zones in the world. Several large magnitude earthquakes (the Prince William Sound Earthquake, March 1964 and the Denali Earthquake, November 2002) have occurred in the state and caused considerable damage to its transportation system, including several highway bridges and other infrastructures. Some of the damages could be related to frozen soil effects. However, only limited research has been carried out to investigate the effects of frozen soils on the seismic site response.

A comprehensive analytical investigation of the effects of frozen soils including seasonally frozen soils and permafrost on the seismic site response has been conducted. Two sites, i.e. the C St-O'Malley Bridge site in Anchorage and the Goldstream Creek Bridge site in Fairbanks, were selected to represent typical sites with seasonally frozen soils and discontinuous permafrost, respectively. Two generic soil profiles were constructed based on the geologic and geotechnical data available for these two sites. A set of input ground motions has been selected from available strong-motion databases and scaled to generate an ensemble of seismic hazard-consistent bedrock motions. One-dimensional equivalent linear analyses were applied to analyze the seismic site response for three levels of seismic hazard, i.e. MCE (2% probability of exceedance in 50 years), AASHTO Design Earthquake (7.5% probability of exceedance in 75 years) and IBC Design Earthquake (two-thirds of MCE). A series of parametric studies were conducted for assessing the sensitivity of the results to the uncertainties associated with shear wave velocity of frozen soils, thickness of seasonally frozen soil, permafrost table/thickness, and bedrock table. Our results show that the presence of frozen soils, particularly permafrost, can significantly change the ground motion characteristics. It is concluded that it is generally conservative to ignore the effects of seasonally frozen ground on site response. It is, however, not always conservative to classify permafrost soil sites by using average shear wave velocity of the upper 30 m frozen or unfrozen soils and use code-defined site coefficients for seismic design. For permafrost sites similar to the GC Site-Worst Case Scenario, that is when the permafrost table is at -50 to -130 ft, and the bedrock table is at -230 ft or shallower, and the soil types are similar to the GC Site - Worst Case Scenario, the average response spectra obtained from this study could be used in seismic design.

## Summary of Findings

Based on this comprehensive study, the following major conclusions or recommendations can be made:

1. Seasonally frozen ground has noticeable impact on the average spectral accelerations for periods shorter than 1.0 sec. While peak ground acceleration, spectral accelerations at 0.2 and 1.0 sec of a site subject to seasonally frozen ground in cold regions decrease with the increase in seasonally frozen soil thickness, spectral acceleration at 0.2 sec is more sensitive to the change in seasonally frozen soil thickness.
2. It is generally conservative to ignore the effects of seasonally frozen soils on seismic site response.
3. The average spectral acceleration, velocity and displacement response is substantially larger than that of site Class D when the permafrost table is located between -50 to -130 ft with the bedrock table at approximately -230 ft or shallower for periods between 0.5 and 1.0 sec.
4. The average spectral values reach the highest when the permafrost table is at -66 ft with the bedrock table at -216 ft. This is designated as the GC Site-Worst Case Scenario.
5. Compared with those suggested by design codes, the average values of spectral acceleration for periods in the range of 0.4 to 1.0 sec are up to 20% larger, those of spectral velocity for periods in the range of 0.4 to 1.0 sec are up to 50% larger, and those of spectral displacement for periods in the range of 0.5 to 1.0 sec are up to 40% larger for all three levels of seismic hazard in the GC Site-Worst Case Scenario.
6. The large amplification in the permafrost site response was mainly caused by the unfrozen top soil layer. The permafrost layer does not amplify the bedrock motions; instead it attenuates high frequency components of the bedrock motions.
7. It is not always conservative to classify permafrost soil sites by using average shear wave velocity of the upper 30 m frozen or unfrozen soils and use code-defined site coefficients for seismic design. For permafrost sites similar to the GC Site-Worst Case Scenario, that is when the permafrost table is at -50 to -130 ft, and the bedrock table is at -230 ft or shallower, and the soil types are similar to the GC Site - Worst Case Scenario, the average response spectra obtained from this study could be used in seismic design. For other permafrost sites, particularly when soft soils and/or sensitive soils are present, site specific investigation should be conducted in a manner similar to the approach used in this study.
8. It is recommended that site exploration beyond the permafrost layer, e.g. drilling or seismic survey, be conducted to detect the bedrock table when other conditions are similar to the GC Site-Worst Case Scenario.
9. The effects of seasonally frozen soils and permafrost are not very sensitive to the variation of shear wave velocity of frozen soils.

## CHAPTER 1 – INTRODUCTION

### 1.1 Background

The state of Alaska is located in one of the most seismically active zones in the world. Several large magnitude earthquakes including the Prince William Sound Earthquake of March 1964 ( $M_w = 9.2$ ) and the Denali Earthquake of November 2002 ( $M_w = 7.9$ ) have occurred in the state and caused considerable damages to its transportation system, including several highway bridges and other infrastructures. Some of the damages could be related to frozen soils effects. However, only limited research has been carried out in this aspect. This research effort focuses on a quantitative assessment of the seismic response of the soil profiles with seasonally frozen soil or permafrost.

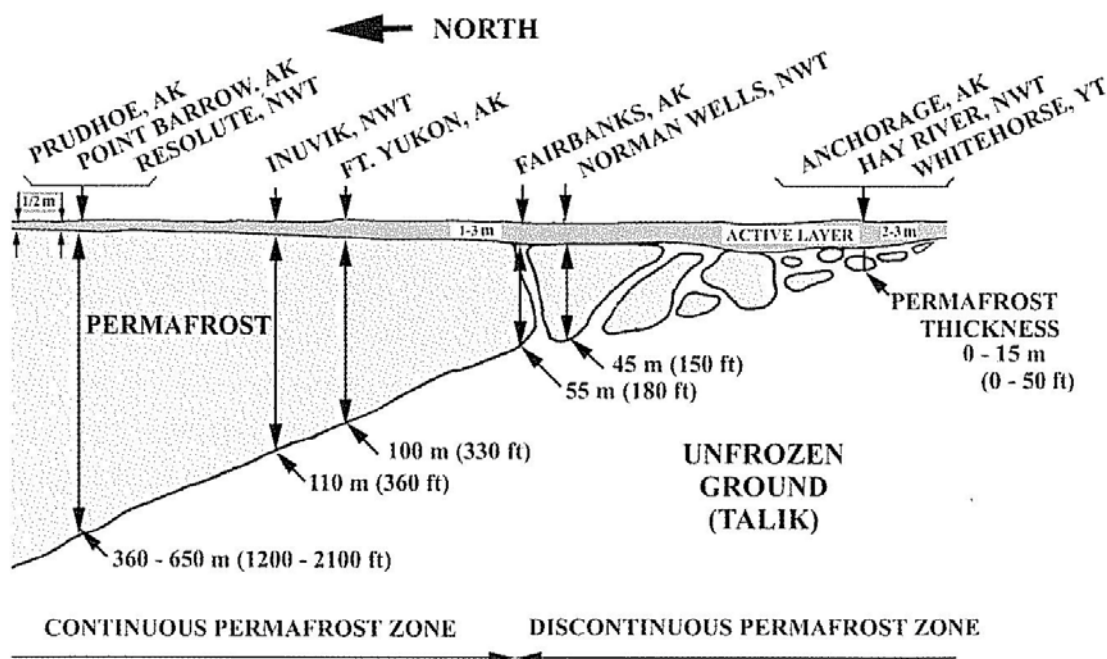


Figure 1.1 Thickness of the active layer and vertical distribution of permafrost in Alaska and western Canada based (Davis, 2001)

Most of the state of Alaska is under arctic or sub-arctic climate. Thick seasonally frozen soils and permafrost (refers to the ground that has a temperature lower than  $^{\circ}\text{B}2$  continuously for at least two consecutive years) exists extensively in the state. Due to the variation of mean annual temperature, the frozen soil profile in Alaska varies, as shown in Figure 1.1 (Davis, 2001). In Southcentral Alaska (Anchorage and its adjoining areas) there exists a seasonally frozen soil of up to 3 m thick and discontinuous permafrost of 0 to 15 m thick. In Interior Alaska, the thickness of the discontinuous permafrost layer increases to about 50 m. To the further north, the discontinuous permafrost becomes continuous permafrost of 360 to 650 m thick. It is noted that most of the permafrost in

Interior Alaska are “warm” permafrost, implying that its temperature is at most a few degrees below the freezing point (V. Romanovsky, Personal Communication, 2007).

Many researchers have studied frozen soil dynamic properties using both laboratory and field measures (e.g. Vinson et al., 1977; LeBlanc et al., 2004). The large variation of temperature causes a drastic change in soil dynamic properties. For instance, the Young’s modulus of the frozen soil is in magnitudes of tens to hundreds times higher than that of unfrozen soil (Tsytovich, 1975). The seasonal changes of soil dynamic properties will very likely affect the seismic site response of the soil column. Moreover, unfrozen soil of low shear wave velocity exists underneath the high velocity permafrost due to increase of ground temperature with depth, which is in contrast to non-permafrost sites where ground stiffness generally increases with depth. Such change in ground stiffness due to existence of permafrost may alter the seismic site response.

However, only limited research has been carried out so far in this aspect. Studies (Singh and Donovan, 1977; Qi et al., 2006) have shown that the presence of a frozen surface layer affects ground motion characteristics and reduces the observed surface acceleration. Finn and Yong (1978) reported a summary of the research efforts on frozen ground including permafrost and concluded that studies on the seismic response of frozen ground were at an elementary stage and were primarily based on field data collected after the Alaska earthquake of 1964 (Eckels 1966; Ferrians 1966). They suggested that as a first order approximation, it might be reasonable to assume the seismic response of a thick permafrost layer would be similar to that of the rock. Vinson (1978) also studied the seismic response of a thick permafrost site. A study on the Qinghai-Tibet railway embankment (Wang et al., 2004) reported that the existence of a permafrost layer would significantly affect the site response spectrum for certain earthquakes with high frequency components. However, this study was based on very limited number of input motions and did not consider different levels of seismic hazard.

Current design codes, such as American Association of State Highway and Transportation Officials (AASHTO, 2007) and International Building Code (IBC) (International Code Council, 2000) are based on site response studies of unfrozen soils and do not include specific recommendations to account for frozen soil effect. In current practice, the effects of permafrost on seismic site response are simply ignored and site exploration depth is typically limited to the depth of the permafrost table (i.e. no drilling and investigation in the permafrost layer). With increasing demand for natural resources, more infrastructure, such as the Alaska Natural Gas Pipeline, is being constructed in the seismically active cold regions. It is therefore imperative to improve our understanding on how seasonally frozen soils and permafrost affect the characteristics of site responses at various levels of seismic hazard in order to provide guidelines for engineering design. This study focuses on a quantitative assessment of the frozen soil effects on the seismic site response.

## **1.2 Objective of Research**

The main objective of this research is to carry out one-dimensional (1-D) site response analyses in order to understand the impact of frozen soils including seasonally frozen soils and permafrost on the seismic response of cold regions sites with high seismic activity. To achieve this objective, three main topics are considered as outlined below:

1. Investigation of the effects of frozen soils including seasonally frozen and permafrost on the seismic site response,
2. Quantification of the uncertainties in the calculated results, and
3. Recommendation of modification to the seismic design codes to account for the effects of frozen ground in the seismic design of bridges and other infrastructures for the state of Alaska as well as for other cold regions.

## **1.3 Scope of Study**

The scope of this study included conducting a series of 1-D equivalent linear site response analyses of two selected sites representative of Alaskan conditions. One site has been selected from Southcentral Alaska with the focus on seasonally frozen ground, and the other from the Interior Alaska with the focus on permafrost. Two generic soil profiles have been established based on the geologic and geotechnical data available for these two sites to make the results applicable to other similar sites. A set of input motions consistent with the tectonic settings of the selected sites has been selected from strong motion databases recorded worldwide and scaled to several seismic hazard levels. These hazard-consistent earthquake ground motions have been used as bedrock motions to simulate the surface motions for studying frozen soil effects on seismic site response.

This study aims to provide a quantitative estimation of frozen soil effects on various ground motion parameters of engineering interest such as peak ground acceleration (PGA) and spectral accelerations (SA) under various frozen soil conditions. Parametric studies have also been conducted to assess the uncertainties in the results due to model assumptions and soil dynamic properties including shear wave velocity and thickness of frozen soils, depth of permafrost table and bedrock table, etc.

## CHAPTER 2 - METHODOLOGY OF SITE RESPONSE ANALYSIS

### 2.1 Introduction

For common engineering applications, site response analysis refers to the analysis to determine the response of soil deposits to the motion of bedrock immediately beneath it (Kramer, 1996). Frozen soils, including seasonally frozen soil and permafrost, constitute unique soil deposits in the state of Alaska. In order to investigate the influence of frozen soils on seismic site response, two bridge sites in the state of Alaska were selected for this study. One is located in seasonally frozen soils and the other in discontinuous permafrost. This chapter describes the general methodology for site response analysis.

The methodology adopted for site response analysis consists of following procedures:

1. Selecting a suitable site response analysis model and constructing a soil profile from the available geotechnical engineering data;
2. Using the available probabilistic seismic hazard map to construct site-specific seismic design spectra for various levels of seismic hazard;
3. Identifying seismic sources (scenario earthquakes) that contribute significantly to the seismic hazard of the study area from the de-aggregation of hazard maps;
4. Generating hazard-consistent strong ground motions for the study sites by appropriate scaling of the time series data of selected earthquakes from other parts of the world based on deaggregation results; and
5. Computing the ground motion parameters at the surface by propagating those hazard-consistent ground motions from the bedrock through the soil column.

In the following sections, we discuss each step.

### 2.2 Site Response Analysis Model

Site response analysis can be performed in one-dimensional (1-D), two-dimensional (2-D) or three-dimensional (3-D) wave propagation analysis. 2-D or 3-D analysis (e.g. Bielak et al., 1999) is capable of modeling the effects of relatively complex basin geometry or topography. For the generic nature of this study, however, 1-D analysis was adopted in this study.

1-D wave propagation analysis is based on the assumption that the response of soil deposits are predominantly caused by the vertical propagation of shear wave from the bedrock (Schnabel et al., 1972). The soil profile is discretized into a multi-degree-of-freedom shear beam system, as shown in Fig. 2.1. Each layer is assumed to be homogenous and isotropic and is characterized by the shear modulus,  $G$ , soil density,  $\rho$ , damping ratio,  $\zeta$ , and thickness,  $h$ . The vertical propagation of shear-wave motion through the system can be calculated based on the solution to the wave equation (Kanai, 1951). Depending on the type of soil model used, site response analysis can be divided into two categories: (a) equivalent linear analysis, and (b) non-linear analysis.

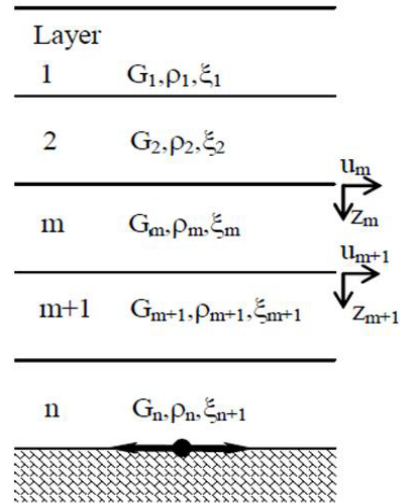


Figure 2.1 One-dimensional idealization of a horizontally-layered soil deposit over a uniform Half-Space

### 2.2.1 Equivalent Linear Analysis

Equivalent linear analysis (Idriss and Seed, 1968; Seed and Idriss, 1970) accounts for the soil nonlinearity using an iterative procedure to obtain values for modulus and damping that are compatible with the equivalent uniform strain induced in each sublayer. The analysis is conducted using soil properties described above and the equivalent uniform shear strain induced in each sublayer is calculated. The shear modulus and the damping ratio for each sublayer are then modified according to the equivalent uniform shear strain based on the applicable relationship relating these two properties to shear strain, which will be discussed next. The analysis is repeated until strain-compatible modulus and damping values are arrived at. It is emphasized that equivalent linear analysis operates in the frequency domain; for each sublayer, time-invariant soil properties are used. While the equivalent linear approach allows the most important effects of nonlinear, inelastic soil behavior to be approximated, it remains a linear analysis method.

Many studies have been carried out to understand soil dynamic properties and to relate shear modulus  $G$  and damping ratio  $\zeta$  with shear strain. Normalized shear modulus  $G/G_{max}$  ( $G_{max}$  is the maximum shear modulus) is typically used in presenting the modulus reduction curve. A number of commonly used relationships between  $G/G_{max}$ ,  $\zeta$  and shear strain for unfrozen soils are available in the literature (e.g. Seed and Idriss, 1970; Seed et al., 1984; Seed et al., 1986; Sun et al., 1988; Vucetic and Dobry, 1991). It is worthwhile to note that there exists a layer of soft clayey soil in the Anchorage basin that is known as the Bootlegger Cover Formation (BCF). Lade et al. (1988) conducted laboratory tests to obtain its modulus reduction and damping ratio properties in relation to shear strain. Vinson et al. (1977) and Czajkowski and Vinson (1980) have obtained the dynamic properties of typical frozen soil of Interior Alaska. A few commonly used

dynamic properties of unfrozen soils and those for frozen soil at “warm” temperature have been plotted in Figures 2.2 and 2.3. Due to lack of in-situ soil testing data at the study sites and the generic nature of this study, these dynamic properties have been used throughout this study.

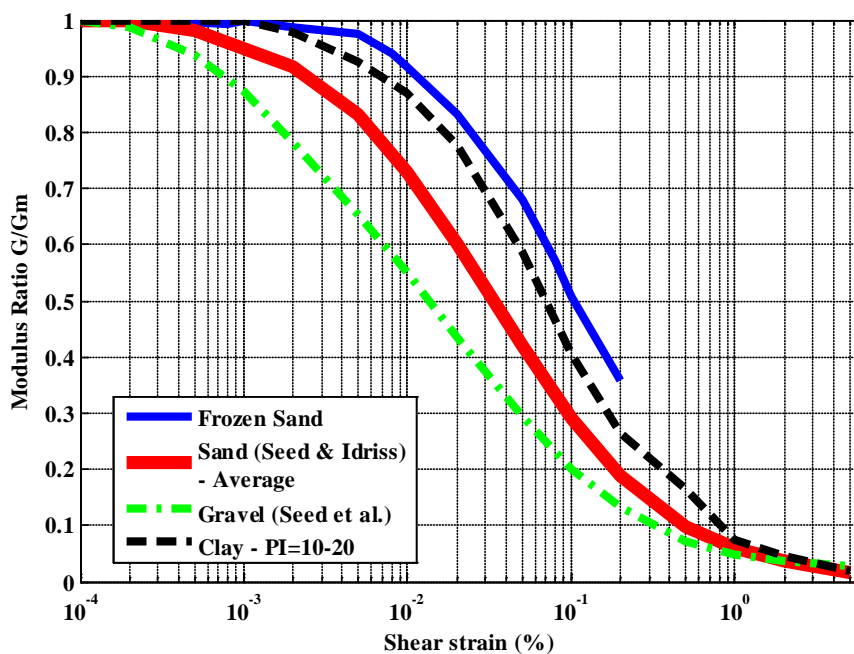


Figure 2.2 Modulus vs. shear strain for unfrozen and frozen soils

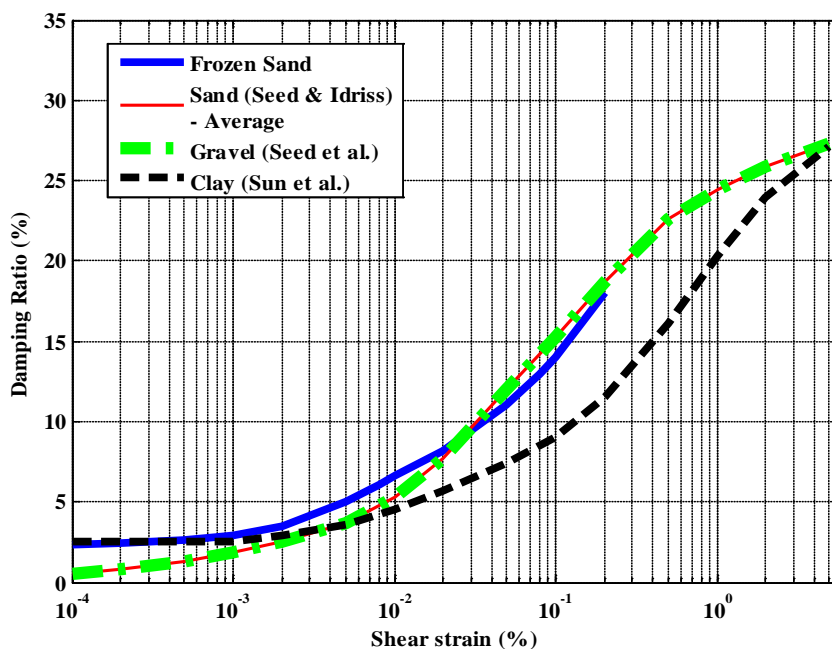


Figure 2.3 Damping ratio vs. shear strain for unfrozen and frozen soils

### 2.2.2 Nonlinear Analysis

Nonlinear time domain analysis is an alternative approach to analyze the nonlinear response of a soil deposit using direct numerical integration in the time domain. It typically uses a fairly complex constitutive soil model to simulate the inherent soil nonlinearity, and allows soil properties within a given layer to change with time as the strains in that layer change. The parameters required for the constitutive soil models generally consist of a backbone curve that models the stress-strain behavior during cyclic loading and rules for loading and unloading, stiffness degradation, and other factors (Kramer, 1996). For example, DEEPSOIL uses an extended MKZ model in time domain analysis of site response (Hashash, 2004; Duhee and Hashash, 2004). These constitutive models typically require physical testing data to carefully calibrate a relatively large set of model parameters. Modified frequency-domain methods (Kausel and Assimaki, 2002; Assimaki and Kausel, 2002) have also been developed in which soil properties in each layer are adjusted on a frequency-to-frequency basis to account for the strong dependency of shear strain amplitude with frequency.

### 2.2.3 Discussion on Analysis Method

The equivalent linear approach has been shown to provide reasonable estimate of soil response, particularly for small shear strains (less than about 1 to 2 percent) and modest accelerations (less than about 0.3 to 0.4g) (Kramer and Paulsen, 2004). Nonlinear analyses may provide an improved estimate of ground motion relative to the equivalent linear analysis when ground strains become large (Stewart and Kwok, 2008). However, a relative large number of soil parameters for soil constitutive models need to be carefully calibrated. According to an informal survey (Kramer and Paulsen, 2004), 1-D equivalent linear analysis was far and away the most commonly used procedure for site response analysis in North America. For these reasons, we chose ProShake (EduPro Civil Systems, Inc., 1998), which uses 1-D equivalent linear procedure, as the research tool in this study.

## 2.3 Identification of Seismic Hazard and De-aggregation of Seismic Hazard

If no recorded ground motion data are available, hazard-consistent bedrock input motions can be generated either by stochastic simulation (Boore, 1983) or by appropriate scaling of recorded strong-motion time histories from other parts of the world. In this study, scaling of recorded ground motions was used. In order to select appropriate strong-motion records major contributing earthquake sources at the study site need to be identified. For this purpose, the Probabilistic Seismic Hazard Maps for Alaska prepared by U.S. Geological Survey have been used (Wesson et al. 1999). Further, de-aggregation of seismic hazard has been used to identify scenario earthquakes to facilitate the selection of ground motions.

### 2.3.1 Identification of Seismic Hazard

From the Probabilistic Seismic Hazard Maps for Alaska, important bedrock motion parameters of engineering interest including peak ground acceleration (PGA), and SA at 0.2 sec ( $S_s$ ) and SA at 1.0 sec ( $S_1$ ) at 5% damping ratio can be retrieved for the study sites. Based on these parameters, response spectrum (RS) of bedrock motion can be constructed according to the procedures defined in AASHTO 2007 or IBC 2000. In this study, three levels of seismic hazard, i.e. 2% probability of exceedance (PE) in 50 years (maximum considered earthquake or MCE), 7.5% PE in 75 years or 5% PE in 50 years (AASHTO Design Earthquake or AASHTO) and two-thirds of MCE (IBC Design Earthquake or DS) have been considered.

### 2.3.2 De-aggregation of Seismic Hazard

De-aggregation of seismic hazard contributions at a site enables the investigators to identify the distance and azimuth to predominant sources in order to generate scenario earthquakes and corresponding time histories for seismic design analysis. The seismic hazard for the selected study sites was de-aggregated in terms of distance and magnitude by using The 1996 De-aggregation Application (<http://eqint.cr.usgs.gov/deaggint/1996/index.php>) prepared by USGS. Based on the de-aggregation results, a series of representative time histories were selected with respect to magnitude, distance and source characterization, as discussed in next section.

## 2.4 Generation of Hazard-Consistent Ground Motions

Several methods of scaling time histories have been proposed. These include frequency-domain methods where the frequency content of the recorded ground motions are manipulated in order to obtain a match (Gasparini and Vanmarcke, 1976; Carballo and Cornell, 2000) and time-domain methods which manipulate only the amplitude of the recorded ground motions (Naeim et al., 2004).

We elect to adopt time-domain scaling method in this study. Due to lack of earthquake ground motion records at the study sites, earthquake ground motion time histories recorded elsewhere were selected based on the source parameters of the scenario earthquakes contributing the most to the seismic hazard of the study sites. Several earthquake strong motion databases are available (e.g. PEER Strong Motion Database and Consortium of Organizations for Strong Motion Observation Systems (COSMOS) Strong Motion Database of California, and KIK-Net and K-Net of Japan) for selecting earthquake strong motion records. Six to ten representative earthquake ground motion records were selected for each study site (Dalal et al., 1976; Seed et al., 1976) to provide reliable site response results. These ground motion time histories were scaled in time domain to various hazard levels. The selection criteria and scaling algorithm used in this study are discussed in detail in this section.

### 2.4.1 Time Histories Selection Criteria

Using the scenario earthquake source parameters as the target, earthquake ground motion time histories recorded elsewhere have been selected based on following criteria:

- 1) The source mechanism of the selected records should be similar to that of the scenario earthquake at the study site;
- 2) Selected records should be from earthquakes whose magnitude is within the range of  $M_w \pm 0.5$ , where  $M_w$  is the moment magnitude of the scenario earthquake of the study sites;
- 3) Peak horizontal acceleration (PHA) of selected time histories should be no more than 5 times smaller than the PGA of the selected hazard level at the study site. This criterion has been imposed to avoid over-scaling; and
- 4) Time histories are selected either from sites underlain by geologic rock or stiff soils or from boreholes in order to minimize the site effects.

### 2.4.2 Time Histories Scaling

The hazard spectra of the study sites are obtained from probabilistic assessment so the RS of selected time histories are inherently incompatible. The spectral levels of the selected data and that obtained from the seismic hazard maps at the study site do not match with each other. For this reason, scaling of time histories is required. The intent of scaling is to provide an ensemble of time histories with its average spectral amplitudes closely matching the probabilistic assessment of bedrock RS for the subject site, while retaining the inherent variability of the time history ensemble. The selected time histories were scaled by the following procedure:

1. Obtain the bedrock RS of a study site as target RS, denoting it as  $RS_{tg}(T_i)$  at period  $T_i$ ;
2. The spectral acceleration (SA) for two horizontal components of a selected time history was calculated, and referred to as  $SA(T_i)$  at period  $T_i$ ;
3. Individual time history  $k$  is simply scaled by a factor  $F_k$  so that the  $L_2$ -norm difference, denoted as  $e_k$  (Eqn. (2.1)), between the target spectrum  $RS_{tg}(T_i)$  and the  $SA(T_i)$  of selected time histories for period  $T_i$  over the range 0-1.0 second is minimum;

$$e_k = \sqrt{\sum_{i=1}^n \{F_k * SA(T_i) - RS_{tg}(T_i)\}^2} \quad (0 \leq T_i \leq 1) \quad (2.1)$$

4. The resulting scaling factor,  $F_k$ , was applied to the individual time histories  $k$  to obtain an input motion.

By selecting a sufficient number of time histories, this procedure can ensure that the average RS of the scaled time histories closely match the target spectrum, while the inherent variability across the time histories is still preserved.

## 2.5 Demonstration of the Effectiveness of Analysis Method

The effectiveness of the site response analysis method adopted in this study has been demonstrated by an example. In this example, an idealized soil profile consisting of a frozen soil layer overlying bedrock, as shown in Figure 2.4. The layer of frozen soil hypothetically extends from surface (0 m) to the top of bedrock (-66 m), and the shear wave velocity  $V_s$  of the frozen soil was taken as 1500 m/s. According to the AASHTO specification, this soil profile can be classified as AASHTO site class B ( the average  $V_s$  of the upper 30 m soils is 1500 m/s), which should not amplify the bedrock motion.

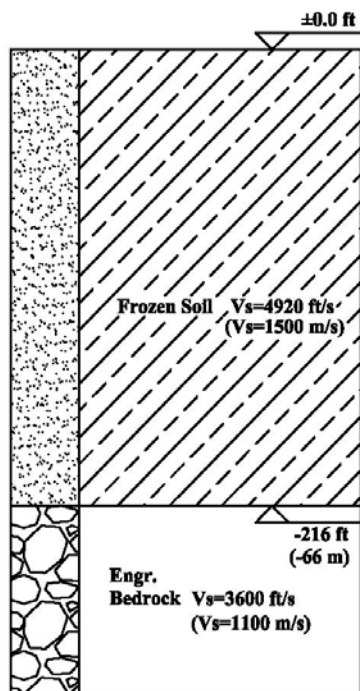


Figure 2.4 A hypothetical soil deposit consisting of frozen soil over bedrock

The Denali earthquake record (listed in Table 4.1) was input at the bedrock, and then propagated through the frozen soil layer. The RS of bedrock and output motions were obtained and shown in Figure 2.5. It can be seen that two RS agree with each other very well except that a subtle difference occurred at short periods, indicating that the frozen soil layer almost did not change the bedrock motion. The difference at short periods may be caused by the frozen soil which tends to attenuate high frequency components of input motions.

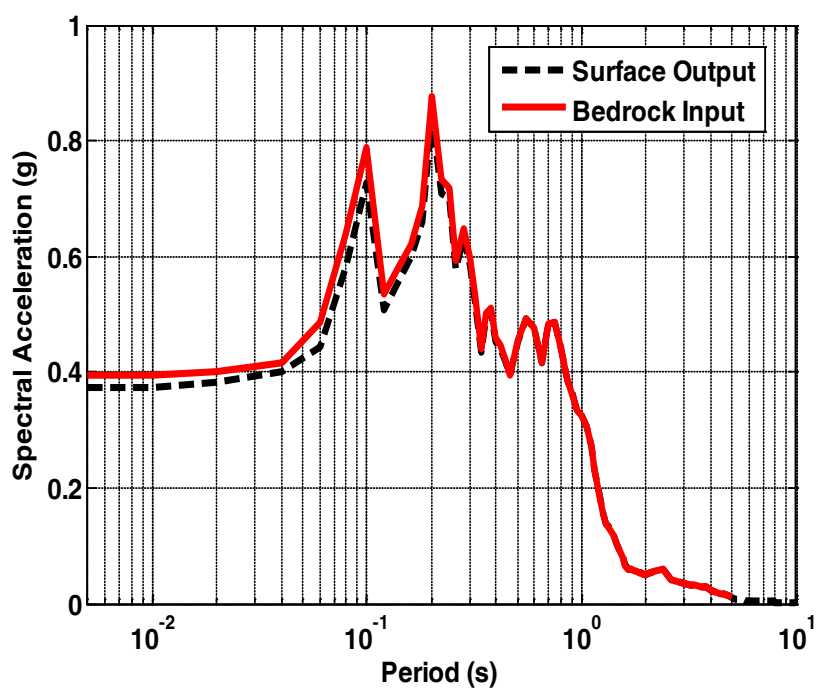


Figure 2.5 Comparison between RS of bedrock and surface motions of the hypothetical soil site

## **CHAPTER 3 - EFFECTS OF SEASONALLY FROZEN SOIL ON THE SEISMIC SITE RESPONSE**

### **3.1 Introduction**

Anchorage is the largest population center in Southcentral Alaska under subarctic climate. It is exposed to considerable frost penetration in winter. This makes Anchorage an ideal site for studying seasonally frozen ground effects on site response. One bridge site at the midtown of Anchorage was selected as the basis of soil profile construction. The outcome of study includes the transfer functions between the generated surface motion and bedrock motion, RS of surface motions and variation of PGA and spectral acceleration (SA) of surface motions. Impact of seasonally frozen ground on the shape and amplitude of seismic site RS was discussed. Parametric studies were conducted to investigate the effects of thickness and shear wave velocity of the frozen soil on site response.

### **3.2 General Geology of the Selected Seasonally Frozen Soil Site**

The C-St/O'Malley Road bridge site (referred to as C-OM site) in Anchorage has been selected for this study. At this site, the soil has a 1-2 m thick surface layer that freezes and thaws annually. A geological section of this bridge site is shown in Figure 3.1 (Combellick, 1999). The soils consist of three layers: a 25 ft (7.5 m) top layer of fine sand and silt (SS) overlies a 49 ft (14 m) thick layer of glacial drift (GD). These two layers overlie the BCF, one of the important Quaternary deposits in the Anchorage basin, which is also embedded in the GD layer. At the very bottom lie Pre-Quaternary sediments (B).

### **3.3 Identification of the Seismic Hazard at the C-OM Site**

The Probabilistic Seismic Hazard Maps of U.S. Geological Survey) has been used to retrieve the bedrock motion parameters of the C-OM site (Latitude 61.1234 N and Longitude -149.8861 W). The values of bedrock motion parameters including PGA,  $S_s$  and  $S_1$  are listed in Table 3.1. The RS constructed based on AASHTO (2007) for this site are plotted in Figure 3.2.

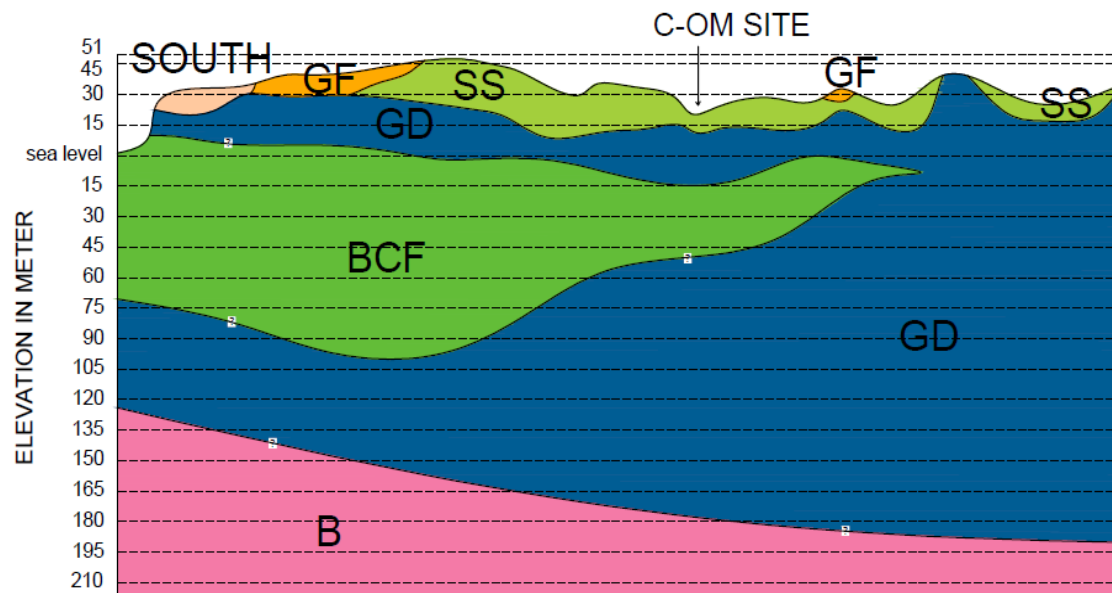


Figure 3.1 A geological cross section at C-OM site based on Combellick (1999)

Table 3.1 Bedrock motion parameters at the C-OM Site

Seismic Hazard Level	PGA (g)	$S_s$ (g)	$S_1$ (g)
MCE (2 % PE in 50 years)	0.665	1.500	0.559
AASHTO Design Earthquake (7.5% PE in 75 years or 5% PE in 50 years)	0.503	1.208	0.411
IBC Design Earthquake (two-thirds of MCE)	0.385	1.007	0.373

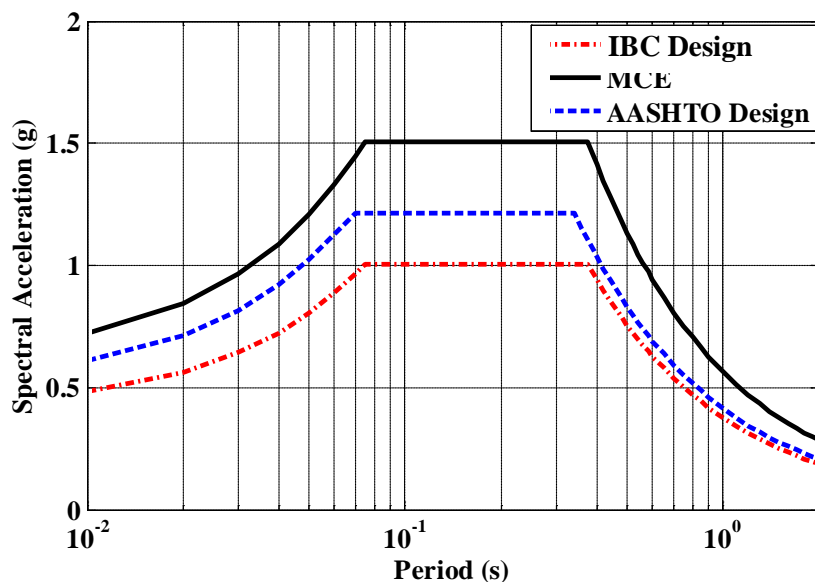


Figure 3.2 Comparison of bedrock motion RS for three levels of seismic hazard

### 3.4 De-aggregation of Seismic Hazard at the C-OM Site

The seismic hazard of the C-OM site has been de-aggregated by moment magnitude ( $M_w$ ) and hypocentral distance. For example, the results of de-aggregation of AASHTO Design Earthquake level seismic hazard for PGA,  $S_s$  and  $S_1$  are shown in Figures 3.3, 3.4 and 3.5, respectively. These figures display the seismic hazard in three-dimensional map views. The X-axis shows the distance between significant seismic sources and the study site; the Y-axis describes the magnitude of potential seismic sources; and the Z-axis indicates the contribution in percentage of each potential seismic source to the total seismic hazard. The height of the bar is proportional to the sum of hazards from all sources at the location. The major sources including crustal faults, plate subduction zone, and random seismicity having more than 10% contribution to the total seismic hazard are listed in Table 3.2.

It is seen from Table 3.2 that the major sources of seismic hazards at this study site for PGA,  $S_s$  and  $S_1$  are subduction zone events including those similar to the 1964 earthquake as well as other local shallow sources. For  $S_1$ , plate subduction zone and megathrust events of 50-60 km hypocentral distance contribute 57.6% of the total seismic hazard, and shallow random sources with a hypocentral distance of 10-12 km and a moment magnitude of 5-7.3 contribute 36.2% of total seismic hazard.

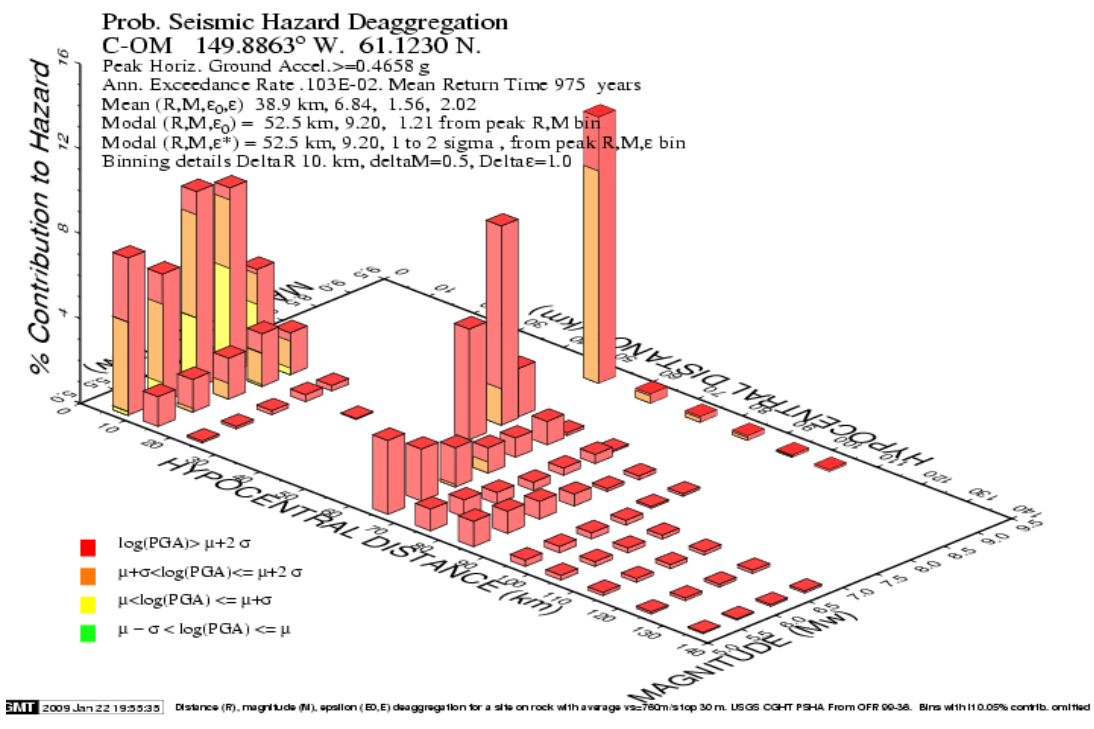


Figure 3.3 De-aggregation of the AASHTO Design Earthquake level seismic hazard (7.5% PE in 75 yrs) at C-OM site for PGA

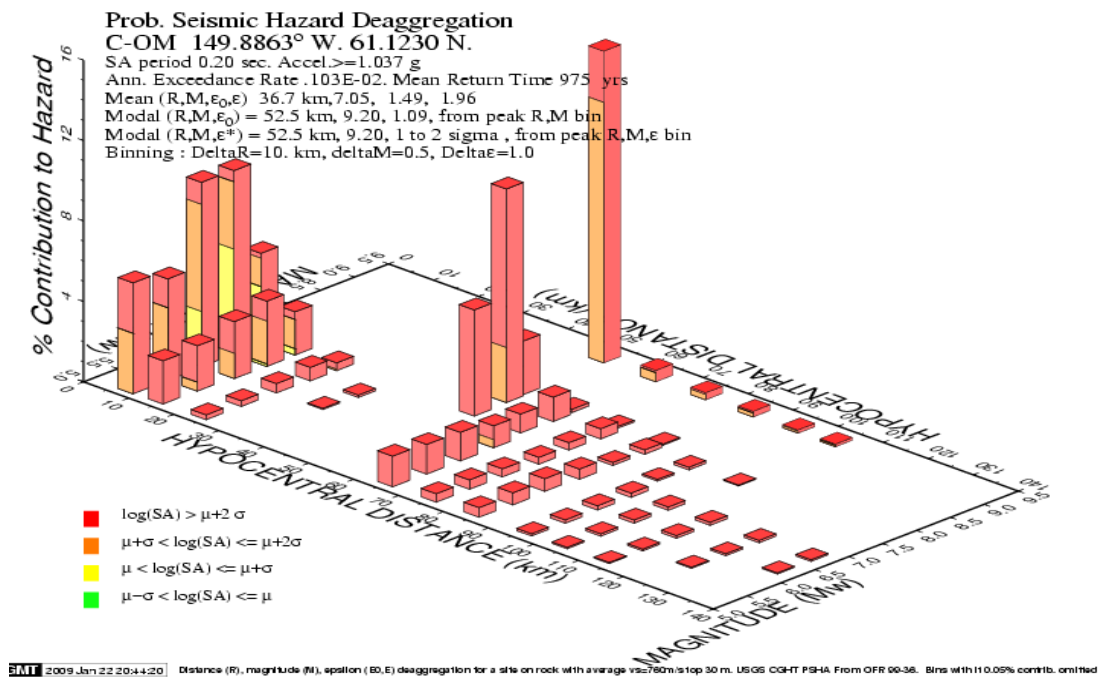


Figure 3.4 De-aggregation of the AASHTO Design Earthquake level seismic hazard (7.5% PE in 75 yrs) at C-OM site for  $S_s$ .

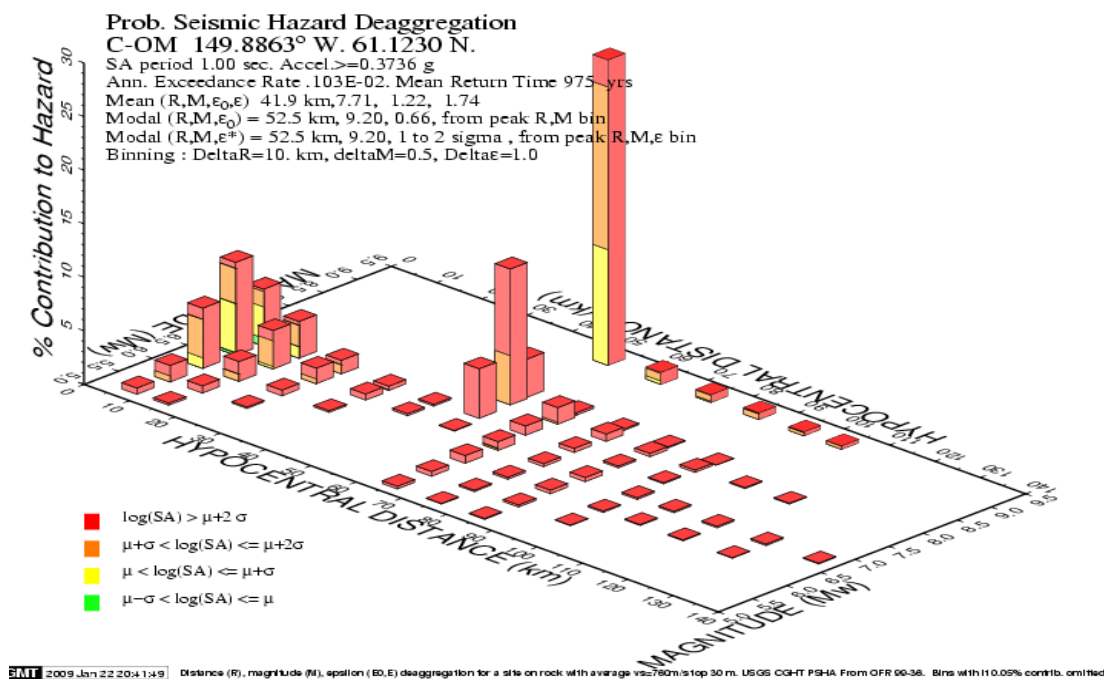


Figure 3.5 De-aggregation of the AASHTO Design Earthquake level seismic hazard (7.5% PE in 75 yrs) at C-OM site for  $S_1$ .

Table 3.2 Summary of major seismic sources for the AASHTO Design Earthquake level hazard (7.5% PE in 75 yrs) of the C-OM site

Source	PGA			
	% contr.	R (km)	M <sub>w</sub>	$\varepsilon_0$
Plate subduction, east zone	10.30	56.8	7.59	2.10
1964-zone subduction M <sub>w</sub> <8.2	10.40	56.8	7.60	2.09
AK 60-km deep seismicity	18.06	76.8	5.82	2.61
Shallow random sources M <sub>w</sub> 5-7.3	46.23	9.1	6.23	0.96
Source	SA at 0.2 sec (S <sub>s</sub> )			
	% contr.	R(km)	M <sub>w</sub>	$\varepsilon_0$
Plate subduction, east zone	11.30	56.9	7.60	2.04
1964-zone subduction M <sub>w</sub> <8.2	11.45	56.9	7.61	2.04
AK 60-km deep seismicity	11.04	76.9	5.98	2.65
Shallow random sources M <sub>w</sub> 5-7.3	48.23	10.1	6.28	1.06
Source	SA at 1.0 sec (S <sub>1</sub> )			
	% contr.	R(km)	M <sub>w</sub>	$\varepsilon_0$
Plate subduction, east zone	12.81	57.8	7.66	1.95
1964-zone subduction M <sub>w</sub> <8.2	13.04	57.9	7.66	1.95
M <sub>w</sub> 9.2 megathrust, east zone	15.12	58.3	9.20	0.71
1964-zone M <sub>w</sub> 9.2 megathrust	16.63	52.4	9.20	0.66
Shallow random sources M <sub>w</sub> 5-7.3	36.19	12.2	6.67	0.93

- M<sub>w</sub>: moment magnitude
- R: hypocentral distance
- $\varepsilon_0$ : standard deviation

### 3.5 Time Histories Selection and Scaling

Five time histories generated by five earthquakes have been selected from the KiK-net strong motion database (<http://www.kik.bosai.go.jp/>) based on the criteria set forth in Sec. 2.4.1. The source parameters and borehole depths at which these five events were recorded are listed in Table 3.3. The ground motion time histories are shown in Figure 3.6.

Table 3.3 Source parameters of the events and recording site conditions of ground motion time histories selected from Kik-net database

Station Code (component)	Origin Time	Source	Depth (km)	Mag. ( $M_w$ )	Epi. Dist. (km)	Borehole PGA (gal)	Borehole depth (m from Mean Sea Level)
IWTH23 (E-W)	05/26/2003	Plate subduction	71	7.0	53	133	-59
KOCH05 (E-W)	03/24/2001	Plate subduction	51	6.4	67	68	160
MYGH11 (E-W)	08/16/2005	Plate subduction	42	7.2	91	98	-202
NIGH01 (N-S)	01/18/2005	Local/ shallow	8	4.8	11.4	104	-15
SMNH01 (N-S)	10/16/2000	Local/ shallow	11	7.3	8	185	69

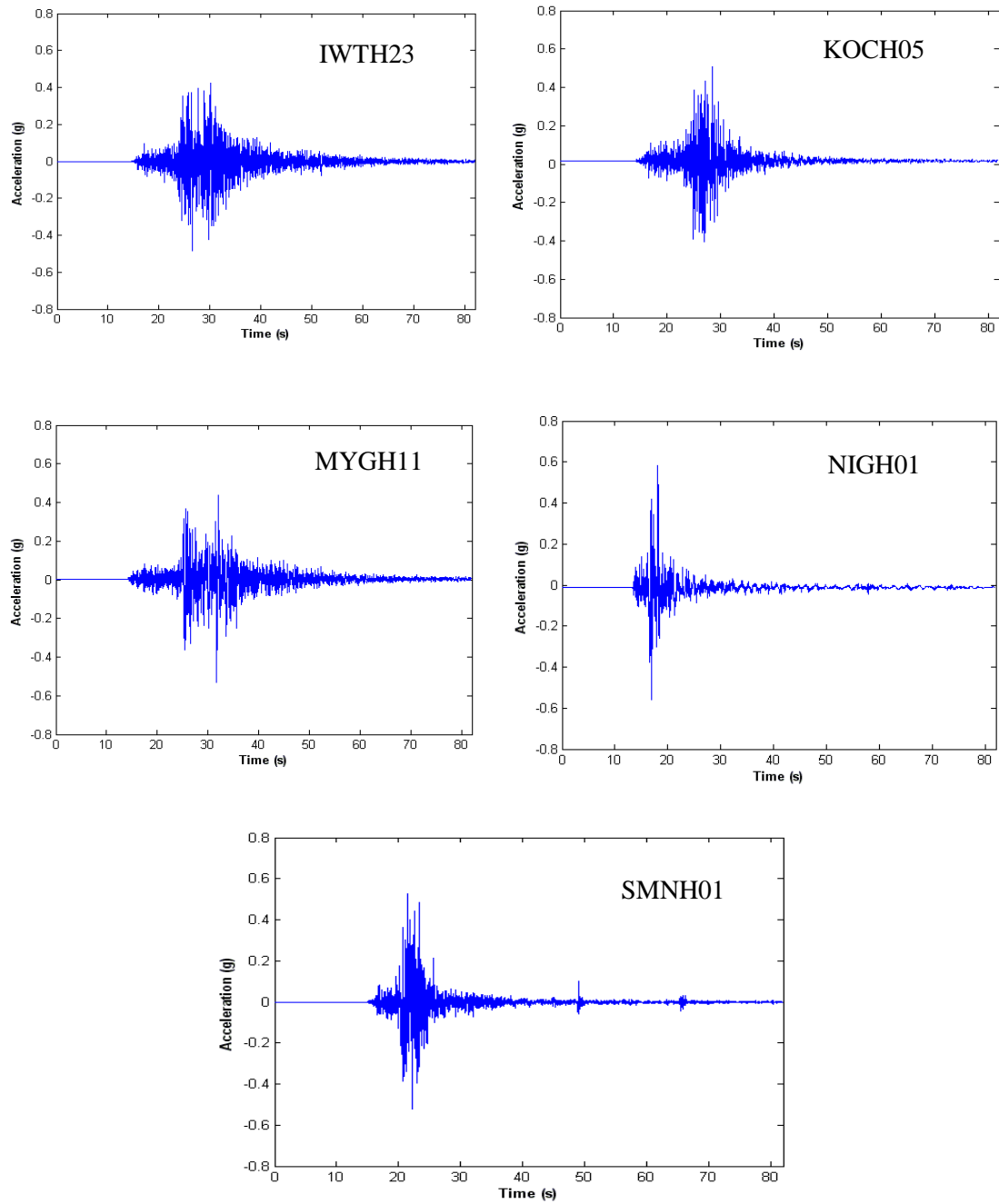


Figure 3.6 Plots of acceleration vs. time for the five time histories selected from the Kik-Net database.

The selected time histories have been scaled to the three levels of seismic hazard of the C-OM site by using the procedure discussed in Section 2.4.2. The scaling factors applied to the selected time histories for generating hazard-consistent input motions are listed in Table 3.4. The RS of the five selected time histories with 5% damping ratio and the target RS for the three levels of hazard are shown in Figures 3.7-3.11, respectively.

Table 3.4 Scaling factor ( $F_k$ ) applied to the selected earthquake ground motion time histories for generating hazard-consistent input motions at the C-OM site

Time Histories ID		IWTH23	KOCH05	MYGH11	NIGH01	SMNH01
Scaling Factor	MCE	5.1	4.8	7.0	3.7	3.8
	AASHTO Design Earthquake	4	3.8	5.9	2.8	3
	IBC Design Earthquake	3.4	3.1	5.2	1.5	2.5

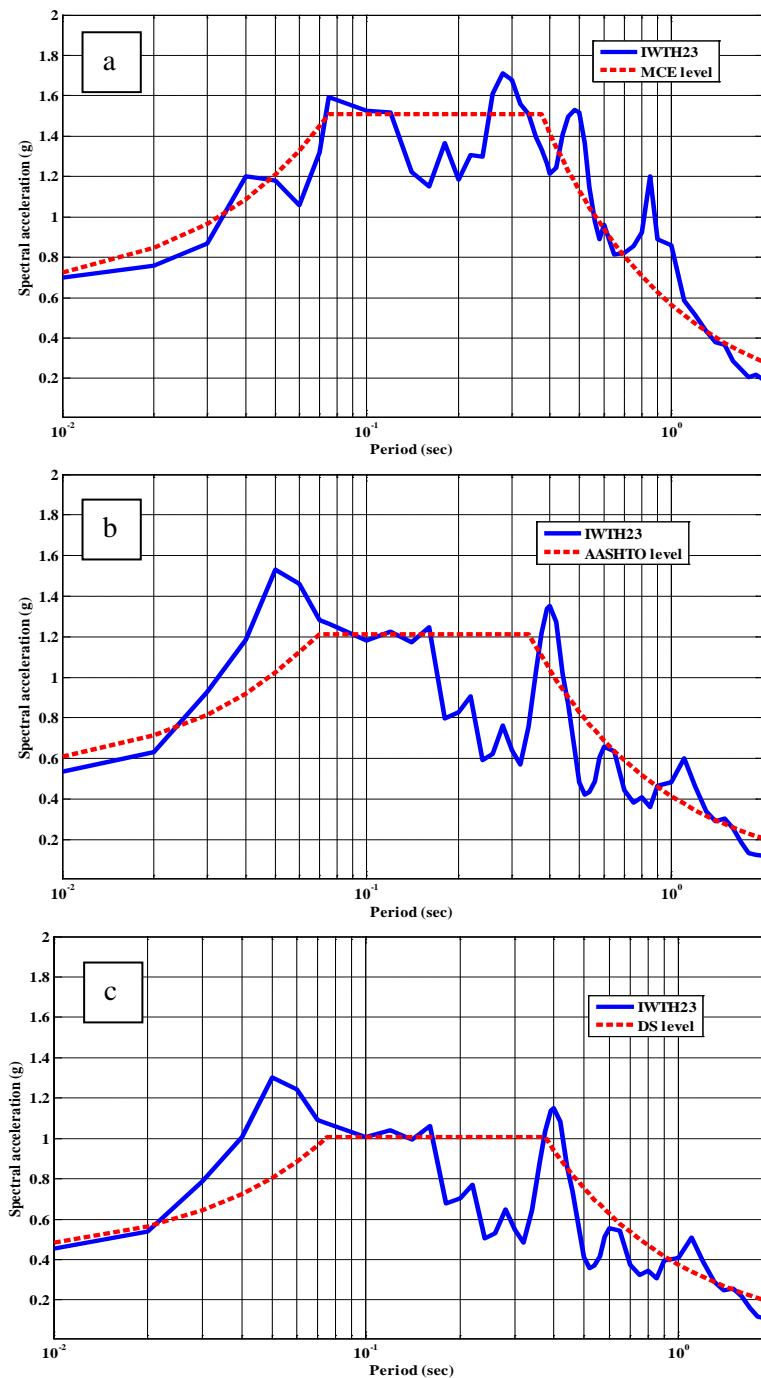


Figure 3.7 Comparison of the RS of IWTH23 ground motion time histories with target bedrock RS for the C-OM site corresponding to (a) MCE, (b) AASHTO Design Earthquake and (c) IBC Design Earthquake levels of seismic hazard.

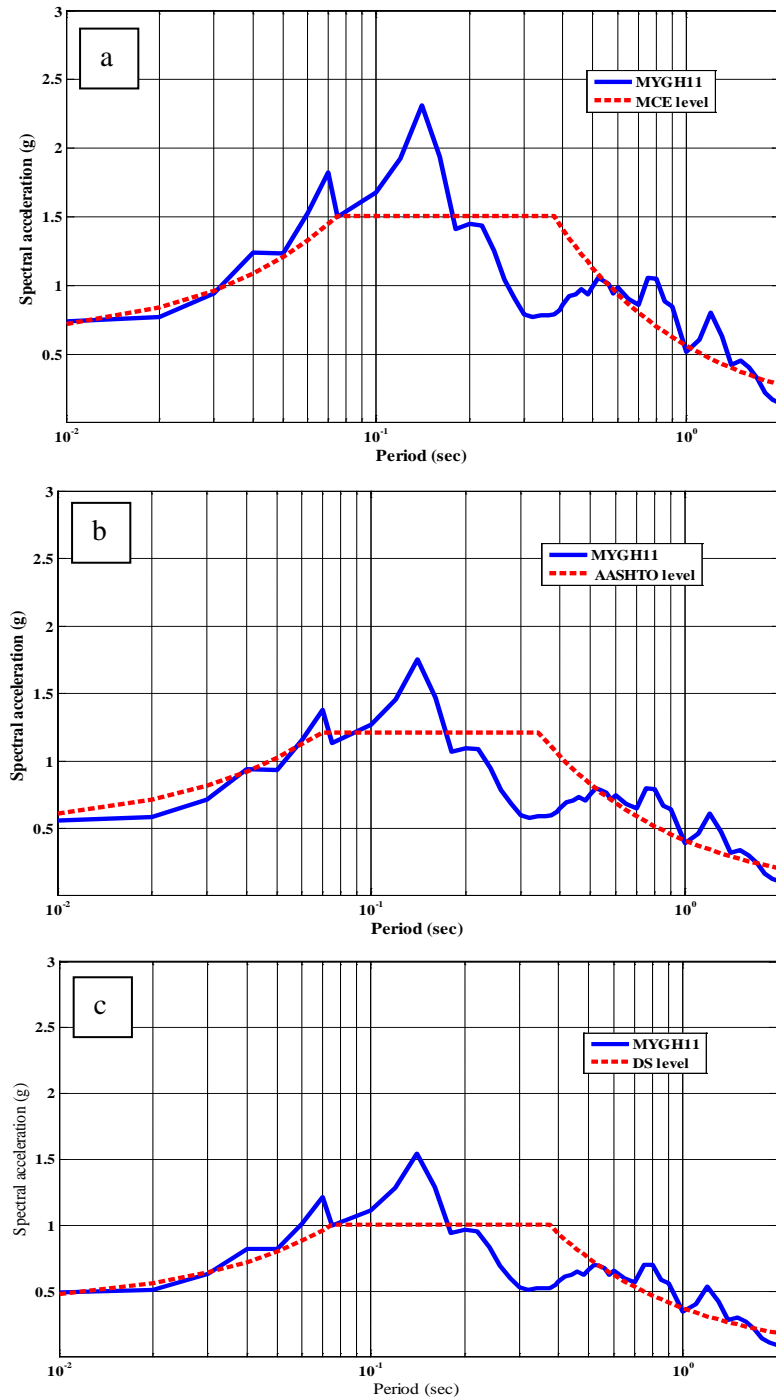


Figure 3.8 Comparison of the RS of MYGH11 ground motion time histories with target bedrock RS for the C-OM site corresponding to (a) MCE, (b) AASHTO Design Earthquake and (c) IBC Design Earthquake levels of seismic hazard.

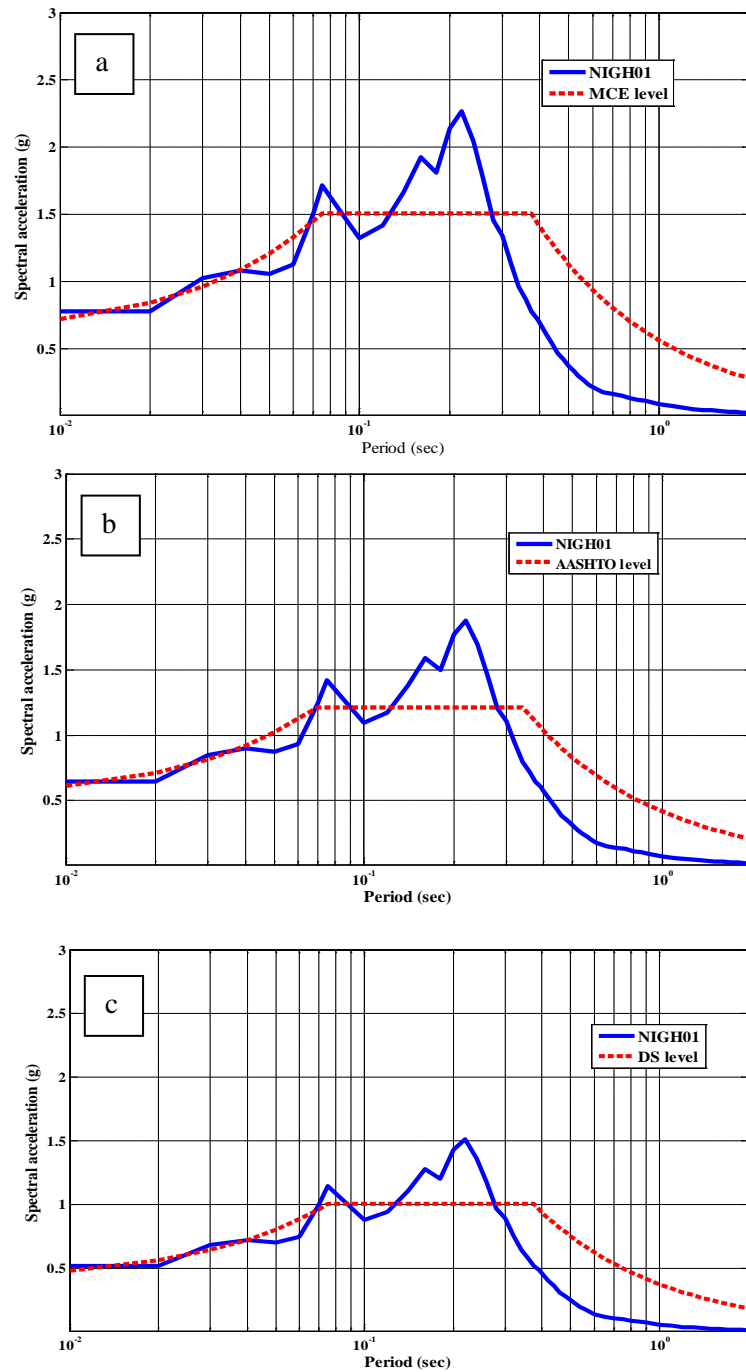


Figure 3.9 Comparison of the RS of NIGH01 ground motion time histories with target bedrock RS for the C-OM site corresponding to (a) MCE, (b) AASHTO Design Earthquake and (c) IBC Design Earthquake levels of seismic hazard.

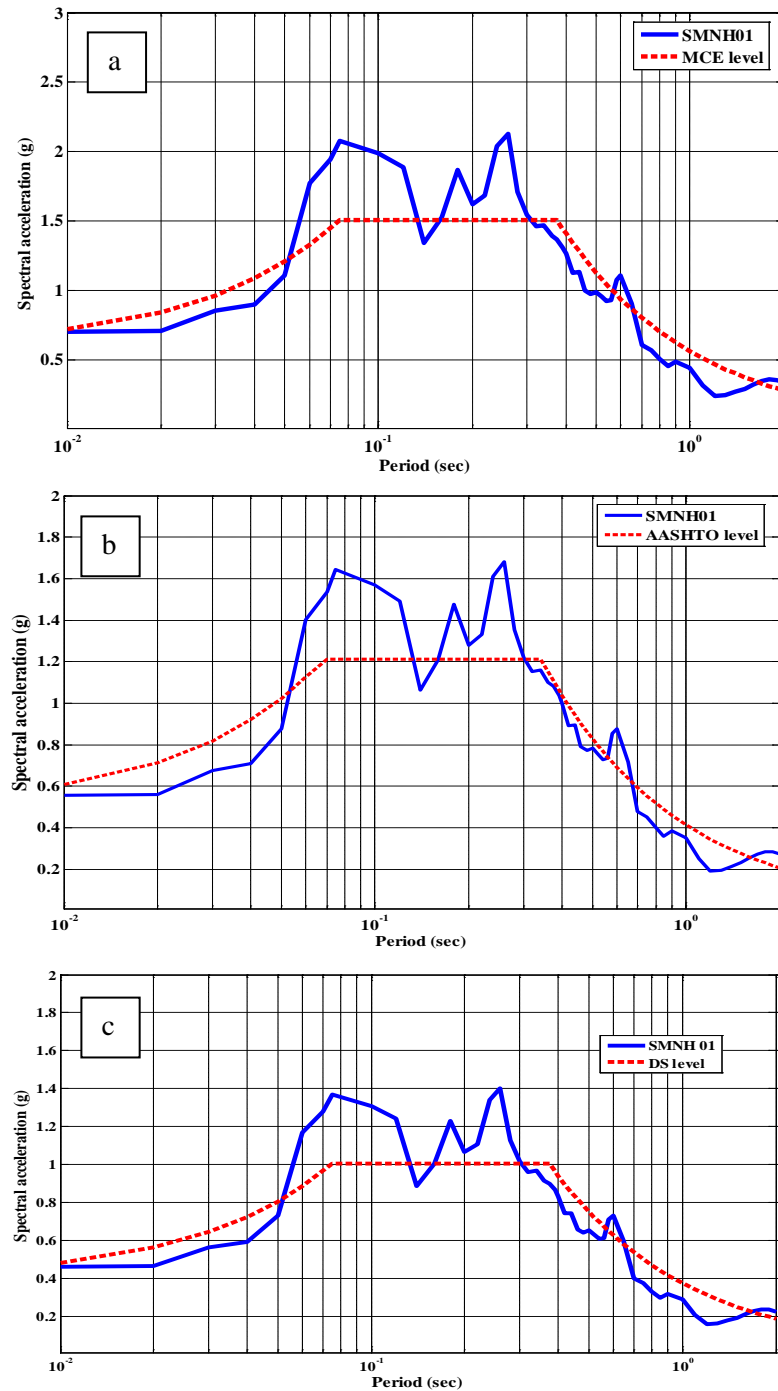


Figure 3.10 Comparison of the RS of SMNH01 ground motion time histories with target bedrock RS for the C-OM site corresponding to (a) MCE, (b) AASHTO Design Earthquake and (c) IBC Design Earthquake levels of seismic hazard.

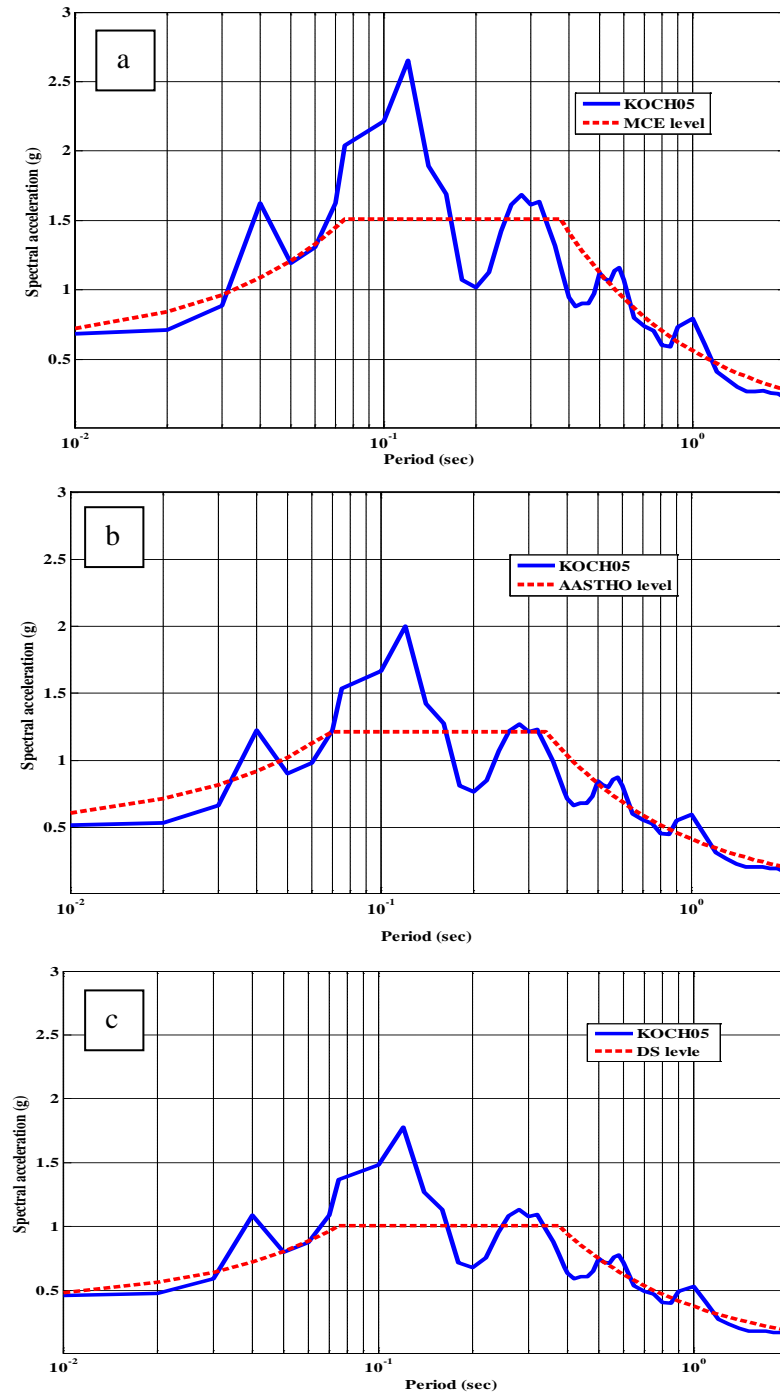


Figure 3.11 Comparison of the RS of KOCH05 ground motion time histories with target bedrock RS for the C-OM site corresponding to (a) MCE, (b) AASHTO Design Earthquake and (c) IBC Design Earthquake levels of seismic hazard.

### 3.6 The Soil Profile with Seasonally Frozen Soil

Combellick (1999) has studied the geologic structures in central and east Anchorage. Figure 3.12 shows the general values of shear wave velocity of different geologic units vs. depth. Based on this information and the geotechnical data reported for the C-OM site (Golder Associates Inc., 2003), a simplified soil profile was constructed, as shown in Figure 3.13. Two important soil properties are identified for different soils: shear wave velocity ( $V_s$ ) and mass density ( $\rho$ ).  $V_s$  for seasonally frozen soils was estimated based on in-situ measurement (Seismic CPT) of frozen soils in northern Quebec of Canada (LeBlanc et al., 2004).

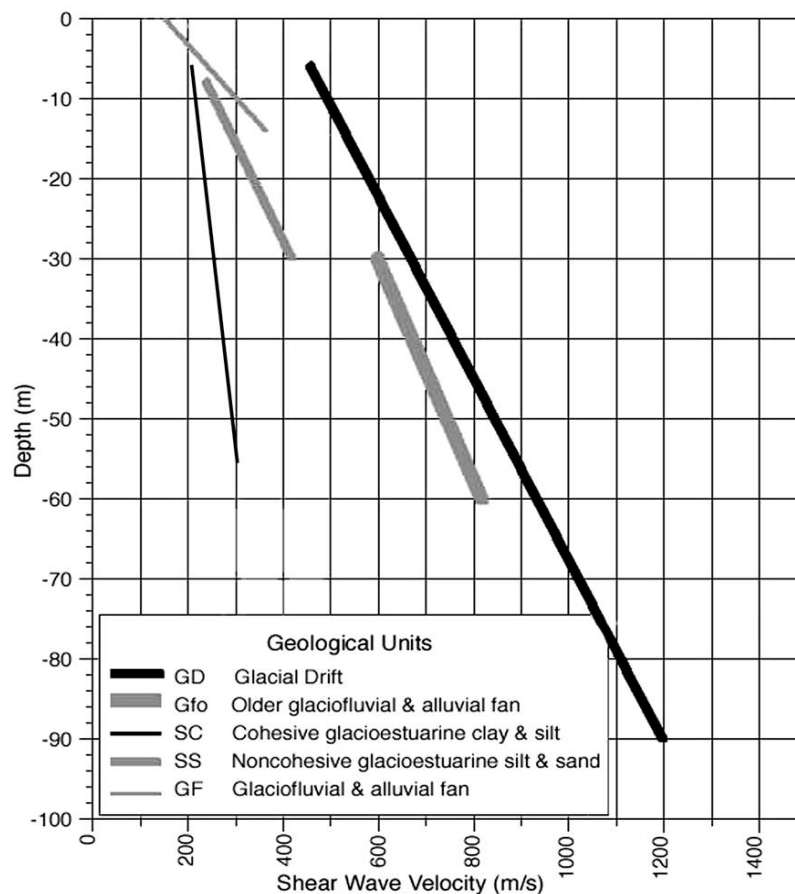


Figure 3.12 Shear wave velocities of different sedimentary units in Anchorage, Alaska (Combellick, 1999)

The maximum frost depth in Anchorage is around 9 ft (2.7 m). However, a frost depth up to 30 ft (9 m) was assumed (as shown in Figure 3.13) in order to assess the sensitivity of site response to frost depth. LeBlanc et al. (2004) showed that  $V_s$  of naturally frozen soils ranges from 3,000 to 5,000 ft/s (900 to 1500 m/s). In this study,  $V_s$  of the middle frozen soil was set to 1,500 m/s. Meanwhile, it is well known that  $V_s$  varies with ice/water

content, temperature, soil type, confining pressure and other factors. For these reasons, two low velocity transition layers with a thickness of 5 ft (1.5 m) were assigned on the top and bottom of the frozen soil layer to account for the surface condition and the partially frozen layer between frozen and unfrozen soils. The  $V_s$  of the transition layers was taken as a half of that for fully frozen soil, i.e. 2,500 ft/s (750 m/s). These transition layers also avoid the abrupt shear wave velocity changes across the layer boundary, which could cause numerical problems for 1-D equivalent linear analysis. It is noted in Figure 3.13 that the Clay with Sand layer represents BCF commonly found in the Anchorage basin.

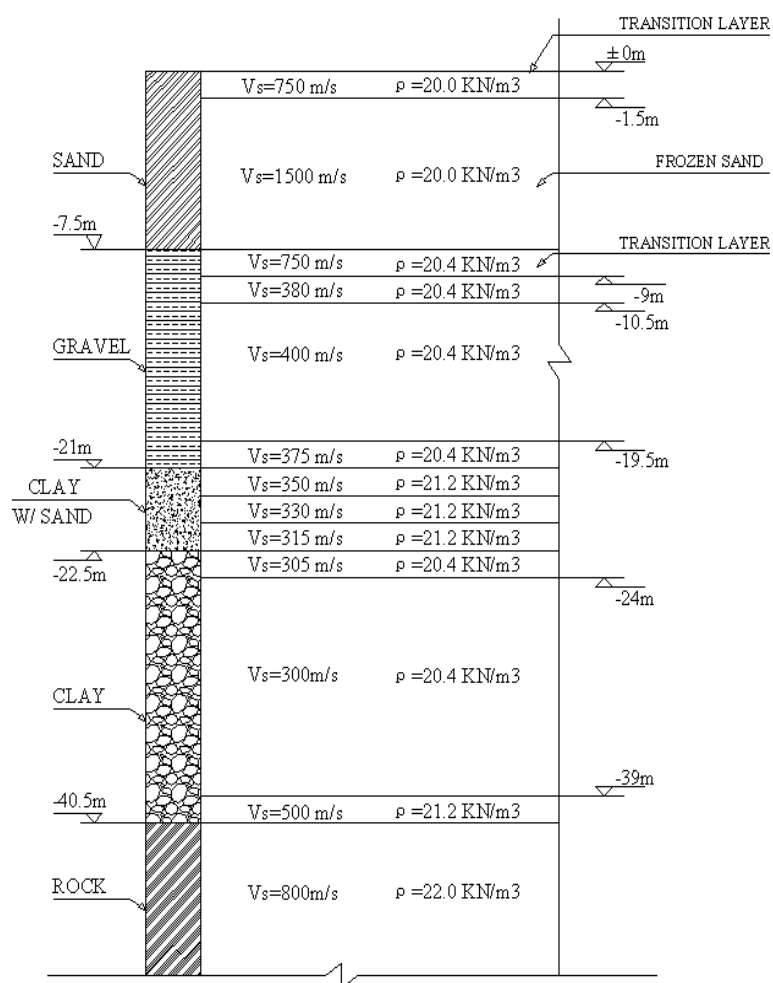


Figure 3.13 A soil profile for the C-OM site

### 3.7 Analyses Results

The five scaled earthquake ground motion time histories were used as the input to the soil profile to conduct site response analysis by using ProShake. The results obtained for site response analyses at three levels of seismic hazard including example acceleration time histories, peak shear strain distribution with depth, RS of surface motions and transfer functions of the soil profile are described in this section.

#### 3.7.1 Acceleration Time Histories and Peak Shear Strain

Figure 3.14 shows one example of the input ground motion and computed surface motion. This surface motion was generated by propagating scaled NIGH01 time histories through the soil profile with 5 ft (1.5 m) thick seasonally frozen soil.

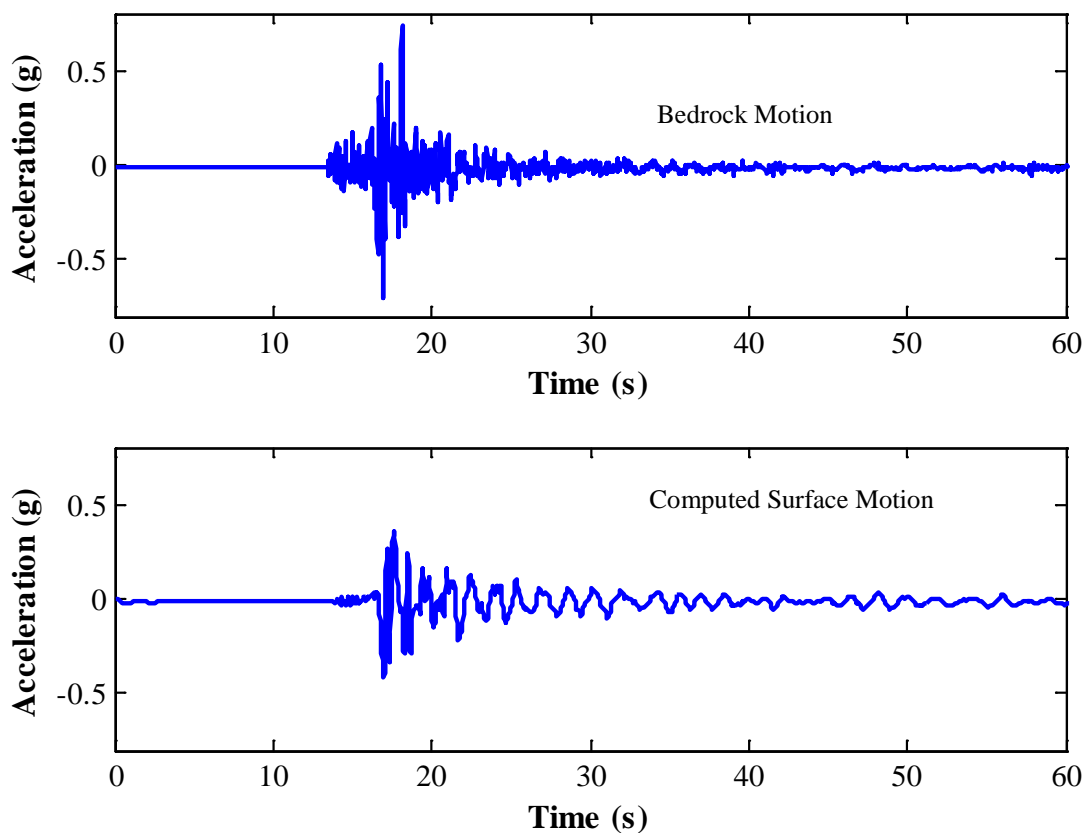


Figure 3.14 Input motion NIGH01 and computed surface motion for the C-OM site

As discussed in Section 2.2.3, the shear strains induced in soil layers should be small in order for equivalent linear analysis to provide reasonable estimate of ground response. The peak shear strains developed within the soil layers for each of the five input motions scaled to MCE level hazard are plotted in Figure 3.15. It can be seen from Figure 3.15 that the maximum peak shear strain is 0.8%, which is at the acceptable level (peak shear

strain less than 1-2%) in order for equivalent analysis to provide a reasonable estimate of ground response.

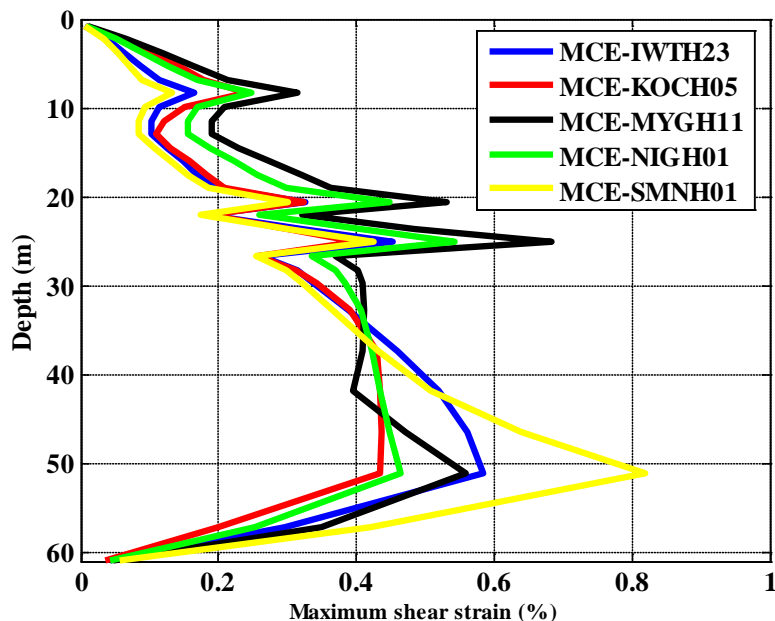


Figure 3.15 Plot of peak shear strain vs. depth for five selected input motions scaled to MCE level hazard.

### 3.7.2 RS of Computed Surface Motions

The 5% damped RS of surface motions were calculated for the five selected input motions and categorized according to different levels of hazard for clarity of presentation.

#### 1) IBC Design Earthquake level hazard

Figures 3.16, 3.17 and 3.18 show the RS of computed surface motions for soil profiles with 0, 5, and 10 ft of seasonally frozen soil, respectively. In each plot the dashed lines are the 5% damped RS of surface motions obtained from the five hazard consistency input motions, and the solid line is the average RS of the five computed surface motion RS. The geometric average RS was computed by using the following equation:

$$aveRS(T) = \sqrt[n]{\prod_{i=1}^n RS_i(T)} \quad (3.1)$$

where  $aveRS(T)$  refers to the average response spectral value at Period T calculated from n response spectra, and  $RS_i(T)$  refers to one of n response spectral values at Period T. Figure 3.19 compares the average RS at different frost depths.

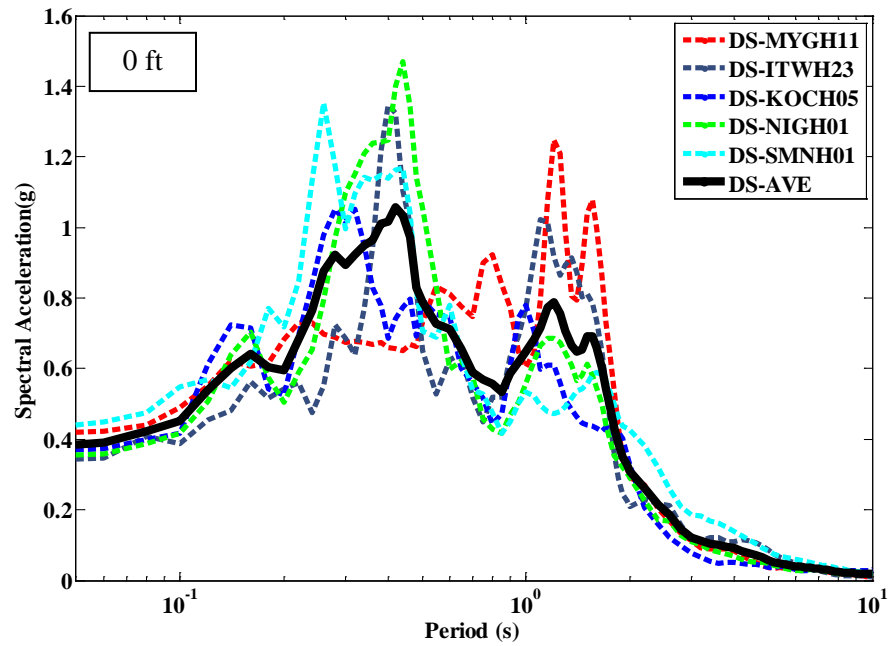


Figure 3.16 Computed surface motions RS and their average RS for the soil profile without seasonally frozen soil (IBC Design Earthquake level hazard)

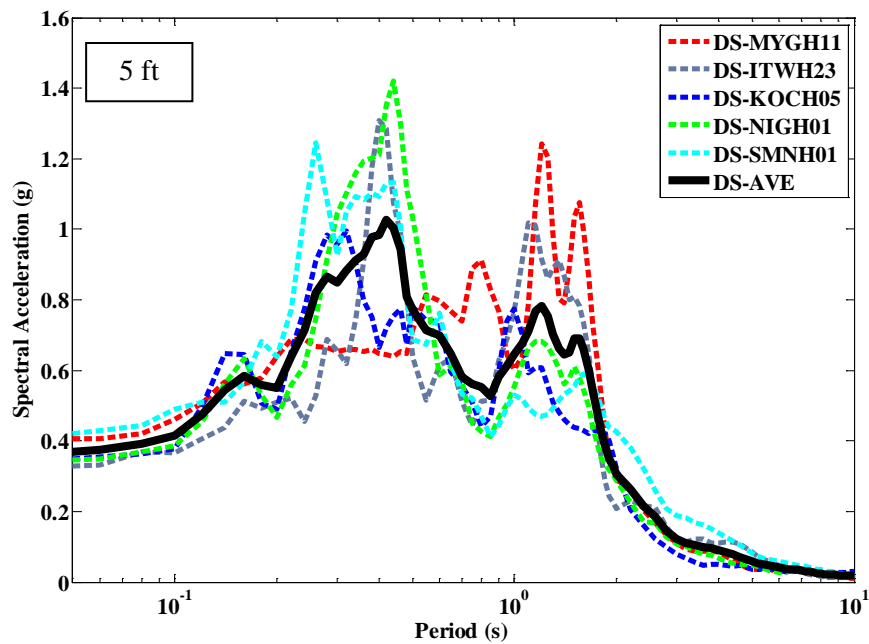


Figure 3.17 Computed surface motions RS and their average RS for the soil profile with 5 ft of seasonally frozen soil (IBC Design Earthquake level hazard)

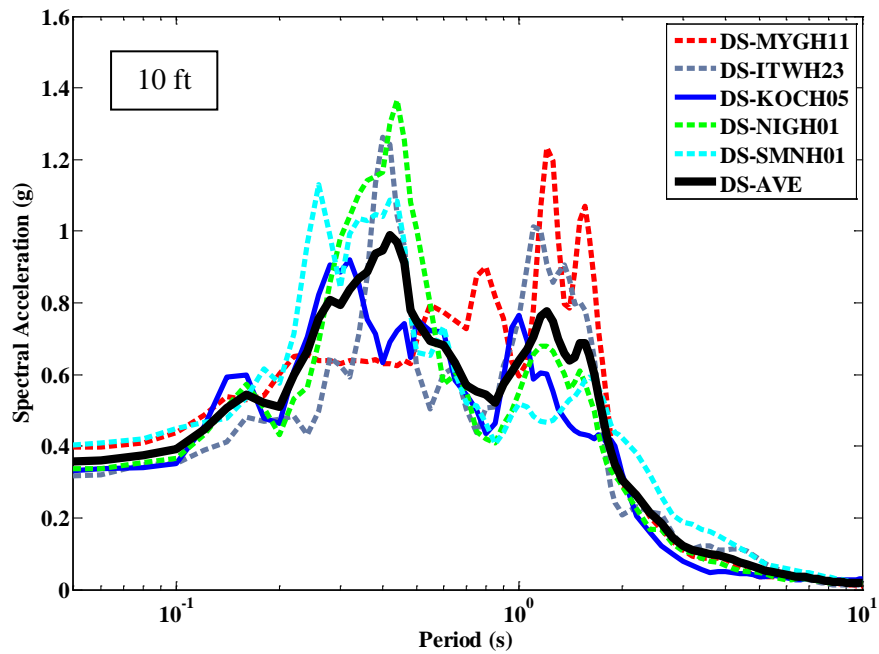


Figure 3.18 Computed surface motions RS and their average RS for the soil profile with 10 ft of seasonally frozen soil (IBC Design Earthquake level hazard)

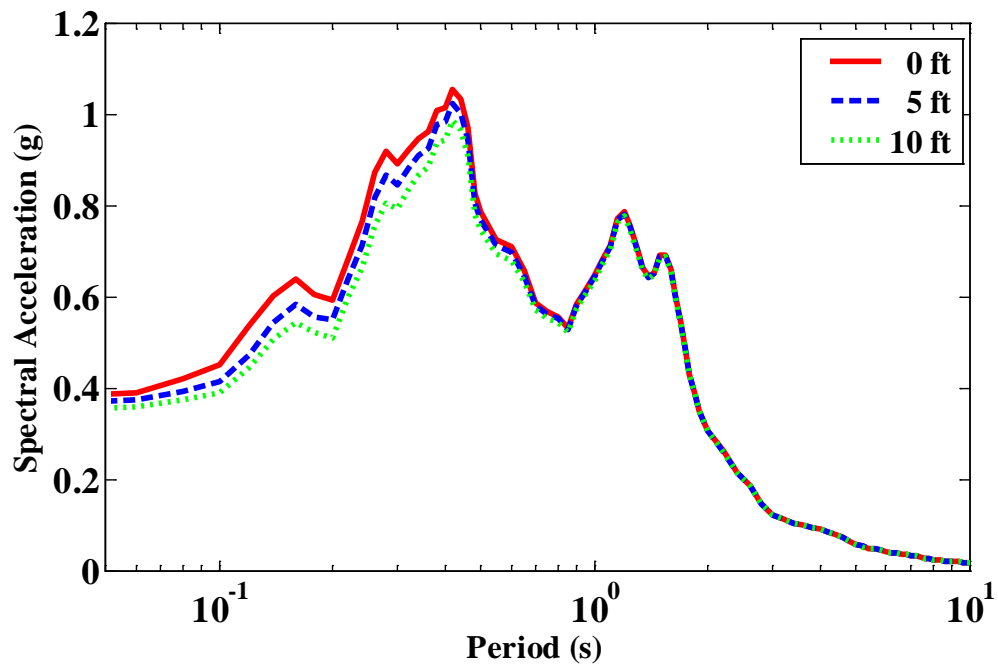


Figure 3.19 Comparison of the average RS for soil profiles with 0, 5 or 10 ft (0, 1.5 or 3 m) of seasonally frozen soil (IBC Design Earthquake level hazard)

## 2) Other Hazard Levels

The 5% damped RS of ground motions obtained from the five selected input motions scaled to AASHTO Design Earthquake and MCE levels of hazard were also calculated and their average RS were compared in Figures 3.20 and 3.21, respectively.

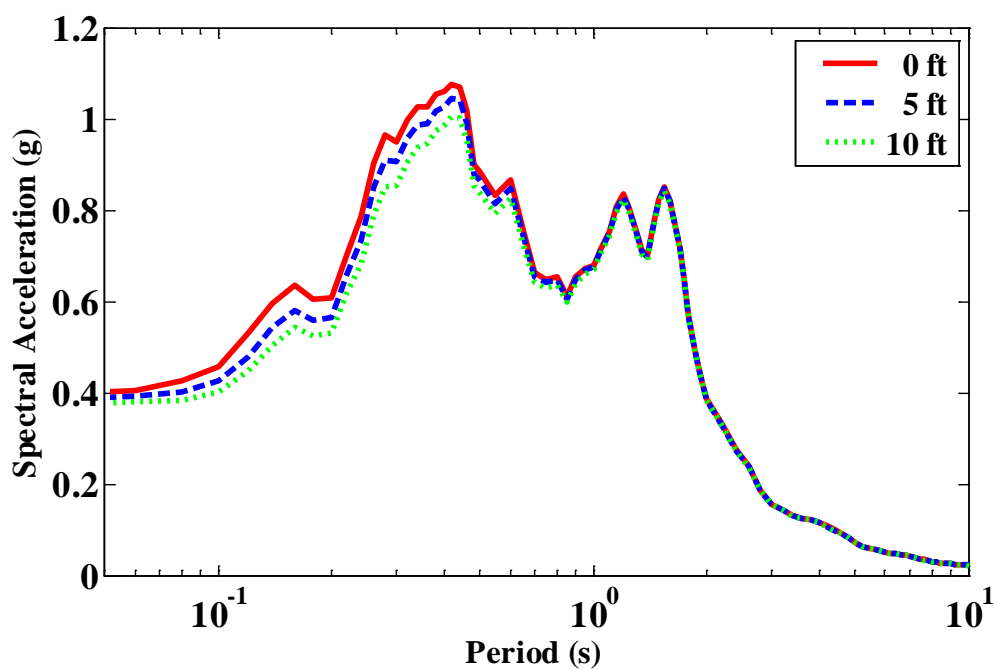


Figure 3.20 Comparison of the average RS for soil profiles with 0, 5 and 10 ft (0, 1.5 and 3 m) of seasonally frozen soil (AASHTO Design Earthquake level hazard)

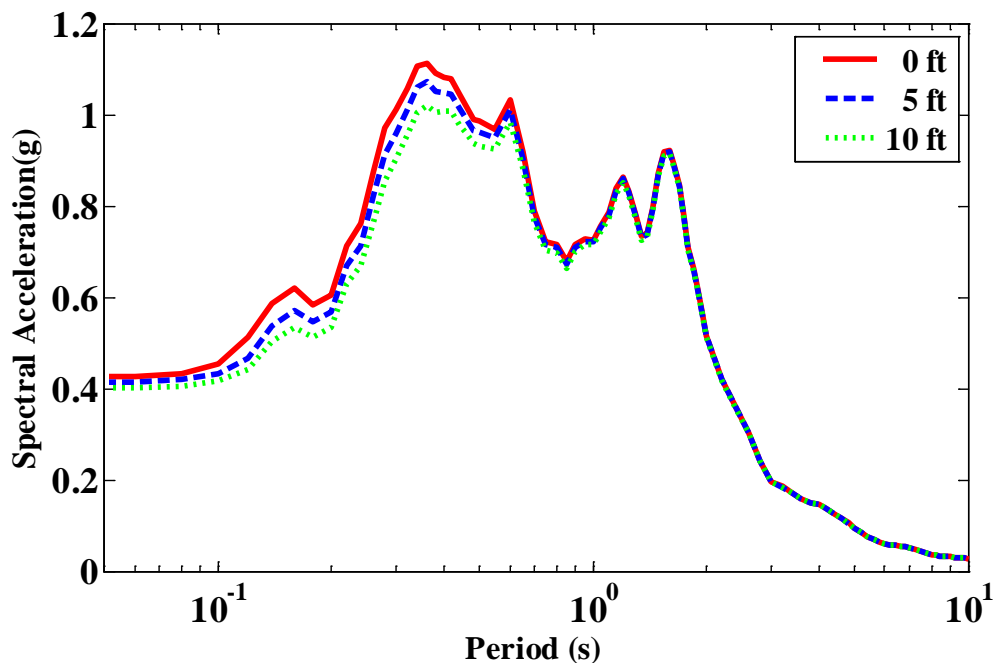


Figure 3.21 Comparison of the average RS for soil profiles with 0, 5 and 10 ft (0, 1.5 and 3 m) of seasonally frozen soil (MCE level hazard)

### 3.7.3 Transfer Function Comparison

In site response analysis, a transfer function is a function that relates the input motion to the surface motion of a soil profile. It provides a different perspective in understanding the effects of seasonally frozen soil. The transfer functions of soil profiles with different seasonally frozen soil depth were computed and examined in this section. For clarity, the results were categorized according hazard levels.

#### 1) IBC Design Earthquake level hazard

Figures 3.22, 3.23 and 3.24 show the amplitude of transfer functions for soil profiles with 0, 5 and 10 ft (0, 1.5 and 3 m) of seasonally frozen soil, respectively. The transfer functions between the surface and input motions obtained from the five input motions are shown by dashed lines. The average transfer function of these five individual transfer functions has also been computed by using the following equation (Eqn. 3.2):

$$aveTF(f) = \sqrt[n]{\prod_{i=1}^n TF_i(f)} \quad (3.2)$$

Where  $aveTF(f)$  refers to the average transfer function value for frequency  $f$ ,  $TF_i(f)$  refers to one of  $n$  transfer function values corresponding to frequency  $f$ . Figure

3.25 compares the average transfer functions of soil profiles with three different seasonally frozen soil depths.

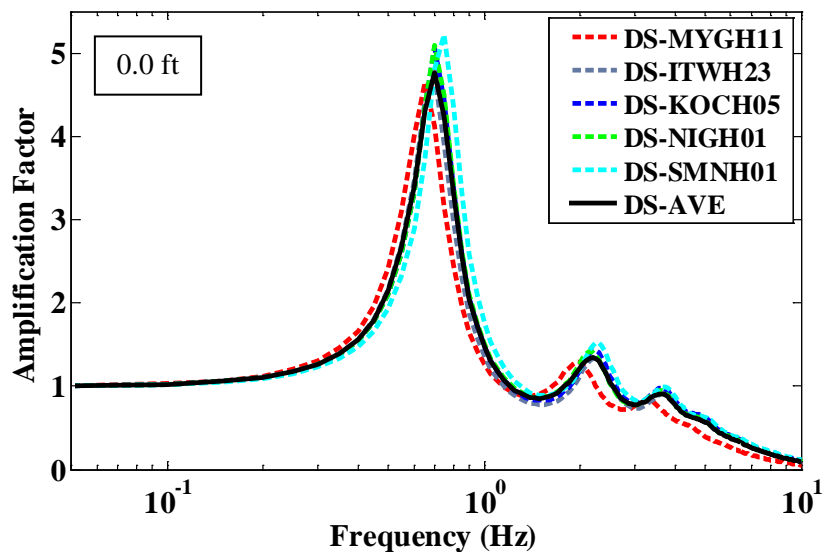


Figure 3.22 Transfer functions for the five computed surface motions and their average for the soil profile without seasonally frozen soil (IBC Design Earthquake level hazard)

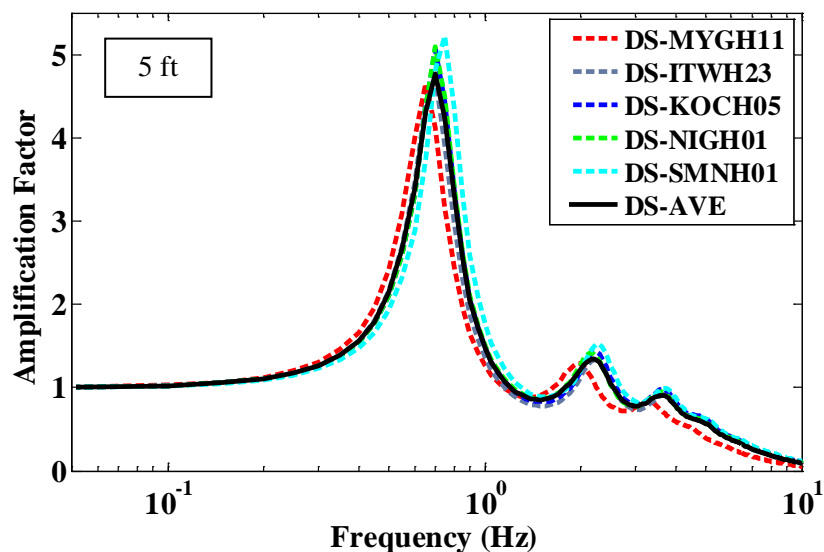


Figure 3.23 Transfer functions of the five computed surface motions and their average for the soil profile with 5 ft of seasonally frozen soil (IBC Design Earthquake level hazard)

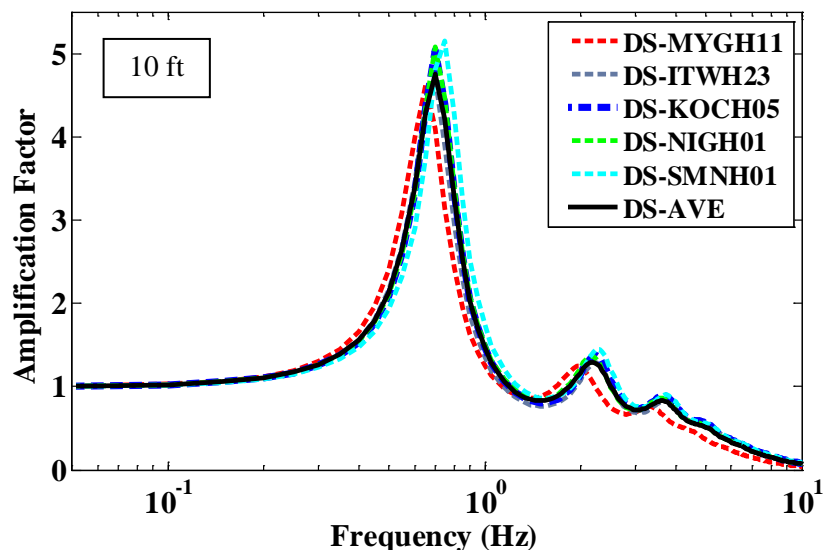


Figure 3.24 Transfer functions of the five computed surface motions and their average for the soil profile with 10 ft of seasonally frozen soil (IBC Design Earthquake level hazard)

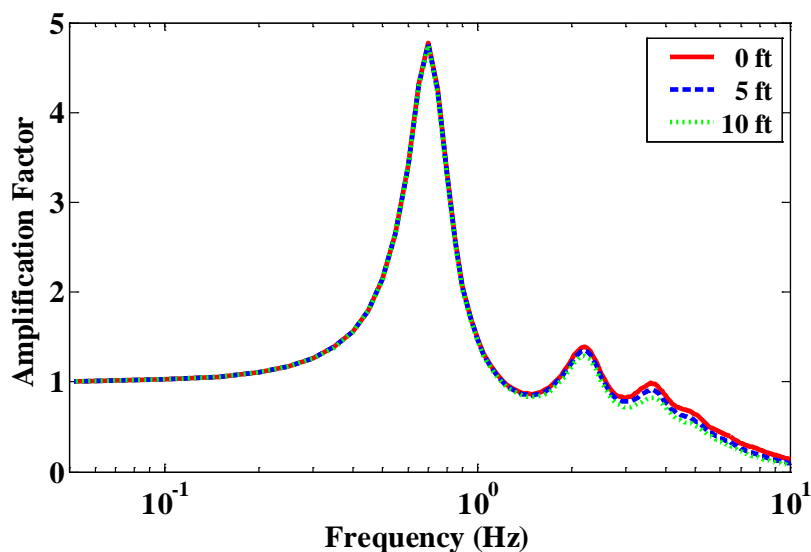


Figure 3.25 Comparison of the average transfer functions for soil profiles with 0, 5 and 10 ft (0, 1.5 and 3 m) of seasonally frozen soil (IBC Design Earthquake level hazard)

## 2) Other levels of hazard

The transfer functions for the five selected input motions scaled to AASHTO Design Earthquake level (7.5% PE in 75 years) and MCE level hazard (2% PE in 50 years) were also computed for soils profiles with 0, 5 and 10 ft (0, 1.5 and 3 m) of seasonally frozen

soil, and their average transfer functions were shown in Figures 3.26 and 3.27, respectively.

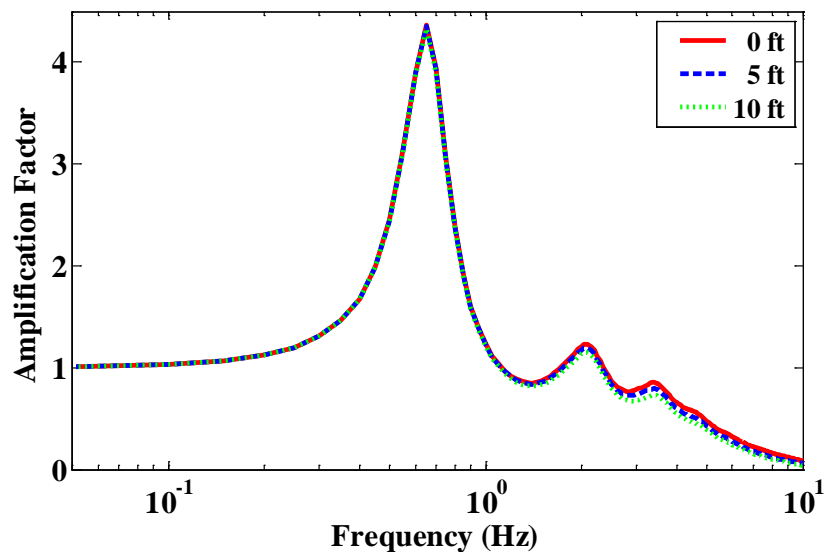


Figure 3.26 Comparison of average transfer functions with 0, 5 and 10 ft (0, 1.5 and 3 m) seasonally frozen soil corresponding to AASHTO Design Earthquake level hazard (7.5% PE in 75 years)

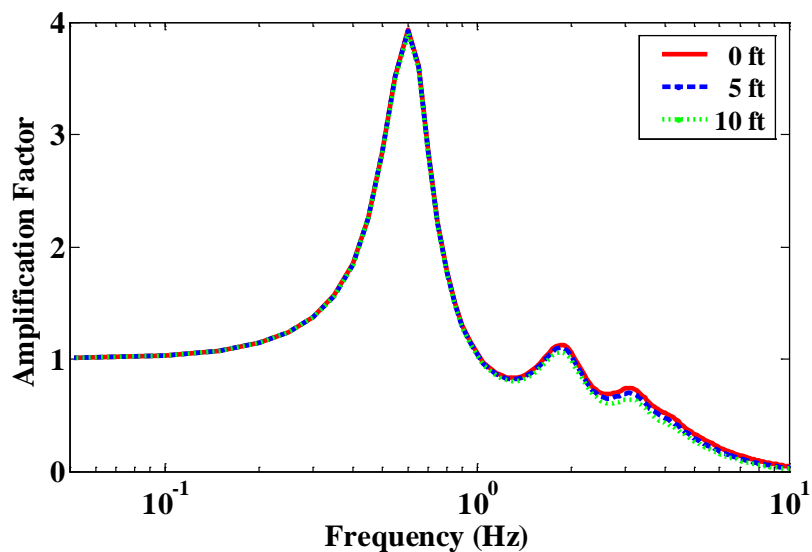


Figure 3.27 Comparison of the average transfer functions for soil profiles with 0, 5 and 10 ft (0, 1.5 and 3 m) of seasonally frozen soil (MCE level hazard)

#### 3.7.4 Effects of Seasonally Frozen Soil Depth on Spectral Acceleration

The variation of peak ground accelerations (PGA),  $S_s$  and  $S_1$  with depth of seasonally frozen soil have been studied for three levels of hazard. The results are shown in Figures 3.28, 3.29 and 3.30, respectively. In this study, the depth of seasonally frozen soil was varied from 0 to 30 ft (0 to 9 m) in order to observe the effects of seasonally frozen soil on site response characteristics. Instead of the average response spectra, the PGA,  $S_s$  and  $S_1$  from the five input time histories have been shown in these figures.

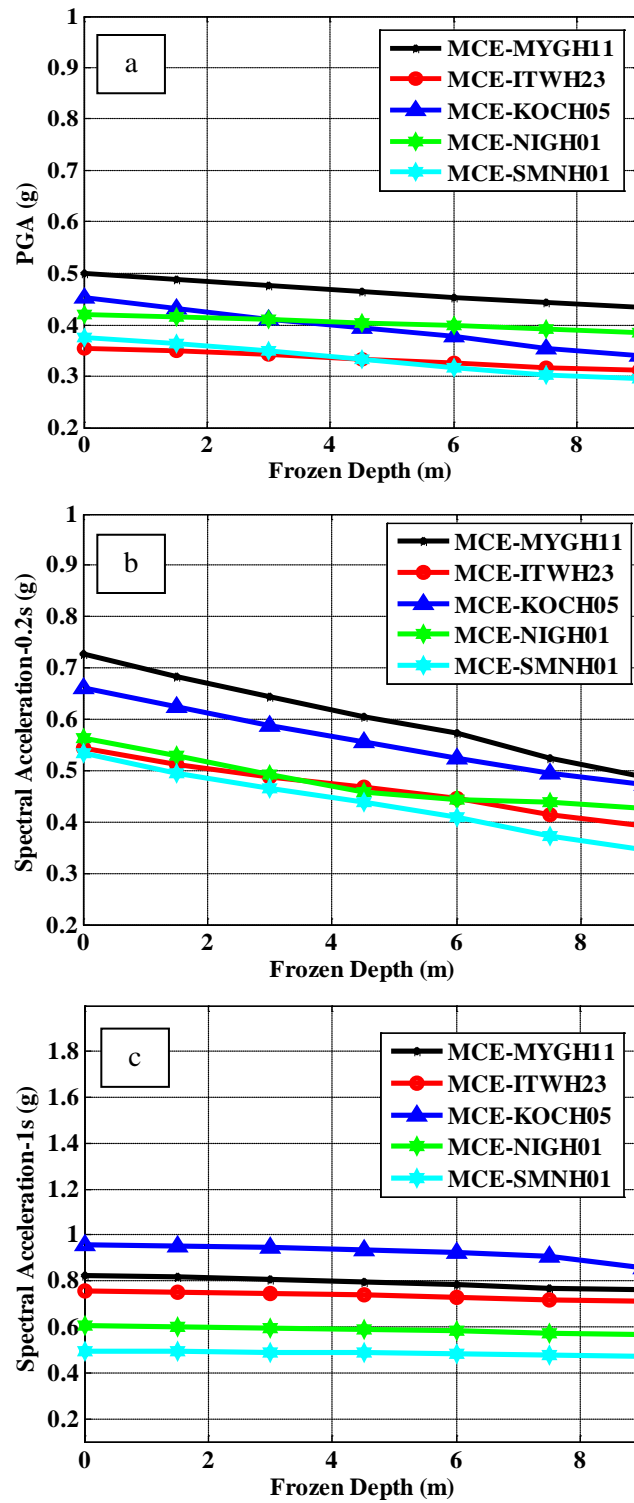


Figure 3.28 Variation of (a) PGA, (b)  $S_s$  and (c)  $S_1$  with seasonally frozen soil depth for MCE level hazard (2% PE in 50 years)

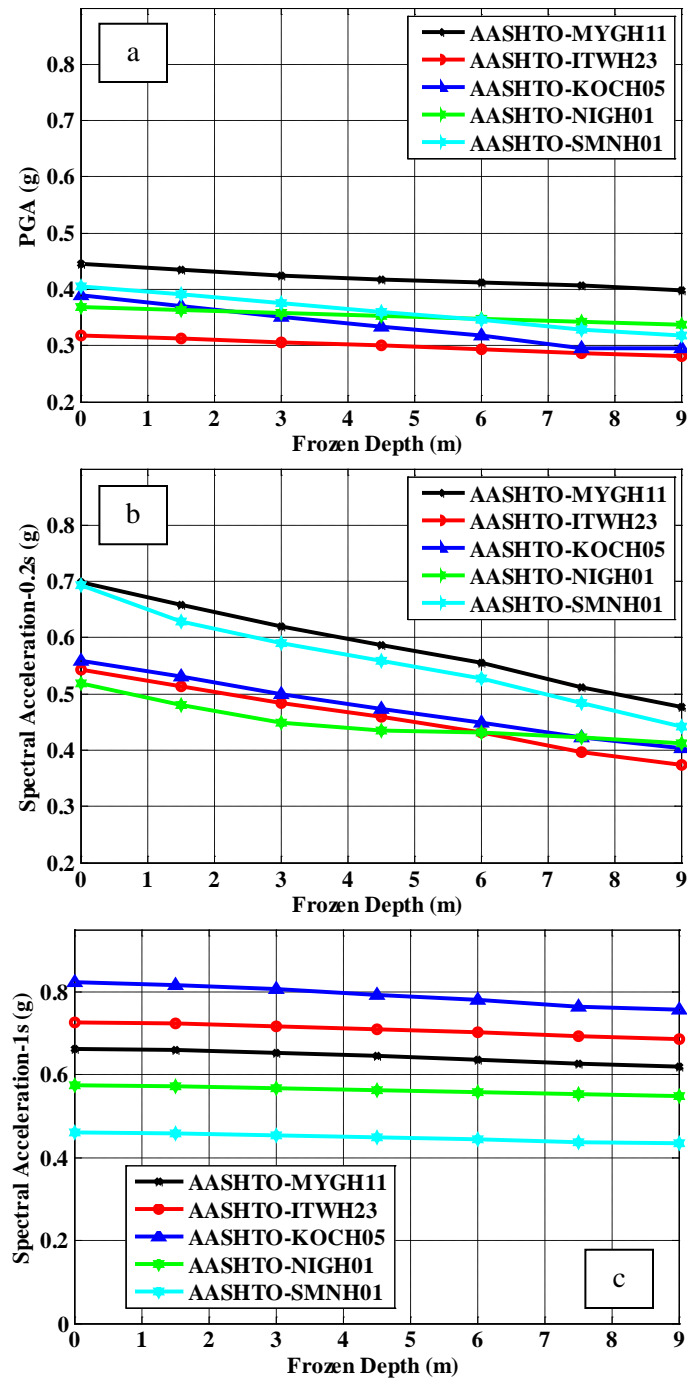


Figure 3.29 Variation of (a) PGA, (b)  $S_s$  and (c)  $S_1$  with seasonally frozen soil depth for AASHTO Design Earthquake level hazard (7.5% PE in 75 years)

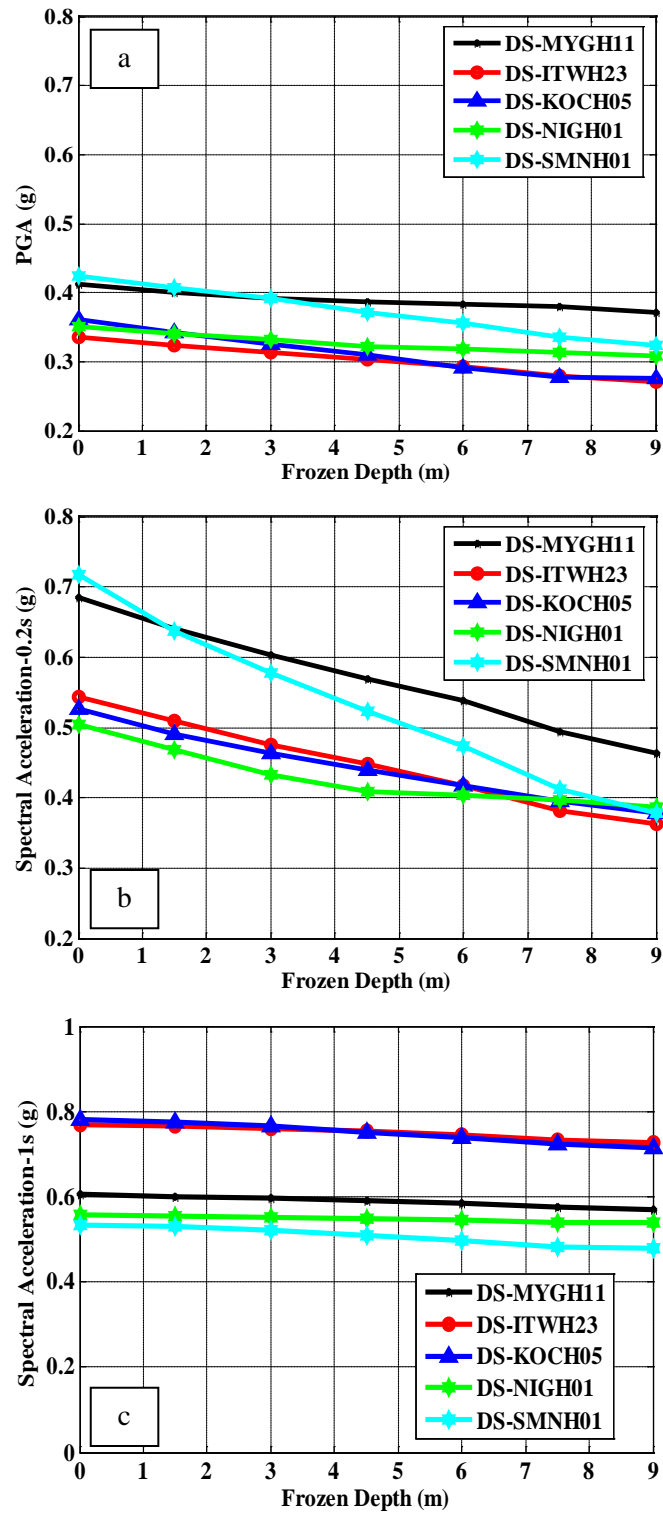


Figure 3.30 Variation of (a) PGA, (b)  $S_s$  and (c)  $S_1$  with seasonally frozen soil depth for IBC Design Earthquake level hazard

### 3.8 Sensitivity of Results on Shear Wave Velocity of Frozen Soil

Shear wave velocity of frozen soil may vary in a certain range depending on soil temperature, ice/water content, soil type, etc. LeBlanc et al. (2004) showed that  $V_s$  of naturally frozen soils ranges from 3,000 to 5,000 ft/s (900 to 1500 m/s). In this section, sensitivity of the results to  $V_s$  has been studied by carrying out a parametric study.  $V_s$  has been varied from 1,600 to 5,000 ft/sec (500 to 1,500 m/s). The variation of site response parameters including PGA,  $S_s$  and  $S_1$  with seasonally frozen soil depth for two input motions (i.e. MYGH01 and NIGH11) scaled to MCE level hazard has been shown in Figures 3.31 to 3.36.

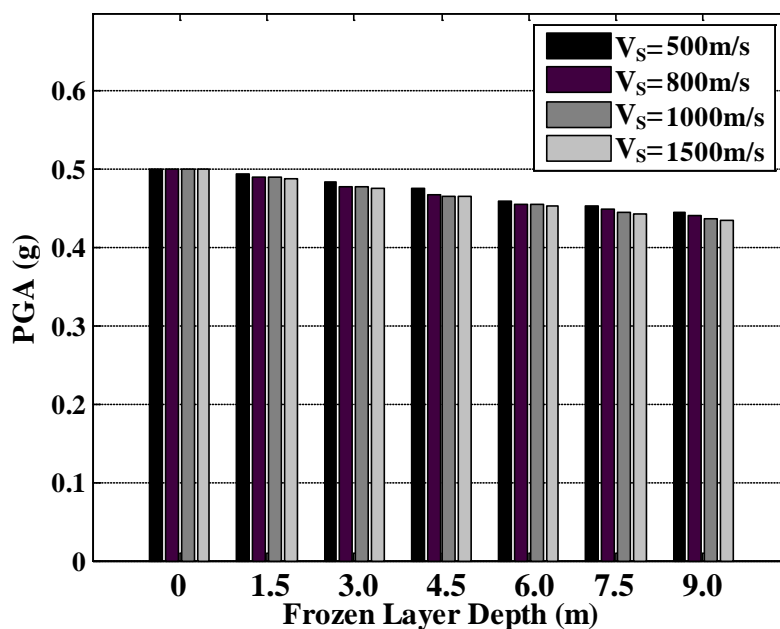


Figure 3.31 Variation of PGA with frozen soil depth and shear wave velocity  $V_s$  for input motion MYGH11

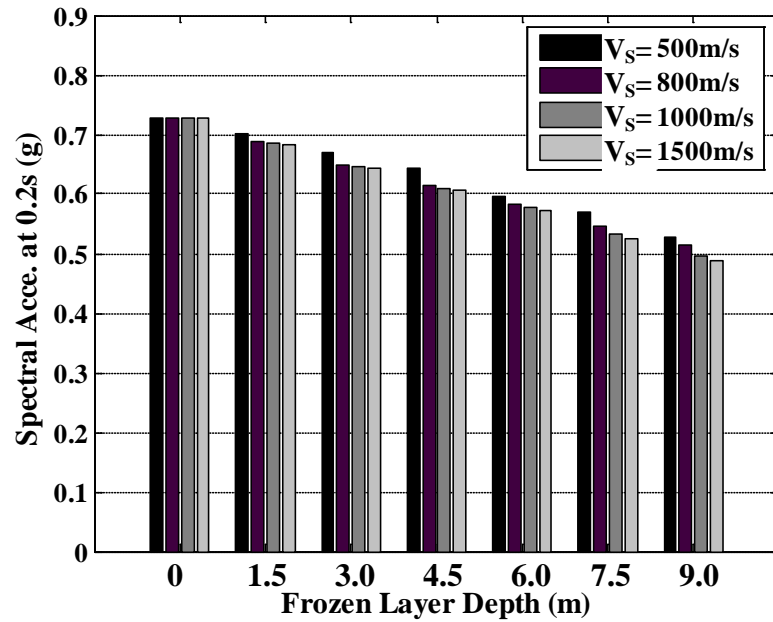


Figure 3.32 Variation of  $S_s$  with frozen soil depth and shear wave velocity  $V_s$  for input motion MYGH11

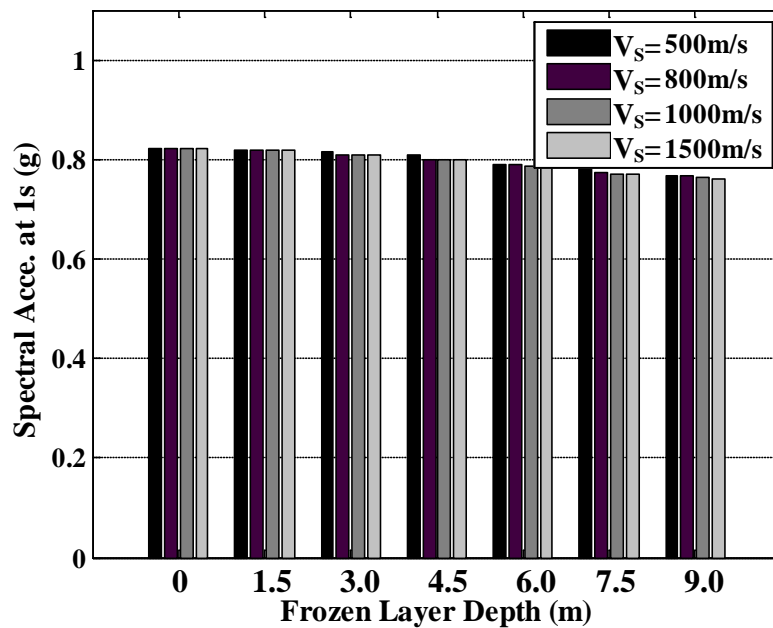


Figure 3.33 Variation of  $S_1$  with frozen soil depth and shear wave velocity  $V_s$  for input motion MYGH11

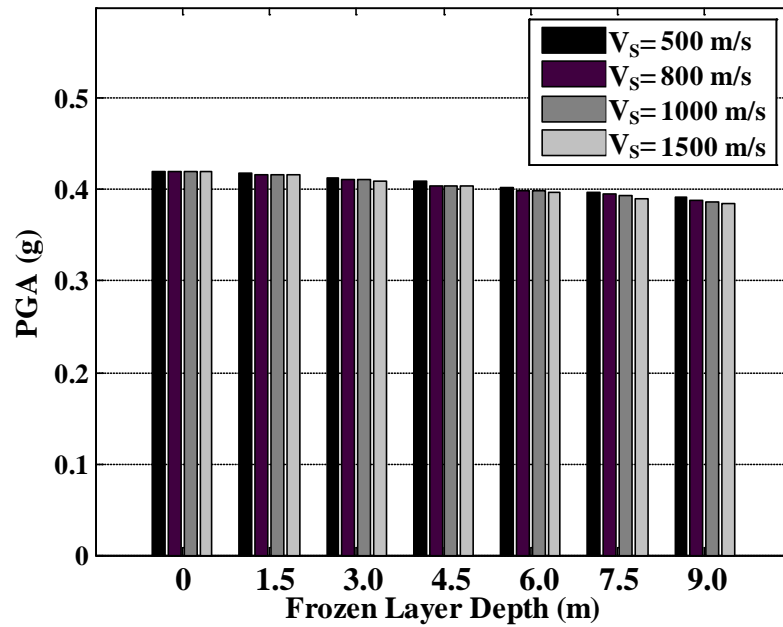


Figure 3.34 Variation of PGA with frozen soil depth and shear wave velocity  $V_s$  for input motion NIGH01

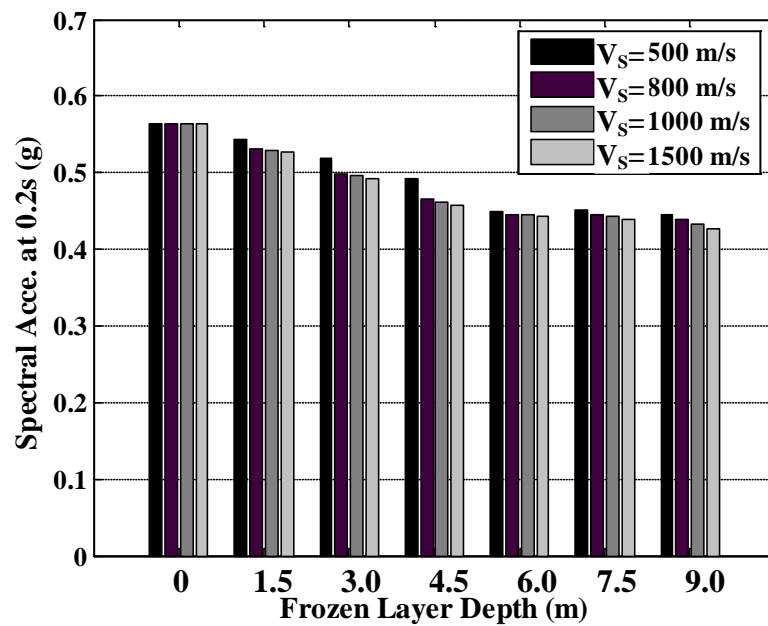


Figure 3.35 Variation of  $S_s$  with frozen soil depth and shear wave velocity  $V_s$  for input motion NIGH01

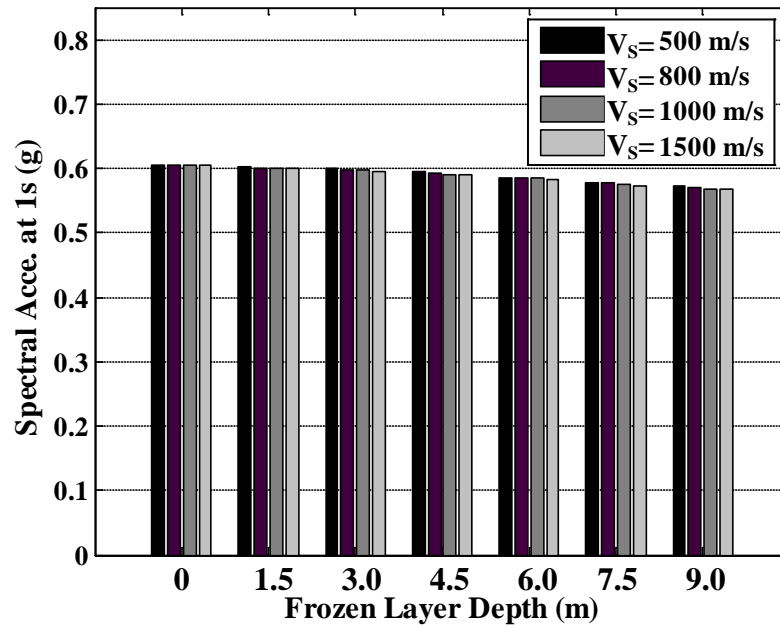


Figure 3.36 Variation of  $S_1$  with frozen soil depth and shear wave velocity  $V_s$  for input motion NIGH01

### 3.9 Discussion of Results

It is seen from Figures 3.19, 3.20 and 3.21 that seasonally frozen ground has noticeable impact on the average spectral acceleration values for periods shorter than 1.0 sec for all three hazard levels. As the thickness of seasonally frozen soil increases, the average spectral acceleration decreases.

From Figures 3.25, 3.26 and 3.27, it is found that seasonally frozen soils have clear impact on the high frequency components (higher than 1 Hz) of transfer functions. With the increase in seasonally frozen soil depth, the transfer function values decrease. This observation is consistent with that made in regard to the RS of the surface motions.

From Figures 3.28, 3.29 and 3.30, it is observed that while PGA,  $S_s$  and  $S_1$  all decrease with the increase in seasonally frozen soil depth,  $S_s$  are more sensitive to the change in seasonally frozen soil depth.

This finding is in general consistent with the fact that a surface stiffer layer (e.g. frozen surface) will act as a low-pass filter that tends to attenuate high frequency components. It agrees with findings reported in previous studies.

From Figures 3.31-3.36, it is observed that there is a slight decrease (<10%) in the spectral values of the surface motions as  $V_s$  varies from 1,600 to 5,000 ft/s (500 to 1,500

m/s), and  $S_s$  is more sensitive to variation in  $V_s$  than PGA and  $S_1$ . This indicates that the seismic site response is not particularly sensitive to variation in the shear wave velocity of seasonally frozen soil.

These findings suggest that seasonally frozen soil reduces the ground motions to certain extent. It is therefore conservative to ignore the effects of seasonally frozen soil on seismic site response.

## **CHAPTER 4 - EFFECTS OF PERMAFROST ON THE SEISMIC SITE RESPONSE**

### **4.1 Introduction**

This chapter presents the effects of permafrost on the seismic site response. Permafrost refers to the ground that has a temperature lower than 32°F (0°C) continuously, for at least two consecutive years (Davis, 2001). The Interior Alaska is underlain by discontinuous permafrost. Fairbanks, the largest population center in the Interior Alaska, is a great candidate site for this study. It is noted that most of the permafrost in Fairbanks area and elsewhere in the Interior Alaska are “warm” permafrost, implying that its temperature is at most a few degrees below freezing point.

The methodology and procedures described in Chapter 2 were applied in the study of permafrost effects. Acceleration, velocity and displacement RS of surface ground motions simulated with site response analyses have been computed. Parametric studies have been conducted to assess the sensitivity of the results to the uncertainties associated with thickness and shear wave velocity of permafrost and bedrock depth. The computed RS have been compared with the RS proposed by AASHTO specifications.

### **4.2 General Geology and Soil Profile of the Selected Permafrost Site**

#### **4.2.1 General Geology**

Based on the recommendation of AK DOT & PF, the Goldstream Creek Bridge site (Latitude 64.9119 N and Longitude -147.8318 W, referred to as GC site) at Ballaine Road in Fairbanks was selected for this study. Péwé (1982) has studied the permafrost distribution in Fairbanks area and constructed a geological section of this area, as shown in Figure 4.1. The GC site is located in the Goldstream Valley just to the north of the hills shown in this figure. In general, a discontinuous layer permafrost of approximately 50 m thick (Davis, 2001; V. Romanovsky, Personal communication, 2007) exists in Fairbanks area. It is underlain by extensive alluvial apron deposits and extends up some distance along the lower slopes of the hills. The bedrock table rises from approximately 500 ft (150 m) at the Chena River flood plain to approximately 200 ft (60 m) at areas close to the hills.

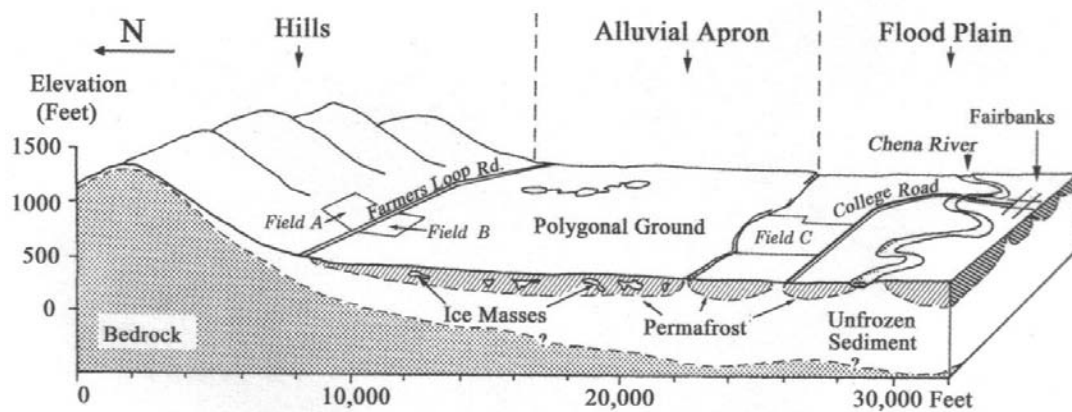


Figure 4.1 A geological cross-section of Fairbanks area (Péwé, 1982)

#### 4.2.2 Soil Profile

Considering the nature of discontinuous permafrost, sensitivity of permafrost table to surface vegetation and topography of the area, it can be concluded that it is impossible to assume a fixed permafrost table in the soil profile. Thus, a set of soil profiles with the permafrost table varying from 0 to -164 ft (-50 m) at an interval of 16 ft (5 m) has been constructed for the GC site according to the geotechnical report (Department of Highways, State of Alaska, 1974) and other geologic data (e.g. Péwé, 1982; Romanovsky, 2007), as illustrated in Figures 4.2a, b and c.

Soil profiles shown in Figures 4.2a, b and c share the same bedrock depth (-216 ft or -66 m) and permafrost bottom depth (-167 ft or -51 m). The only variable is the permafrost table which varies from 0 m (corresponding to a very shallow permafrost table case, a) to -40 m (corresponding to the case with significantly degraded permafrost table, b). A case with no permafrost or permafrost table at -164 ft (50 m) (c) has also been included for comparison. In all profiles, the permafrost layer has been assumed to overlie on a 6 m thick gravel layer at a depth of -167 ft (-51 m), which in turn overlies on a weathered rock layer with a thickness of 30 ft (9 m). Transition layers were assigned for the top portion of the permafrost layer and for the partially frozen layer between the permafrost and unfrozen gravel layer.

No in-situ  $V_s$  data are available for frozen soils at the study site or from near-by areas. Shear wave velocity  $V_s$  for unfrozen soil was evaluated based on geotechnical report, and  $V_s$  for permafrost and transition layers were set in a similar way as the seasonally frozen soil case described in Chapter 3. The width of shading areas in Figures 4.2a, b and c illustrate the magnitude of shear wave velocity.

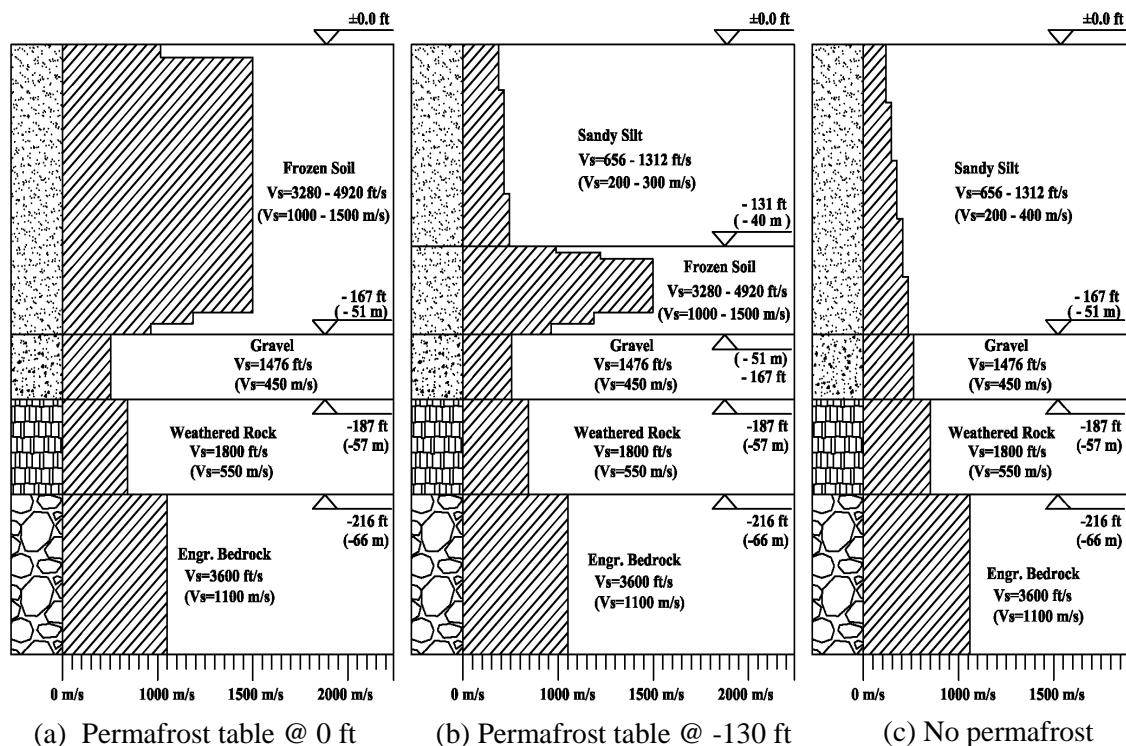


Figure 4.2 Soil profiles with varying permafrost table

### 4.3 Identification of the Seismic Hazard at the GC Site

The Probabilistic Seismic Hazard Maps for Alaska (Wesson et al. 1999) has been used to retrieve bedrock motion parameters including PGA,  $S_s$  and  $S_1$  for the construction of the bedrock motion RS. Three levels of seismic hazard, namely MCE, AASHTO Design Earthquake and IBC Design Earthquake have been considered. The values of ground motion parameters for the GC site are listed in Table. 4.1.

Table 4.1 Ground motion parameters at the GC Site

Seismic Hazard Level	PGA (g)	$S_s$ (g)	$S_1$ (g)
MCE (2% PE in 50 Years)	0.425	1.103	0.304
AASHTO Design Earthquake (7.5% PE in 75 Years)	0.289	0.646	0.201
IBC Design Earthquake (two-thirds of MCE)	0.294	0.735	0.203

#### 4.4 De-aggregation of Seismic Hazard at the GC Site

The seismic hazard was de-aggregated in terms of moment magnitude ( $M_w$ ) and hypocentral distance by the 1996 Deaggregation Application (<http://eqint.cr.usgs.gov/deaggint/1996/index.php>) prepared by U.S. Geological Survey. For example, the results of seismic hazard de-aggregation for PGA, SA at period of 0.2 and 1 sec corresponding to AASHTO Design Earthquake level hazard are shown in Figures 4.3, 4.4 and 4.5, respectively. The major sources of seismic hazard are listed in Table 4.2.

It is seen from Table 4.2 that for the GC site more than 90% of the total seismic hazard was contributed by shallow random sources of magnitude 5-7.3 with hypocentral distance less than 20 km. This clearly indicates that the shallow random sources have dominant influence on the seismic hazard of the GC site.

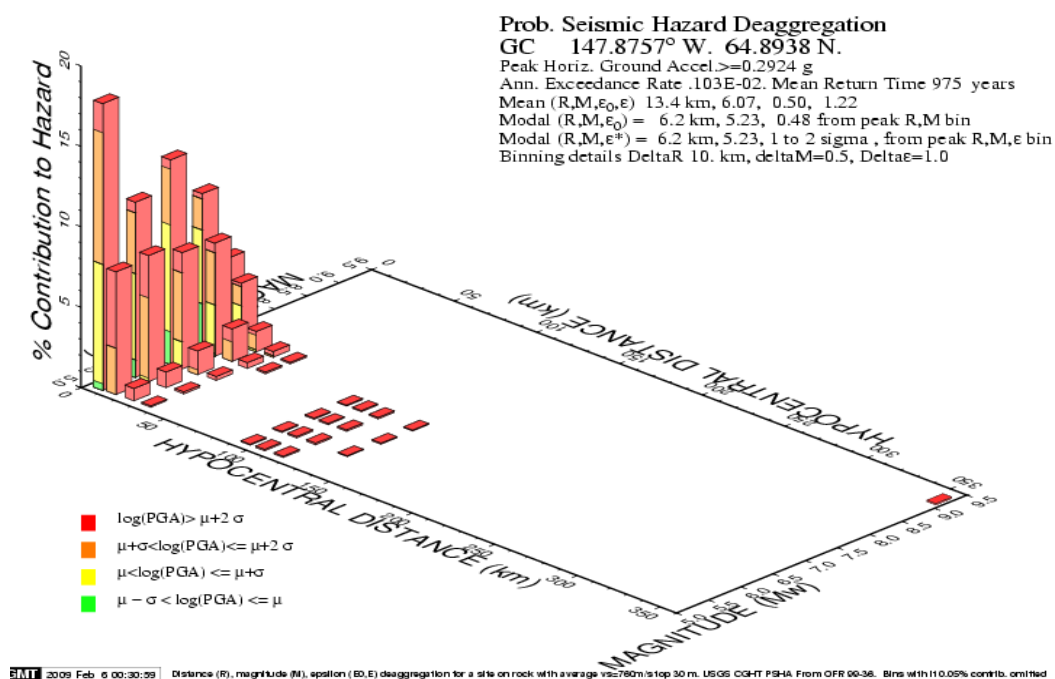


Figure 4.3 De-aggregation of the AASHTO Design Earthquake level seismic hazard (7.5% PE in 75 yrs) of the GC site for PGA

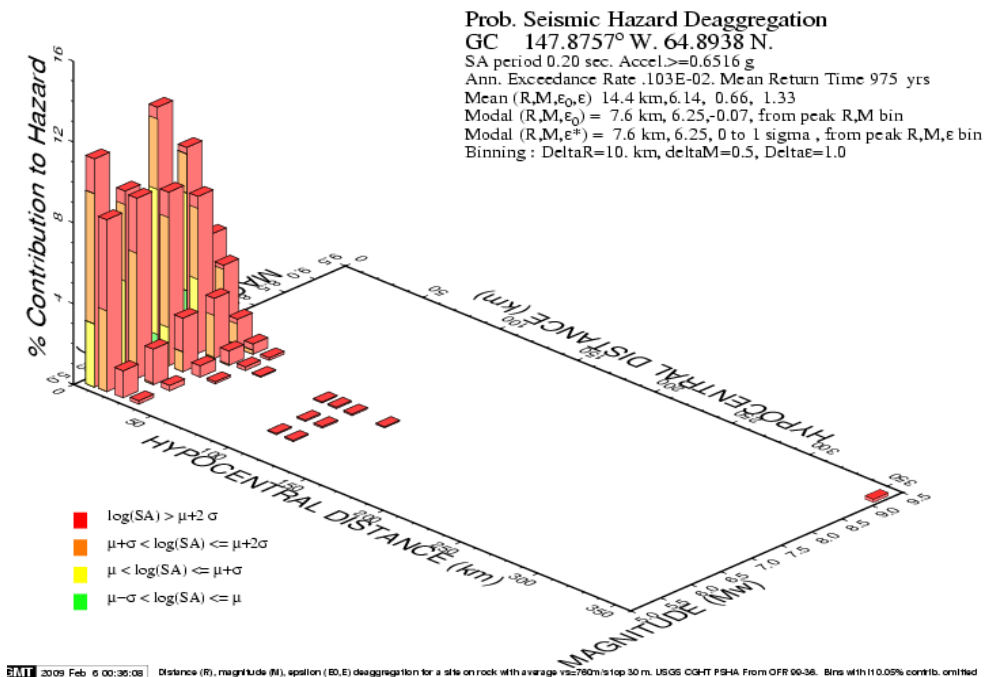


Figure 4.4 De-aggregation of the AASHTO Design Earthquake level seismic hazard (7.5% PE in 75 yrs) of the GC site for  $S_s$

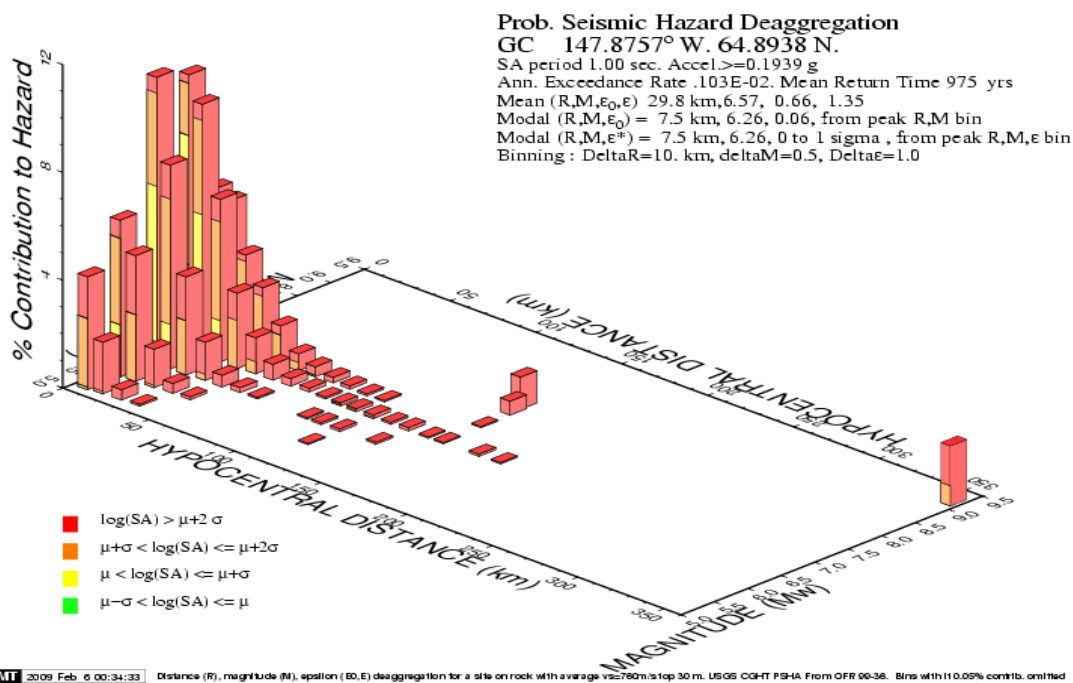


Figure 4.5 De-aggregation of the AASHTO Design Earthquake level seismic hazard (7.5% PE in 75 yrs) of the GC site for  $S_1$

Table 4.2 Summary of major sources of seismic hazard for the GC site

	<b>PGA</b>			
Source	% contr.	R (km)	$M_w$	$\varepsilon_0$
Shallow random sources $M_w$ 5-7.3	98.17	11.1	6.07	0.45
	<b>SA at 0.2 sec (<math>S_s</math>)</b>			
Source	% contr.	R (km)	$M_w$	$\varepsilon_0$
Shallow random sources $M_w$ 5-7.3	98.65	12.5	6.14	0.64
	<b>SA at 1.0 sec (<math>S_1</math>)</b>			
Source	% contr.	R (km)	$M_w$	$\varepsilon_0$
Shallow random sources $M_w$ 5-7.3	94.31	17.9	6.48	0.57

- $M_w$ : moment magnitude
- R: hypocentral distance
- $\varepsilon_0$ : standard deviation

## 4.5 Time Histories Selection and Scaling

### 4.5.1 Time Histories Selection

Ten time histories from nine individual earthquakes have been selected from the COSMOS strong motion database (<http://www.cosmos-eq.org>). The source parameters of these events and the recording site conditions of these time histories are listed in Table 4.3. The ten ground motion time histories are shown in Figures 4.6 and 4.7.

Table 4.3 Selected ground motion time histories and their source parameters

Time Histories ID (component)	Origin Time	Dep. (km)	Mag. ( $M_w$ )	PGA (gal)	Station Code	Site Condition	Epicentral Dist. (km)
Denali (N-S)	11/03/2002	4.9	7.9	98.0	UA Station Carlo	stiff soil	64.2
Hector Mine (N-S)	10/16/1999	5.0	7.1	143.0	CSMIP 22170	Shallow alluvium over granite bedrock	51.5
Hector Mine (N-S)	10/16/1999	5.0	7.1	76.6	CSMIP 12647	weathered rock	75.4
Imperial Valley (E-W)	10/15/1979	9.9	6.5	153.6	Cerro Prieto	Rock	20.0
Landers (N-S)	06/28/1992	7.0	7.3	39.4	CSMIP 12206	Weathered granite	52.4
Loma Prieta (E-W)	10/18/1998	17.5	7.0	426.6	CSMIP 47379	weathered rock	Closest dist to fault: 2.8
North Palm Springs (N-S)	07/08/1986	11.0	6.2	107.5	CSMIP 12206	weathered granite	19.5
Park Field (E-W)	09/28/2004	7.9	6.0	178.2	CSMIP 36431	soil sand stone	Closest dist to fault: 0.5
Petrolia (N-S)	08/17/1991	10.0	6.0	128.8	CSMIP 89005	Cretaceous Rock	15.4
SMNH01 (N-S)	10/16/2000	11.0	7.3	185.0	SMNH01	Borehole	8

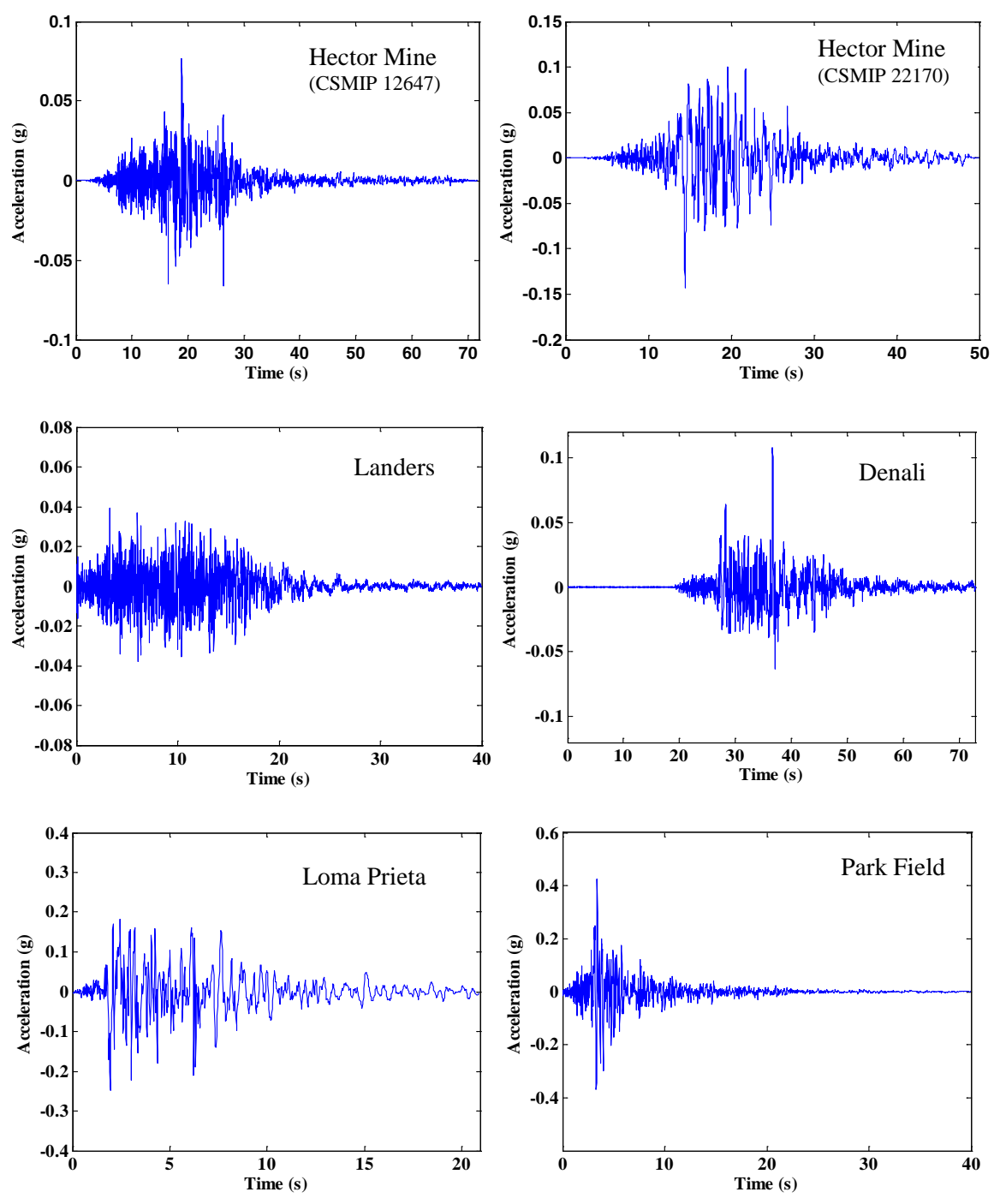


Figure 4.6 Earthquake ground motions selected for the GC site

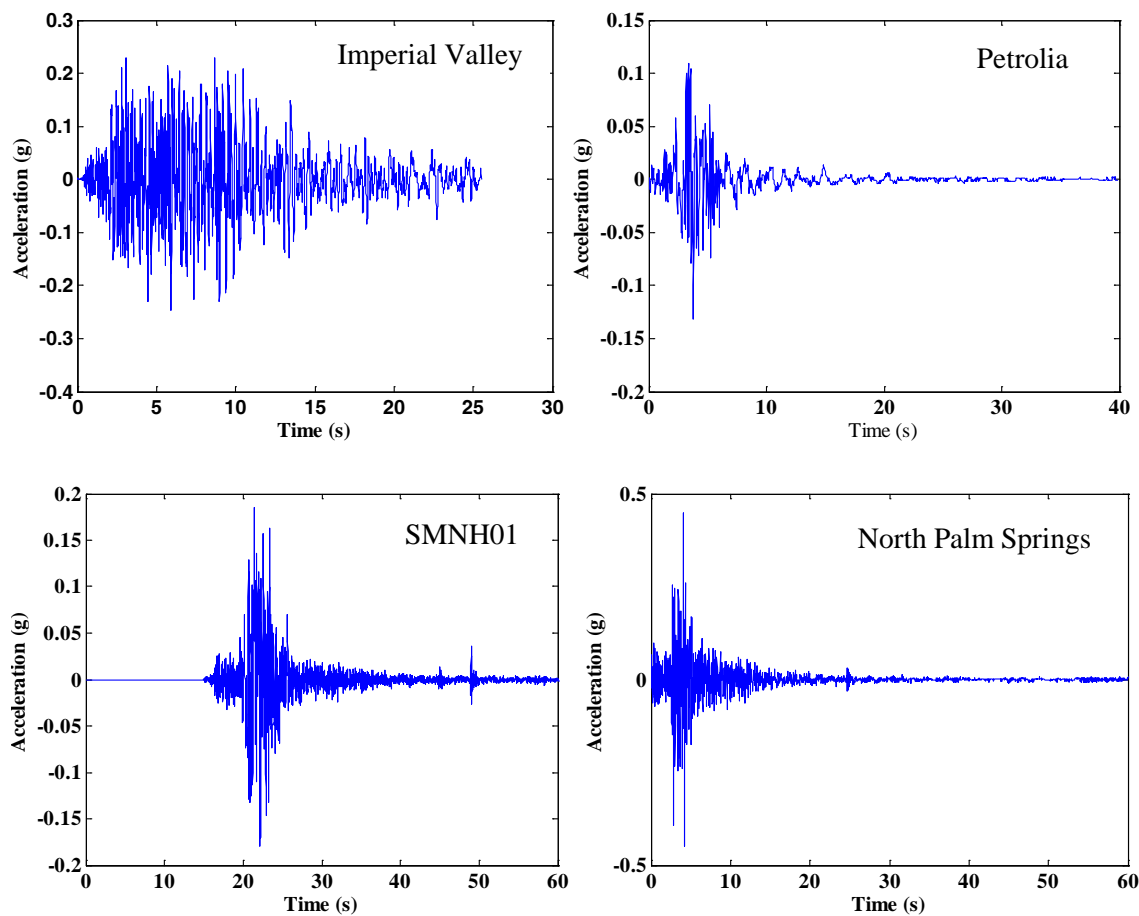


Figure 4.7 Earthquake ground motions selected for the GC site (cont'd)

#### 4.5.2 Time History Scaling

The selected time histories were scaled to match the RS of the three levels of hazard of the GC site by using the procedure discussed in Section 2.4.2. The scaling factors applied to each ground motion time histories are listed in Table 4.4. It is noted that most of the scaling factors used are less than 5. However, there are a few cases (for example, Landers earthquake record) that the scaling factor exceeds 5, due to lack of any other strong motion time histories recorded from a site with similar seismic settings. As an example, the 5% damped RS of selected earthquake ground motions scaled to AASHTO Design Earthquake level hazard is shown in Figures 4.8 and 4.9. The scaling target, i.e. the bedrock RS at the GC site, is also shown for comparison.

Table 4.4 Scaling factor ( $F_k$ ) applied to the selected earthquake ground motions for generating hazard-consistent input motions at the GC site

Event ID	Scaling factor		
	MCE	AASHTO Design Earthquake	IBC Design Earthquake
Denali	4.9	3.2	3.8
Hector Mine (22170)	3.5	2.2	2.3
Hector Mine (12647)	5.8	3.4	3.6
Imperial Valley	2.4	1.6	1.8
Landers	9.4	6	6.3
Loma Prieta	1.4	0.9	1.1
North Palm Springs	6.2	4.1	4.3
Park Field	1.7	1.1	1.2
Petrolia	3.6	2.3	2.5
SMNH01	2.3	1.5	1.6

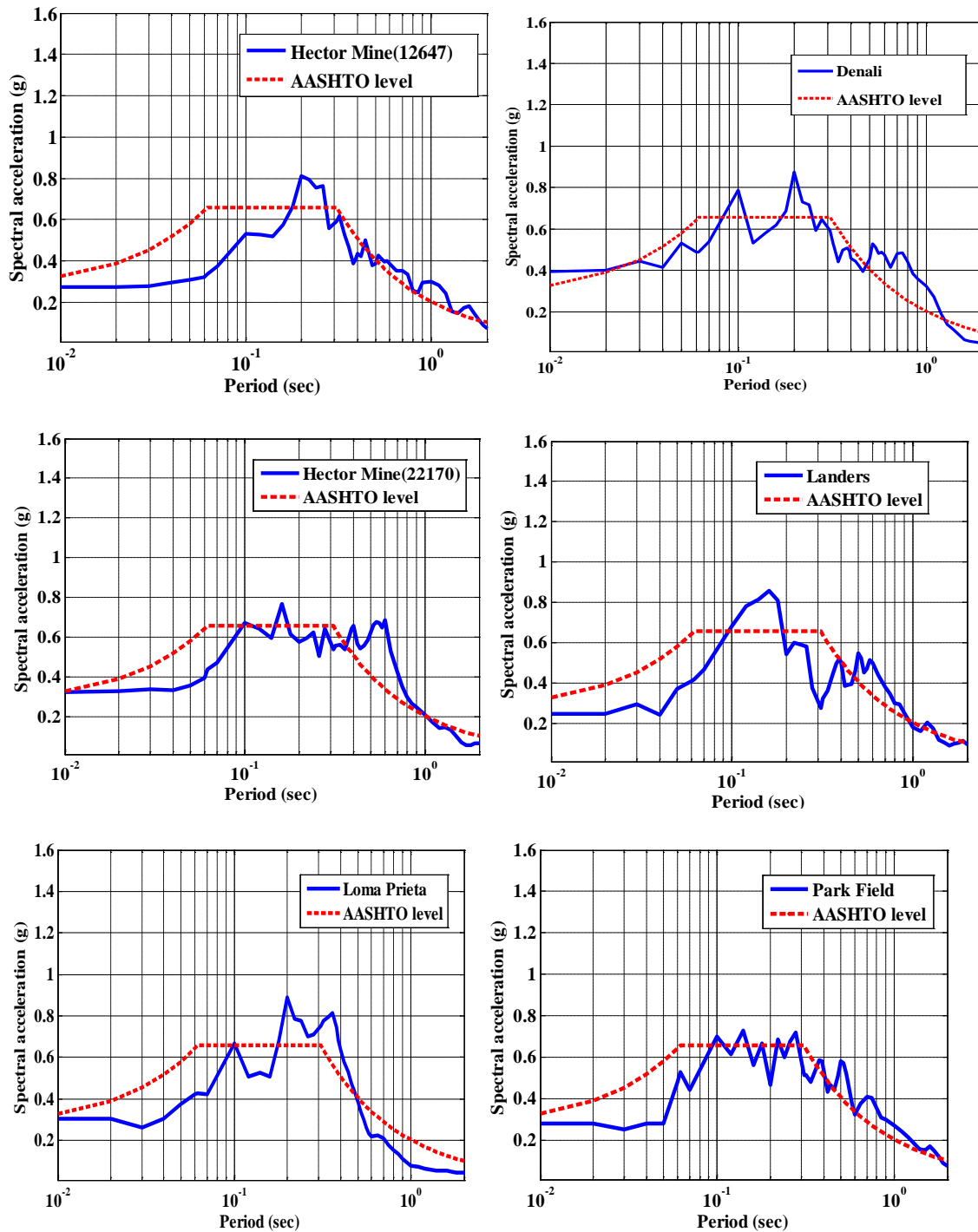


Figure 4.8 Comparison of the RS of scaled input motions with target bedrock RS for the GC site (AASHTO Design Earthquake level hazard)

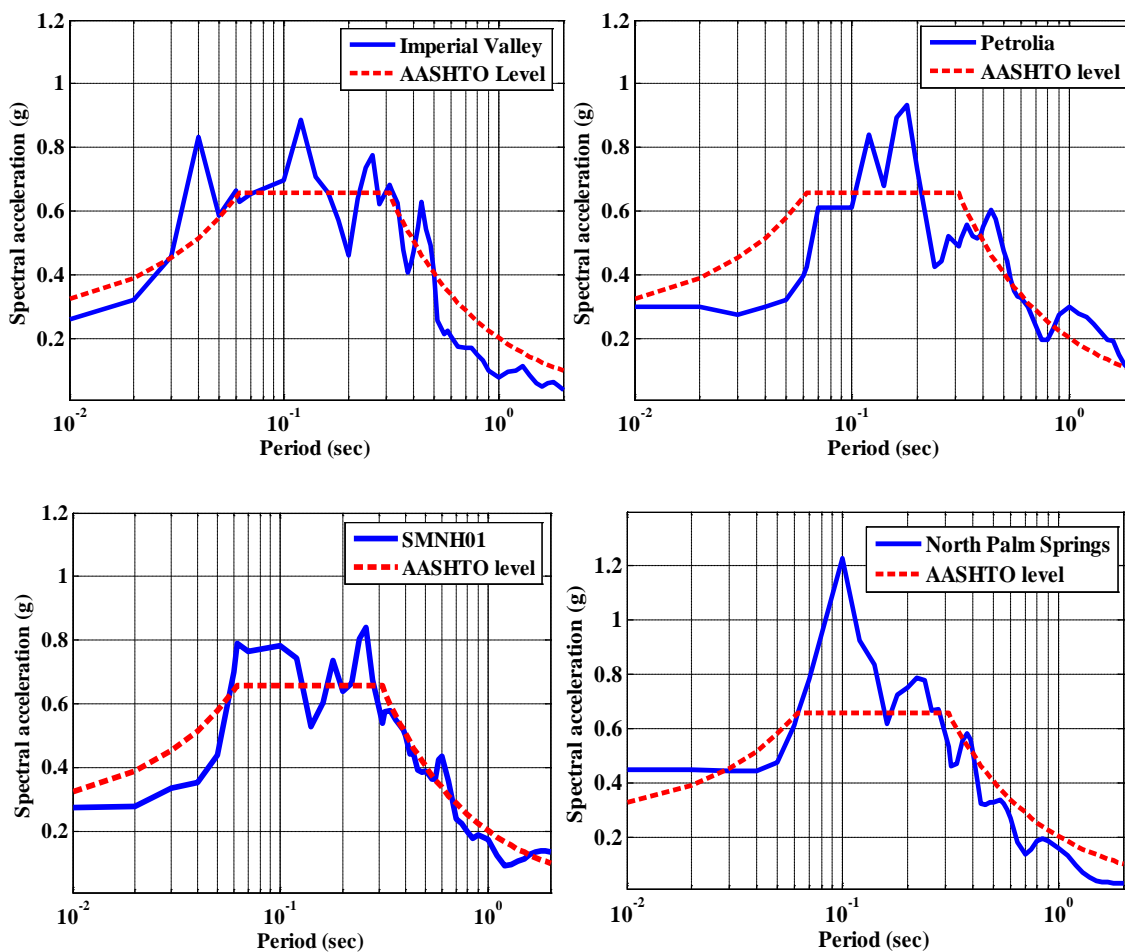


Figure 4.9 Comparison of the RS of scaled input motions with target bedrock RS for the GC site (AASHTO Design Earthquake level hazard) (cont'd)

#### 4.6 Discussion on the representativeness of selected input motions

In order to verify the scaling procedure and the representativeness of the selected earthquake ground motions, the 5%-damped geometric average RS of all selected input time histories for the three levels of hazard were calculated by using Eqn. 3.1 and are shown in Figures 4.10, 4.11 and 4.12, respectively. For comparison, the bedrock site RS are also plotted. It can be observed that the average RS agree well with the target RS for all three levels of hazard. This confirms that the selected and scaled earthquake motions are representative of the seismic hazard as expressed by the design RS at the study site.

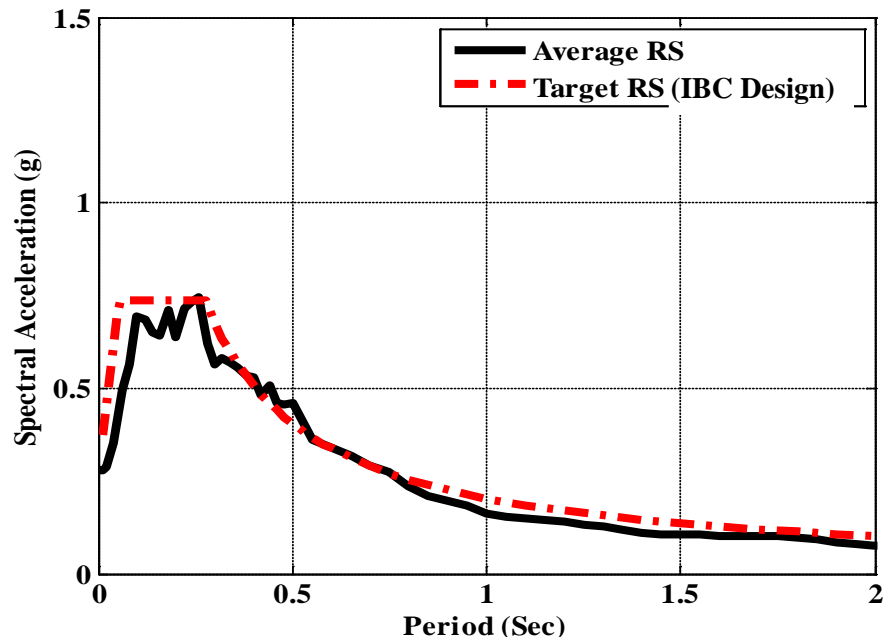


Figure 4.10 Comparison of the average RS of the ten input motion time histories with bedrock RS of the GC site (IBC Design Earthquake level hazard)

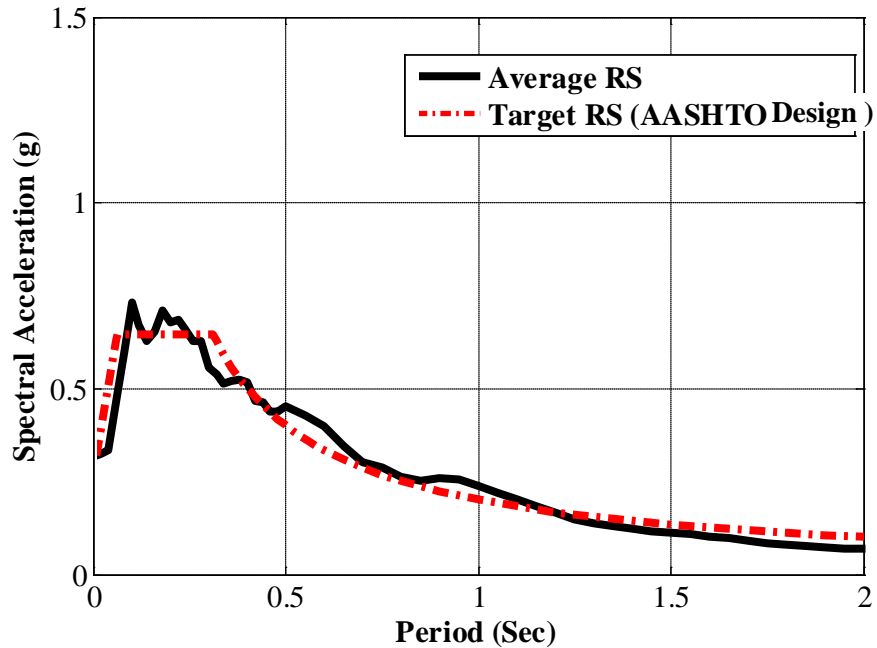


Figure 4.11 Comparison of the average RS of the ten input motion time histories with bedrock RS of the GC site (AASHTO Design Earthquake level hazard)

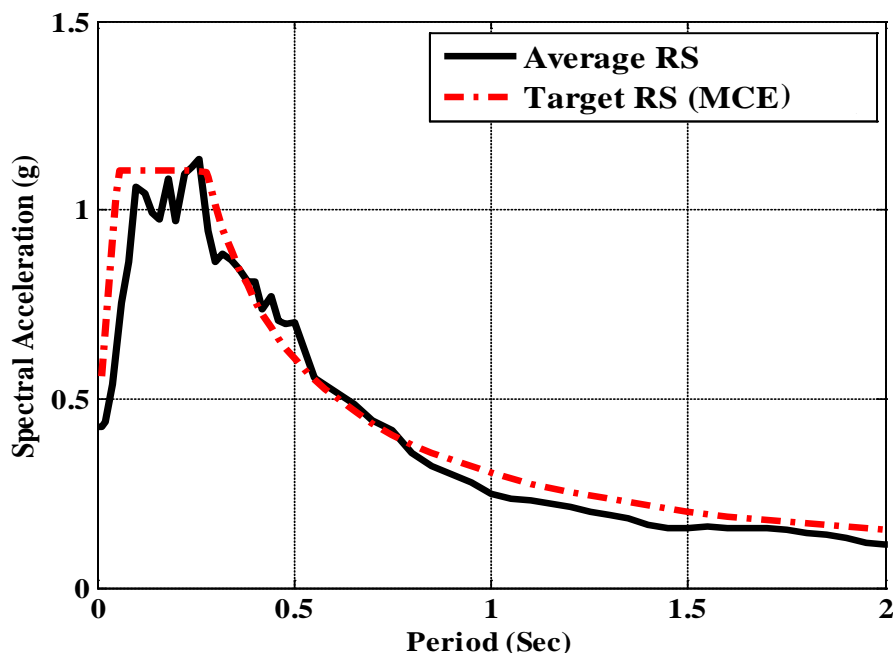


Figure 4.12 Comparison of the average RS of the ten input motion time histories with bedrock RS of the GC site (MCE level hazard)

Due to the amount of computation involved in parametric studies, we have used six input motions, identified as Loma Prieta, Hector Mine 22170, Hector Mine 12647, Denali, Landers, and Park Field, out of the ten input motions to study the effects of variation in permafrost table, permafrost shear wave velocity and bedrock table on the site response characteristics. Once the parameters that produce the largest site response (referred to as worst case scenario) was identified, all ten input motions were used to obtain the average site response spectra.

The average RS for the six selected input motions and ten input motions are compared with the AASHTO Design Earthquake RS for bedrock at the GC site in Figure 4.13. It is seen from Figure 4.13 that the average RS of the six input motions is very similar to that of the ten input motions, and both of them are close to the AASHTO Design Earthquake RS. This confirms the representativeness of the selected input motions used in different stages of the study.

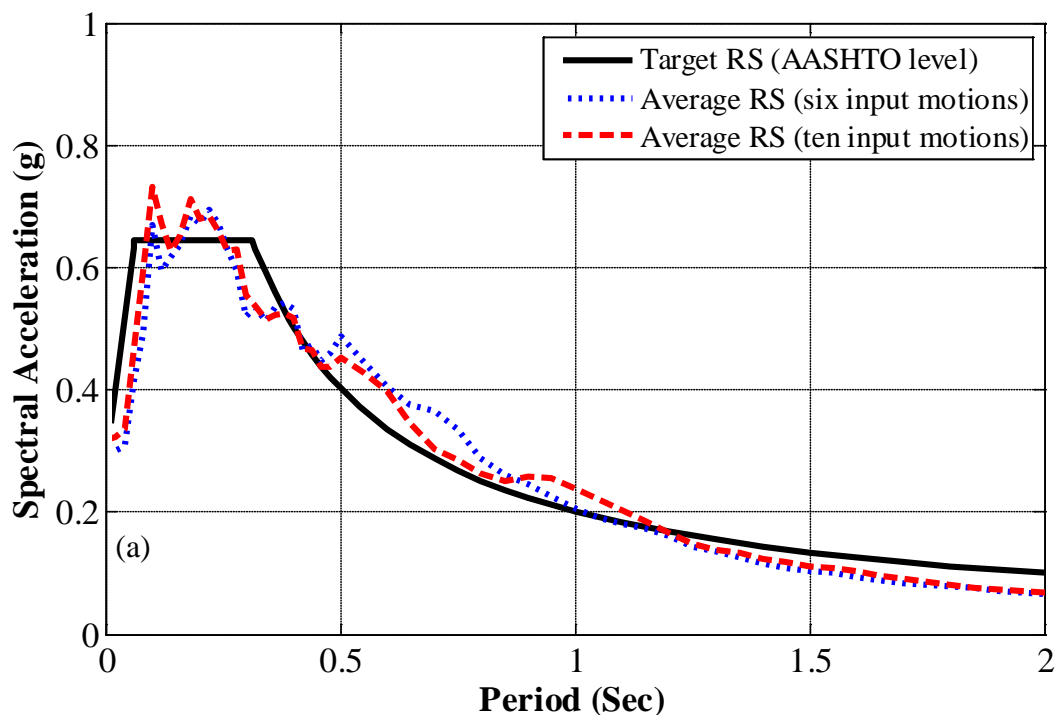


Figure 4.13 Comparison of the average RS of selected input motions with the target RS of the GC site for AASHTO Design Earthquake level hazard

## 4.7 Analysis Results

### 4.7.1 Time History of Acceleration and Peak Shear Strain

Site response analyses were conducted for this site with 1-D equivalent linear procedure. Figure 4.14 shows examples of computed time histories at the surface and within the permafrost layer for the profile with the permafrost table at -20 m. For comparison, the input motion, i.e. Denali earthquake ground motion is also shown.

The peak shear strain developed in the soil profile with the permafrost table at -20 m for input ground motions scaled to MCE level hazard is shown in Figure 4.15. It is seen that the maximum shear strain is less than 0.3%, which is well below 1~2%, required for equivalent linear analysis to produce acceptable results.

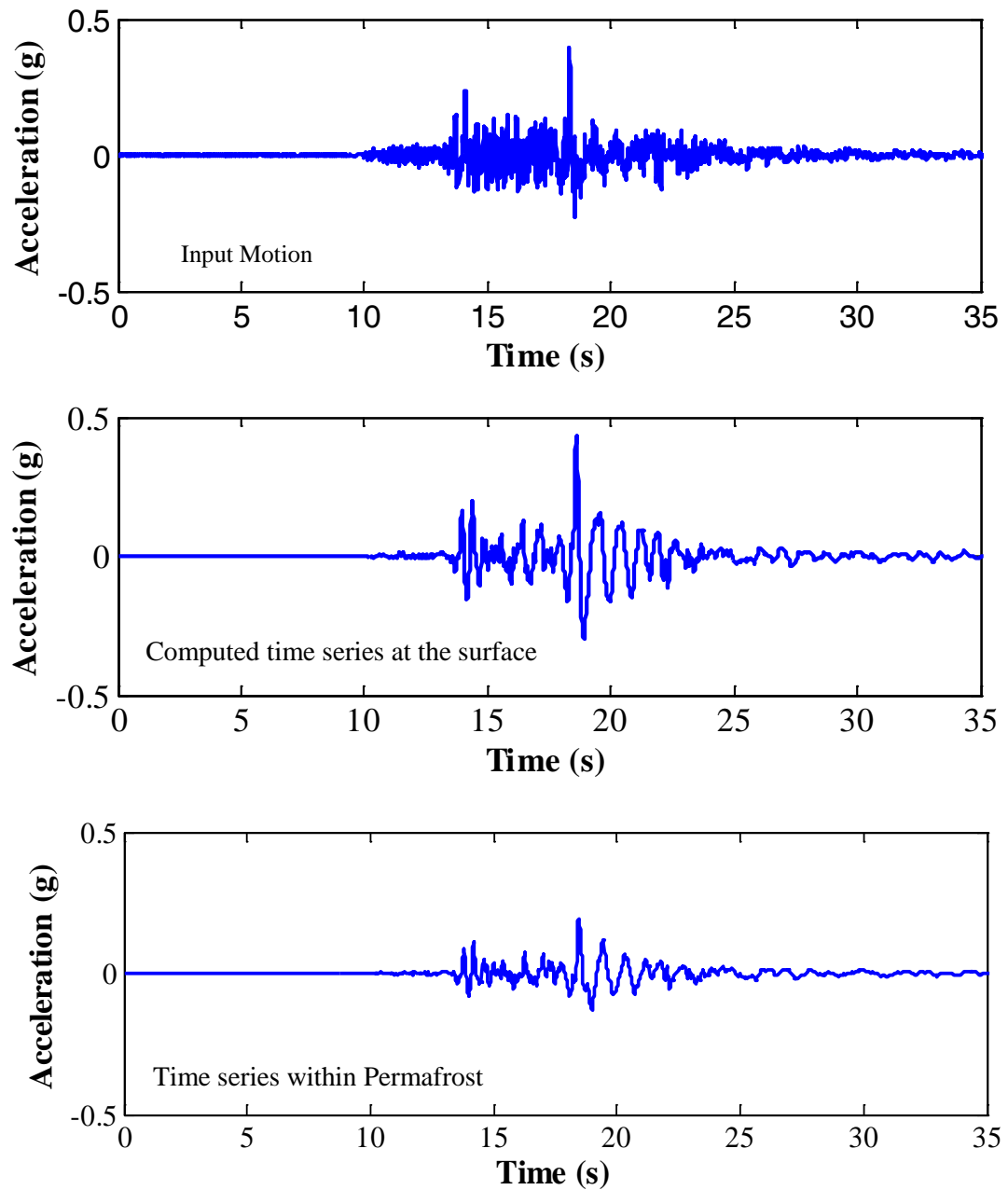


Figure 4.14 Comparison between the input time series (Denali) and computed time series at the surface and within permafrost.

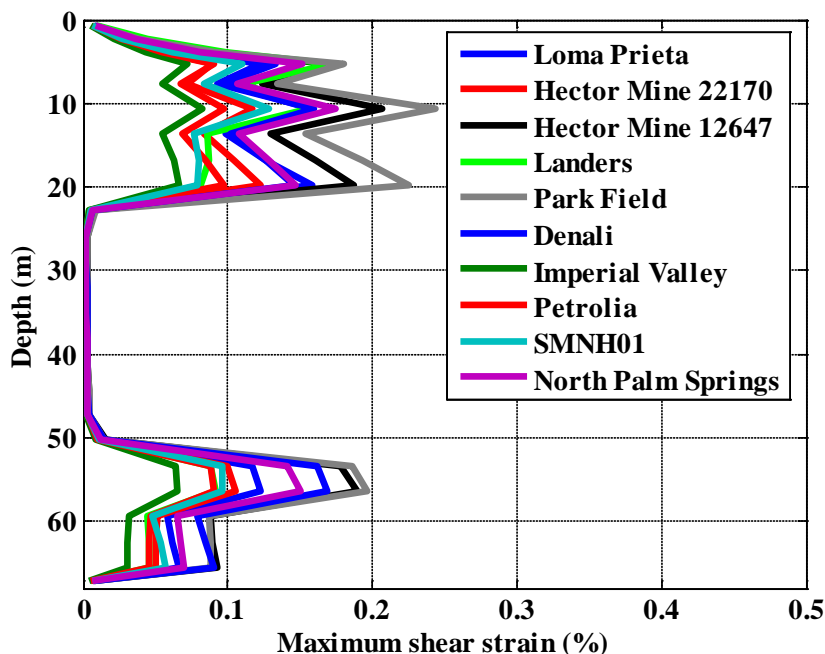


Figure 4.15 Peak shear strain vs. depth for ten input motions scaled to MCE level hazard for a soil profile with permafrost table at -20 m and bedrock table at -66 m.

#### 4.7.2 Site Response for Different Permafrost Table

The RS were computed by propagating each of those six input motions scaled to the AASHTO level hazard through the soil profile with permafrost table varying from 0 to -164 ft (-50 m) (Figure 4.2). The RS of simulated ground surface motions and their average RS are shown in Figures 4.16-4.24. The average RS was calculated using the following equation:

$$aveRS(T) = \sqrt[n]{\prod_{i=1}^n RS_i(T)} \quad (4.1)$$

Where  $aveRS(T)$  refers to the average RS,  $RS_i(T)$  refers to one of  $n$  RS used to calculate the average RS.

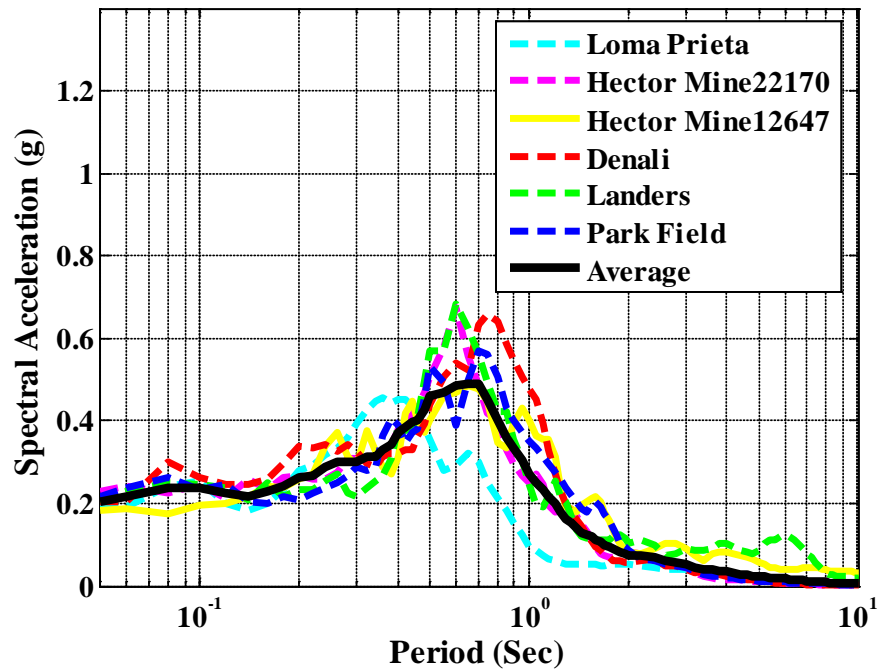


Figure 4.16 RS of the surface motions and their average for the soil profile with permafrost table at 0 ft (0 m) (AASHTO Design Earthquake level)

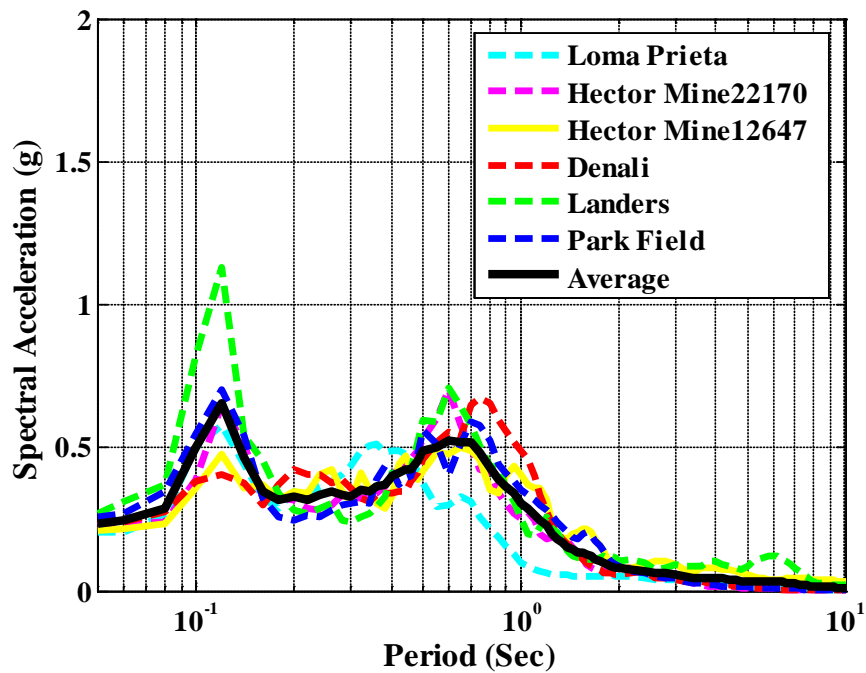


Figure 4.17 RS of the surface motions and their average for the soil profile with permafrost table at -16 ft (-5 m) (AASHTO Design Earthquake level)

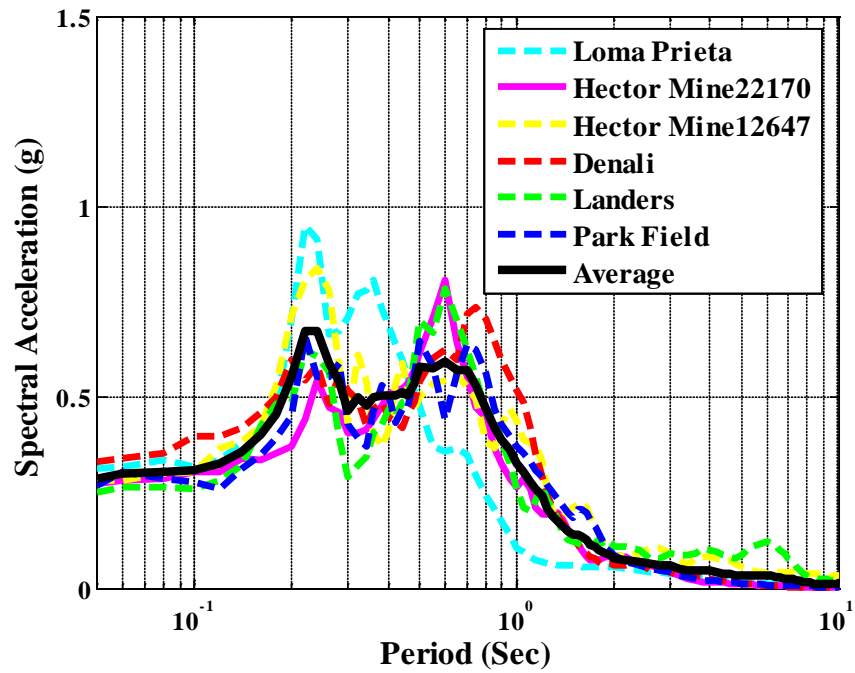


Figure 4.18 RS of the surface motions and their average for the soil profile with permafrost table at -33 ft (-10 m) (AASHTO Design Earthquake level)

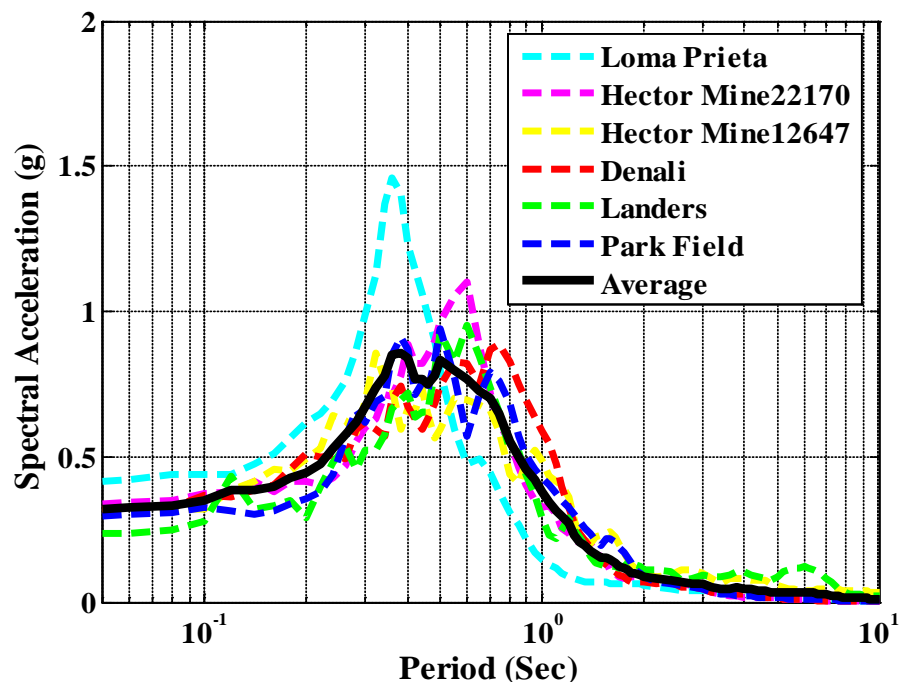


Figure 4.19 RS of the surface motions and their average for the soil profile with permafrost table at -50 ft (-15 m) (AASHTO Design Earthquake level)

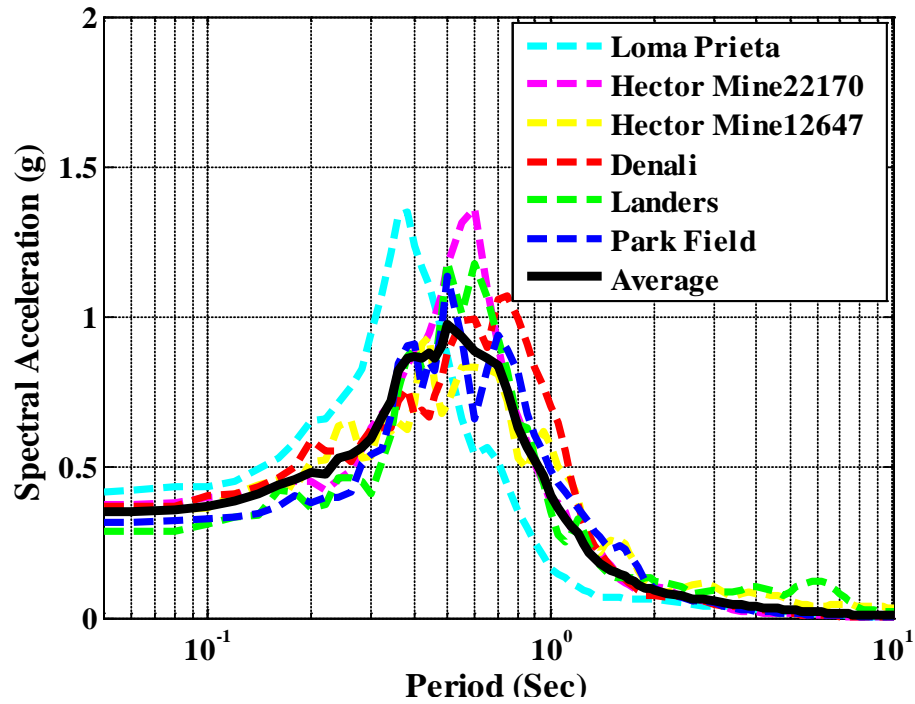


Figure 4.20 RS of the surface motions and their average for the soil profile with permafrost table at -66 ft (-20 m) (AASHTO Design Earthquake level)

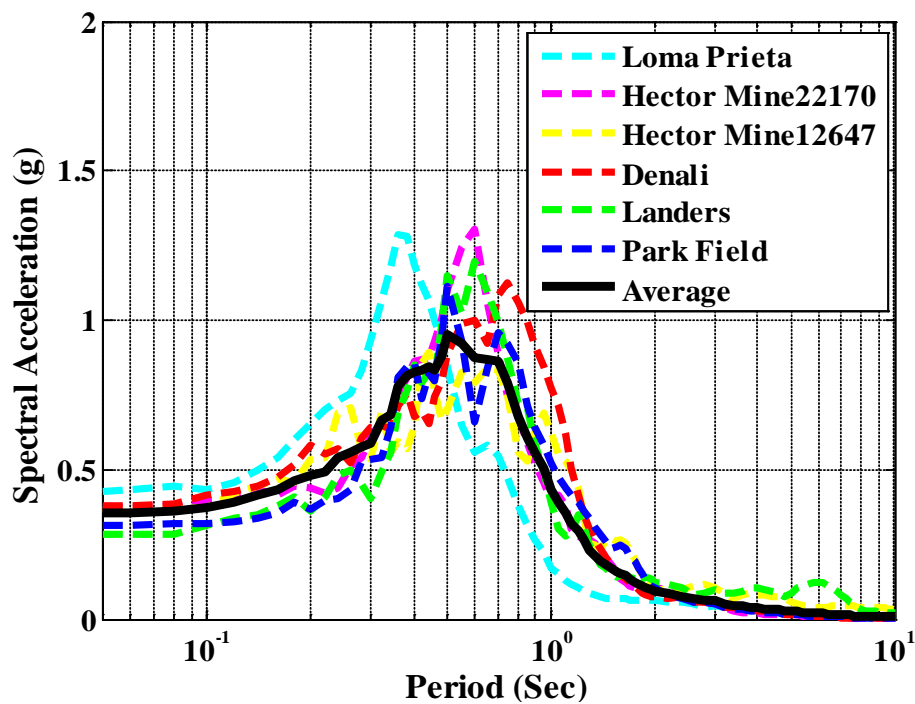


Figure 4.21 RS of the surface motions and their average for the soil profile with permafrost table at -82 ft (-25 m) (AASHTO Design Earthquake level)

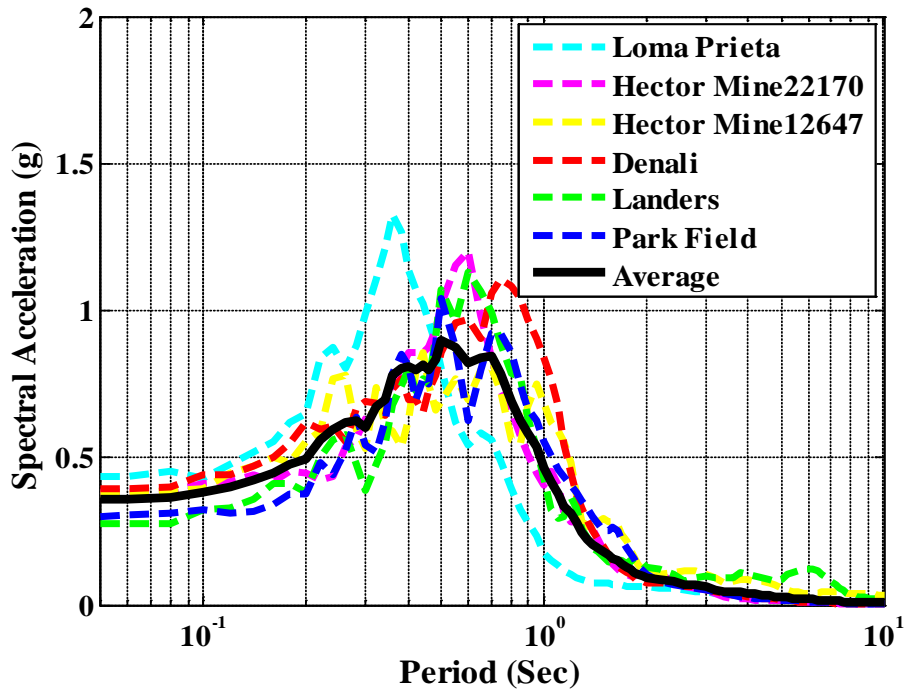


Figure 4.22 RS of the surface motions and their average for the soil profile with permafrost table at -100 ft (-30 m) (AASHTO Design Earthquake level)

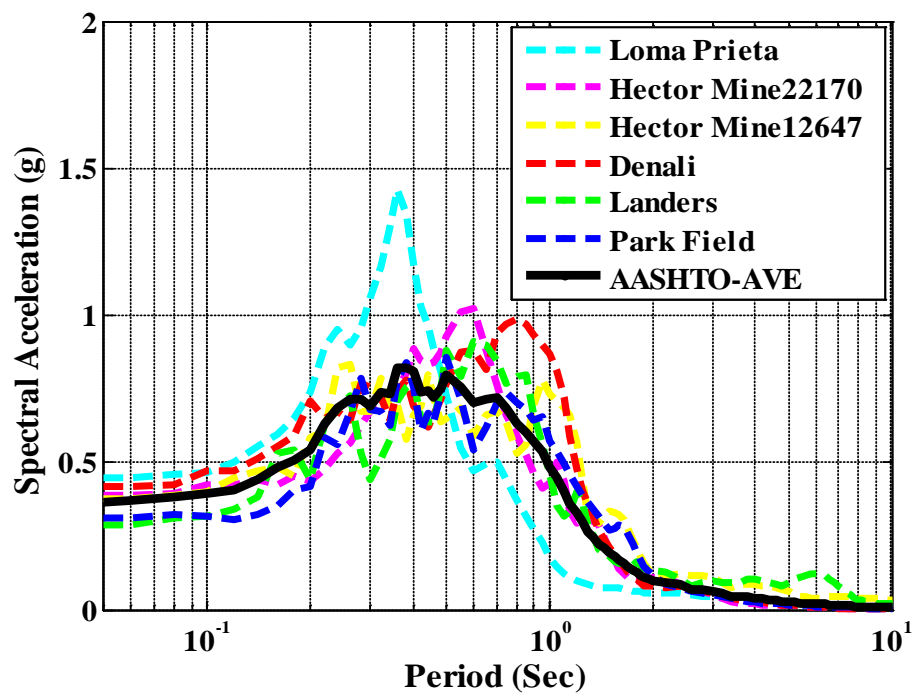


Figure 4.23 RS of the surface motions and their average for the soil profile with permafrost table at -130 ft (-40 m) (AASHTO Design Earthquake level)

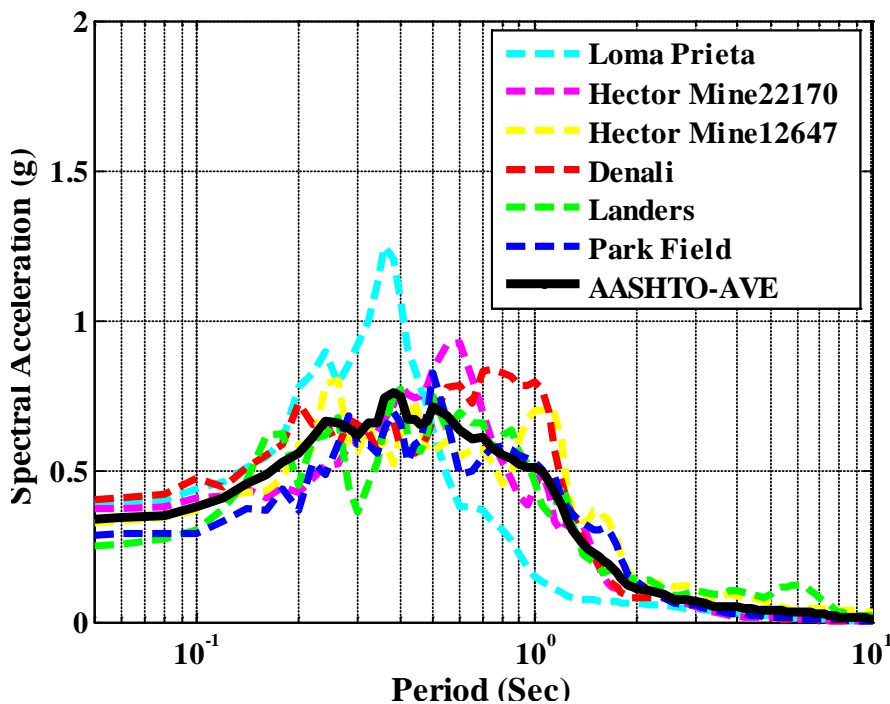


Figure 4.24 RS of the surface motions and their average for the soil profile with permafrost table at -160 ft (-50 m) or no permafrost (AASHTO Design Earthquake level)

#### 4.7.3 Effects of Permafrost Table Variation on Site Response

A set of soil profiles with the permafrost table varying from 0 to -40 m at an interval of 5 m has been constructed (Figure 4.2). All models assume that the bedrock table is located at a depth of -66 m. The RS were computed by propagating each of the scaled six input motions through the soil profile with varying permafrost table. The average RS for permafrost table varying from 0 to -164 ft (-50 m) are shown in Figure 4.25 along with the AASHTO Design Earthquake spectra for Class B (bedrock), D (medium) and E (soft) soil types. The design spectrum for Class D is chosen because for non-permafrost condition the site would have been classified as site Class D (the average shear wave velocity of upper 30 m soil profile is within 183 to 366 m/s) based on NEHRP criteria (BSSC, 1997). The design RS for site Class E is shown for reference.

It is observed from Figure 4.25 that the SA values of the computed response are smallest when the permafrost table is close to the surface (0 ft). For the 0 ft permafrost table, the SA values are found to be well below that of Class D type soil. The SA values increase gradually with the decrease of permafrost table till it reaches -66 ft (-20 m), when the SA values peak. With the further drop of permafrost table beyond -66 ft, the SA values again start to decrease.

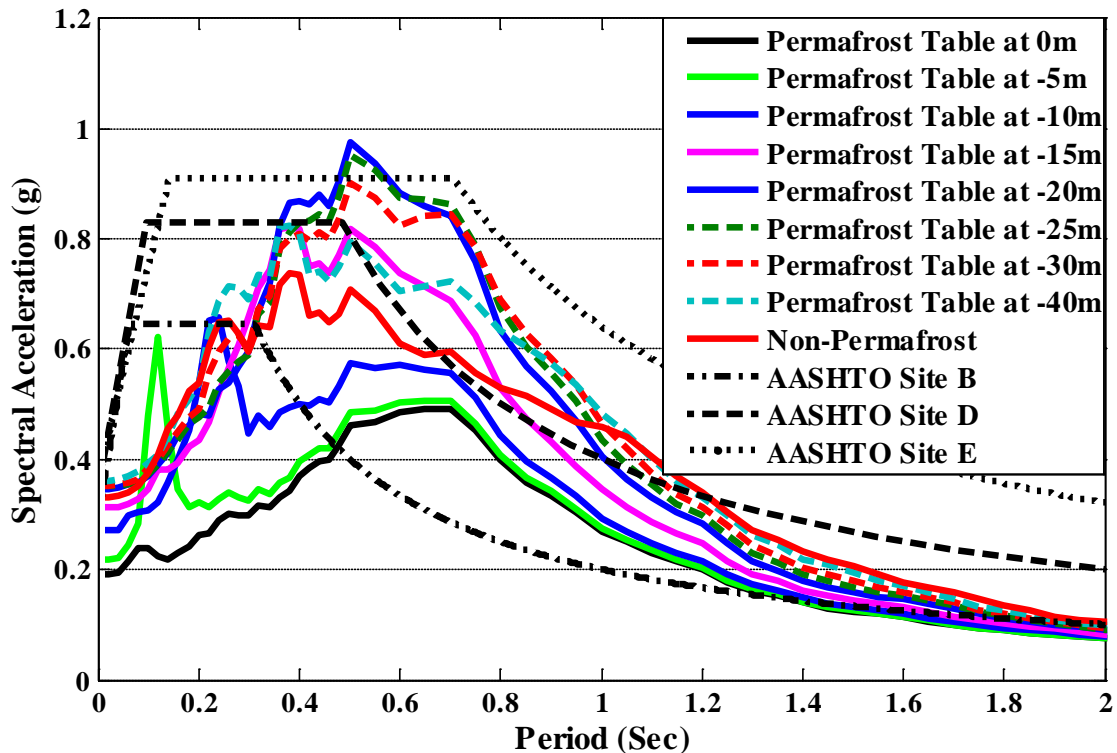


Figure 4.25 Comparison of the average RS with varying permafrost table for input motions scaled to AASHTO Design Earthquake level hazard for the GC site

It is important to note that the SA values for period ranging from 0.35 to 0.9 sec when the permafrost table falls into the range of -50 to -130 ft (-15 to -40 m) is greater than those of AASHTO Site Class D and is up to 20% greater when the permafrost table is at -66 ft. The RS are generally below that of Site Class E except for periods around 0.55 sec. However, for the soil profile with no permafrost, SA values are within the envelope of Site Class D, as expected. Therefore it is not always conservative to classify a permafrost site in the same manner as a non-permafrost site. It is also interesting to note that the SA values for the soil profile with permafrost table at -66 ft is much smaller than those of AASHTO site class D for period ranging from 0 to 0.3 sec; this pronounced reduction is due to the presence of permafrost which attenuates higher frequency components, as will be discussed in the next section.

#### 4.7.4 Effects of Permafrost with Variation in Bedrock Table

Considering the dipping of the bedrock table in the Fairbanks area (Péwé, 1982), a parametric study has been conducted to investigate the effects of bedrock table on the site response. According to previous analysis results, the average RS of surface motions

reaches the highest values when permafrost table is at -66 ft. In the soil profile used for this parametric study, the portion above -164 ft (-50 m) is retained; the bedrock table is varied from -200 to -500 ft (-66 to -150 m). Correspondingly the gravel layer thickness is varied from 20 to 300 ft (6 to 92 m). The soil profiles and  $V_s$  values are shown in Figure 4.26.

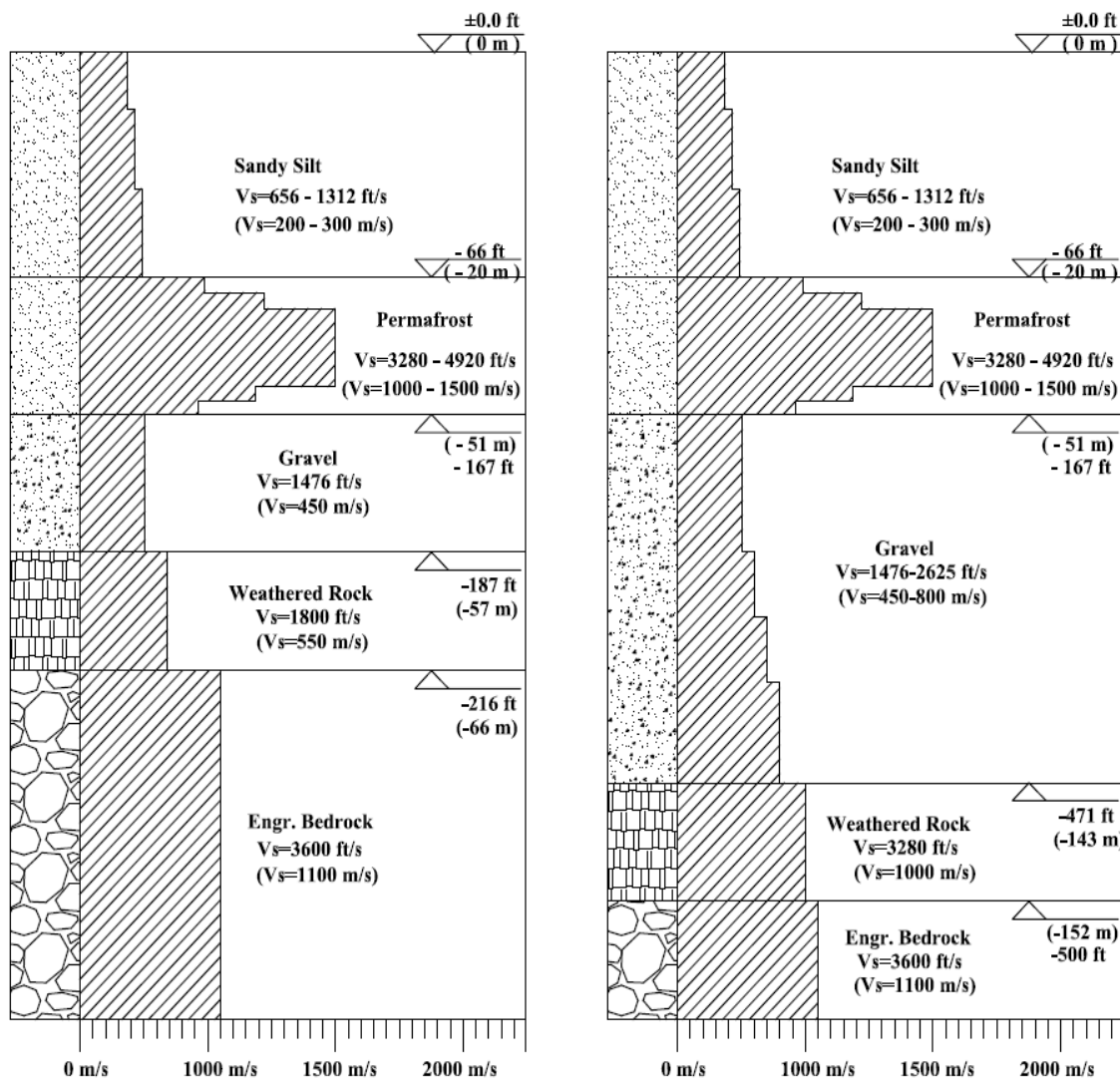


Figure 4.26 Soil profiles with varying bedrock table

The average RS simulated for different bedrock tables have been obtained and shown in Figure 4.27. It is seen from Figure 4.27 that the SA values decreases as the bedrock table drops, and it is higher than those of site Class D when the bedrock table is shallower than approximately -230 ft (-70 m). It is believed that the main reason for this is the thicker

deposits of gravels and sands below the permafrost attenuate more input energy, therefore reducing the surface response.

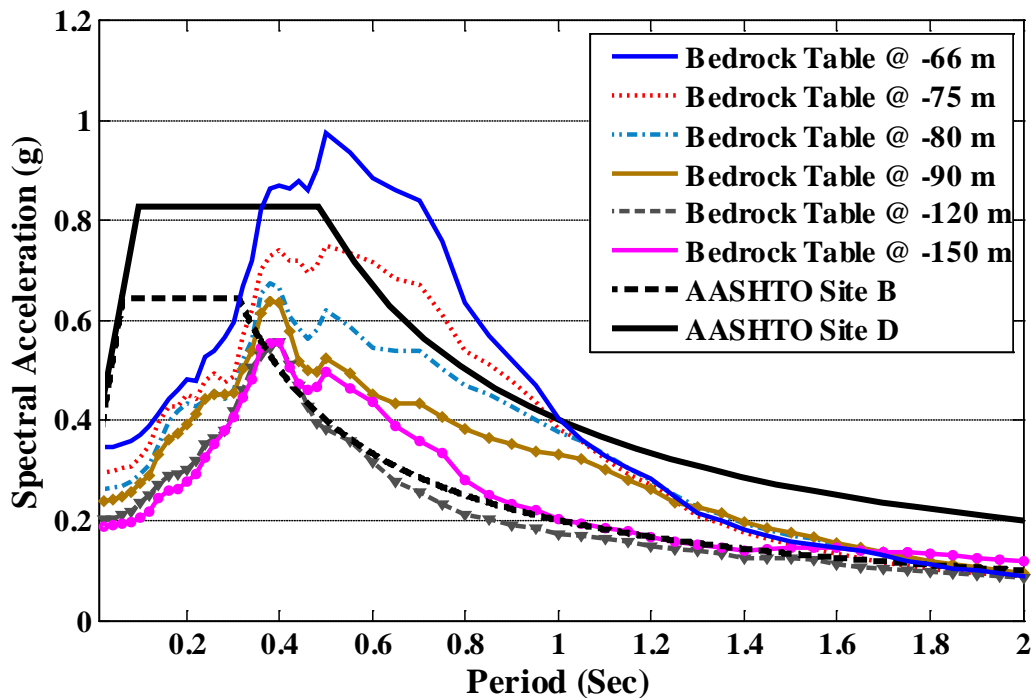


Figure 4.27 Average RS of surface motions for soil profiles with varying bedrock table for AASHTO level hazard

#### 4.7.5 Discussion on Role of Permafrost

In order to explain the effects of permafrost on the site response, the transfer functions of the unfrozen top layer and the underlying permafrost layer for selected permafrost tables are illustrated in Figures 4.28a and b, respectively. From Figure 4.28a, it is observed that as the permafrost table drops from 0 to -35 m, the predominant period shifts from 0.25 to 0.85 sec, while the peak amplification factor for the top unfrozen layer varies from 4 to 5. Meanwhile, it is seen from Figure 4.28b that the peak amplification factor for the permafrost layer is no more than 1.5. In particular, the permafrost layer attenuates the input motions components for period less than 0.6 sec. This indicates that the top unfrozen layer plays a dominant role in amplifying ground motion components with relatively longer period and shifting the predominant period to longer period, and the permafrost layer attenuates ground motion components with relatively shorter period.

For the soil profile with permafrost table at -66 ft, it amplifies the components around 0.4-0.75 sec by more than 200%, therefore forming a peak around 0.55 sec in the average

response spectra, which is significantly larger than the SA values in the AASHTO Design Earthquake RS. This is analogue to the resonance phenomenon in structural dynamics: when the period for the top unfrozen layer moves closer to the predominant period of the input motion as the permafrost table drop to -66 ft, resonance occurs, hence producing maximum ground response.

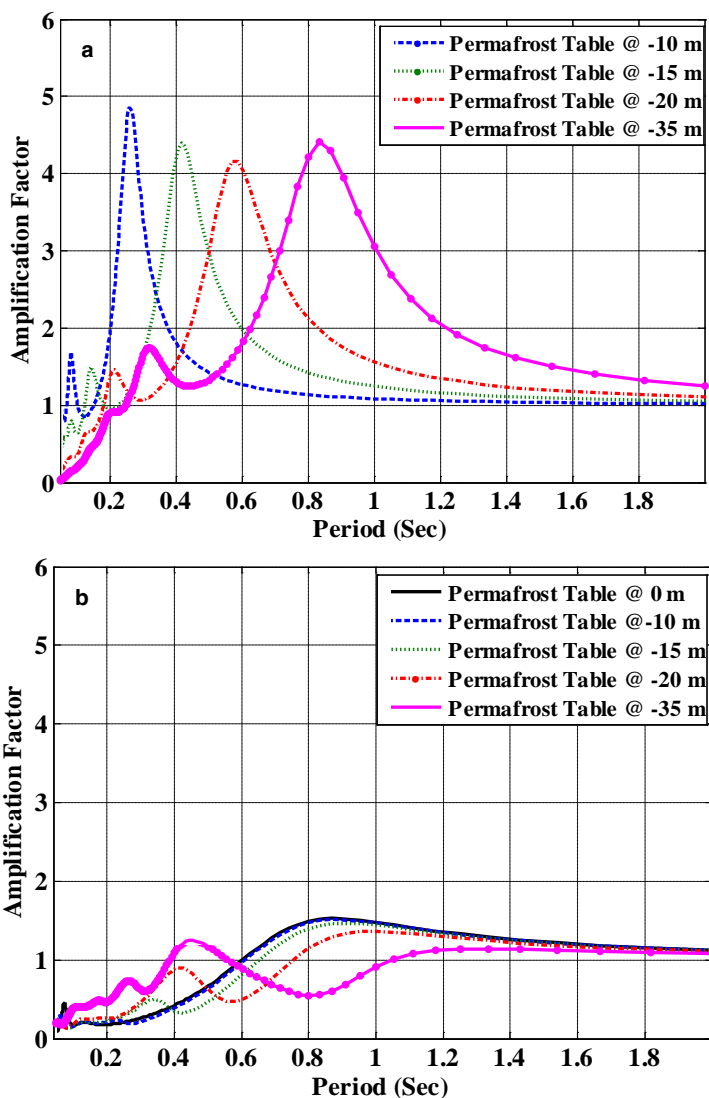


Figure 4.28 Transfer functions of (a) the top unfrozen layer and (b) underlying permafrost for soil profiles with permafrost table varying from 0 to -115 ft (-35 m)

#### 4.7.5 Sensitivity of Results to Permafrost Shear Wave Velocity

To assess the dependence of results to variation in shear wave velocity of permafrost, a sensitivity study has been carried out by using the profile with permafrost table at -66 ft.

The site RS for varying  $V_s$  values for input motions Denali and Hector Mine are shown in Figures 4.29a and b, respectively. The input motions have been scaled to AASHTO Design Earthquake level hazard. It is seen from Figures 4.29a and b that the SA values increase by less than 10% when permafrost shear wave velocity decreases from 4,900 to 2,600 ft/s (1,500 to 800 m/s). It is therefore concluded that the effect of varying permafrost shear wave velocity on seismic site response is insignificant.

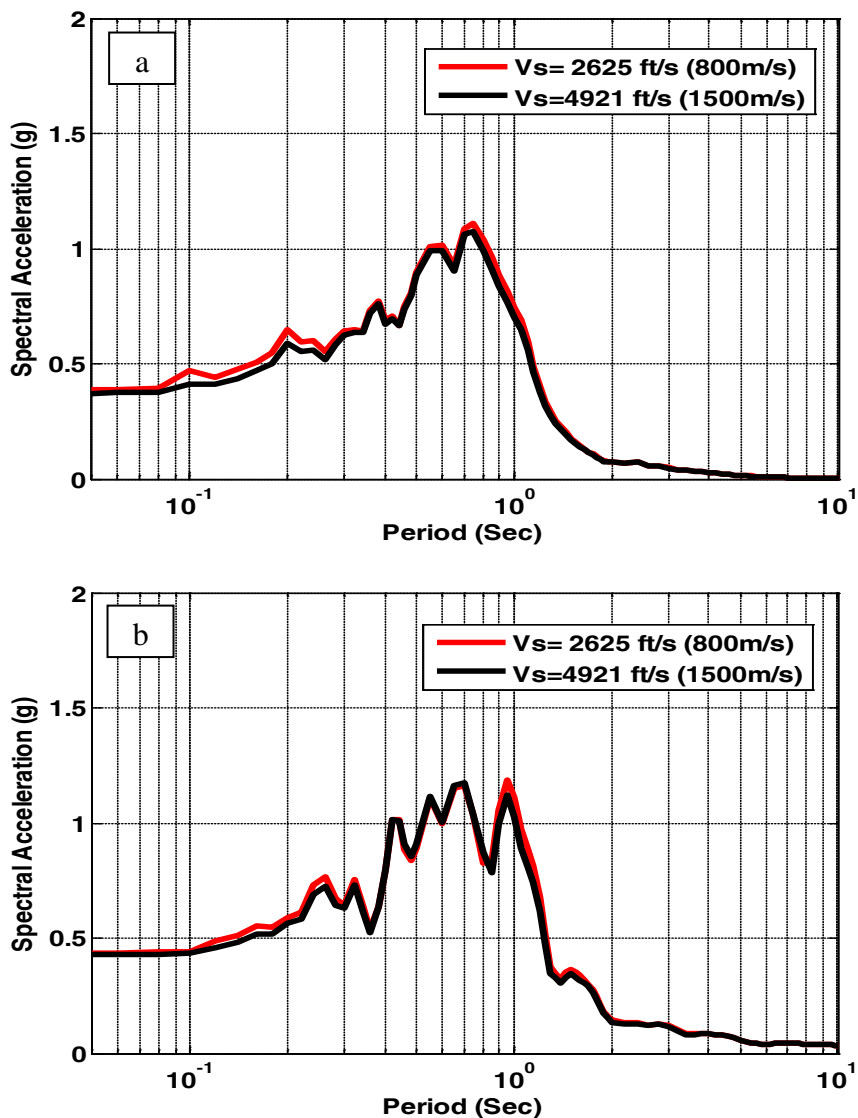


Figure 4.29 Variation of RS with permafrost shear wave velocity for input motions Denali (a) and Hector Mine (b) scaled to AASHTO Design Earthquake level hazard

#### 4.8 Average Response Spectra for Similar Sites

These parametric studies confirm that the soil profile with a permafrost table at -66 ft (-20 m) and the bedrock table at -216 ft (-66 m) produces the largest SA values in the average surface RS. This soil profile is referred to as the GC Site-Worst Case Scenario in this report. This profile was further used to produce the average surface displacement, velocity and acceleration RS for the GC site by using all ten input motions scaled to MCE, AASHTO Design Earthquake and IBC Design Earthquake level hazards, as shown in Figures 4.30, 4.31 and 4.32, respectively. For comparison, the RS for site Class D were also plotted. The spectral accelerations ( $S_a$ ) were directly obtained from analysis results. The spectral velocities ( $S_v$ ) and displacements ( $S_d$ ) were obtained by using  $S_v(i) = S_a(i) \frac{T_i}{2\pi}$ , and  $S_d(i) = S_a(i) \left(\frac{T_i}{2\pi}\right)^2$  (where  $T_i$  is period, and  $S_a(i)$  the spectral acceleration corresponding to  $T_i$ ), respectively (Chopra, 2007).

Figures 4.30, 4.31 and 4.32 show that compared with those suggested by design codes for Class D soils (IBC 2000, AASHTO 2007), the  $S_d$  values for periods in the range of 0.4 to 1.0 sec are up to 20% larger, those of  $S_v$  for periods in the range of 0.4 to 1.0 sec are up to 50% larger, and those of  $S_a$  for periods in the range of 0.5 to 1.0 sec are up to 40% larger for the three levels of seismic hazard. For periods outside of those ranges, the spectral values are generally smaller than those suggested by design codes. It is also interesting to observe that the average surface displacement RS level off at around 0.8 sec, which is in contrast to the observation that the design displacement RS flatten at around 4 sec. Therefore, it is not always conservative to ignore the effects of permafrost in seismic design of bridges and other civil infrastructure. Our parametric study indicates that a permafrost site with a permafrost table at around -66 ft and a bedrock table at about -216 ft may produce substantially higher site response than that proposed by design codes. In this sense, a site exploration beyond the permafrost layer is highly recommended when permafrost is present, particularly as the permafrost table is at around -66 ft (-20 m).

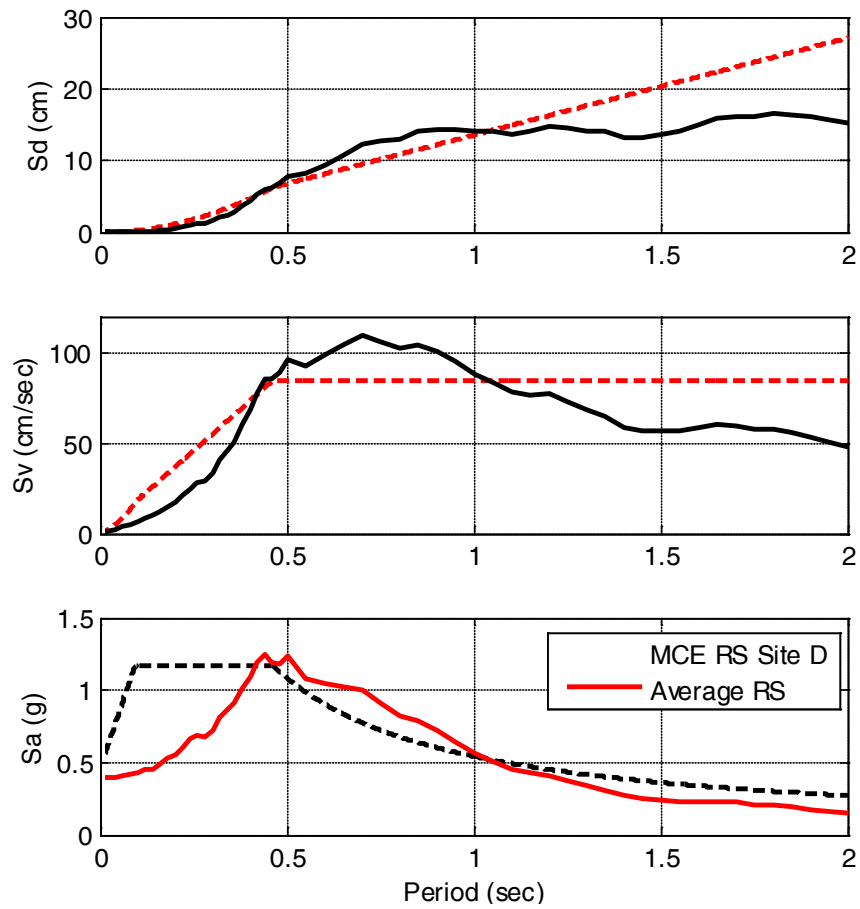


Figure 4.30 Average surface displacement, velocity and acceleration RS for the GC Site-Worst Case Scenario at MCE level hazard (2% PE in 50 years)

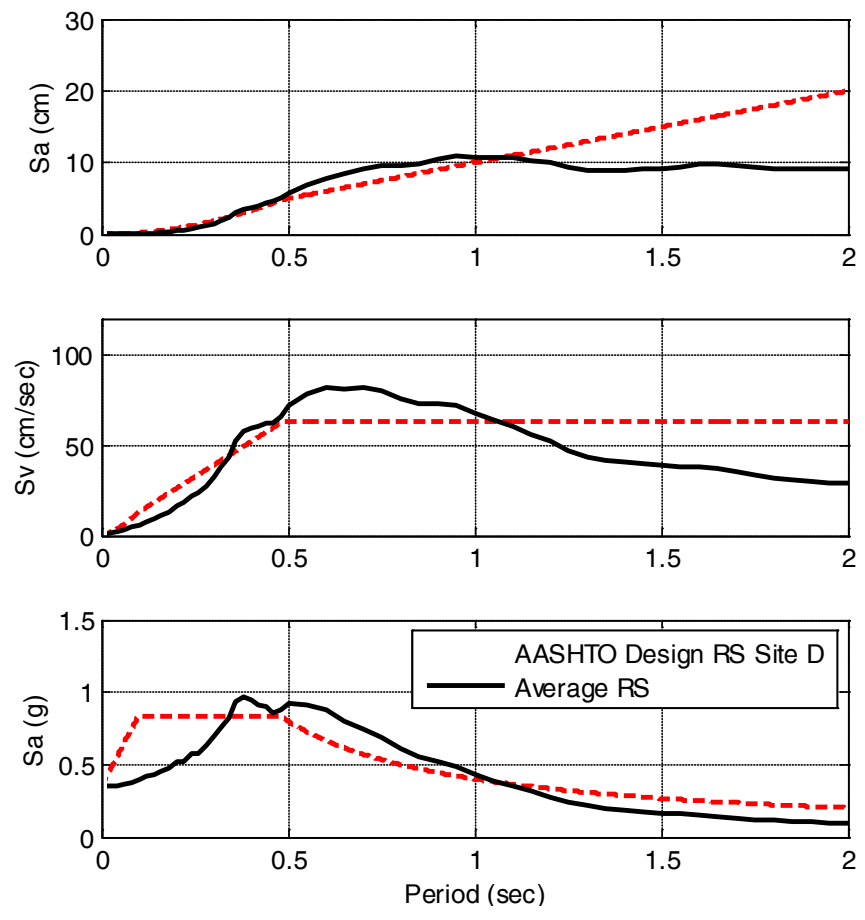


Figure 4.31 Average surface displacement, velocity and acceleration RS for the GC Site-Worst Case Scenario at AASHTO Design Earthquake level hazard (7.5% PE in 75 years)

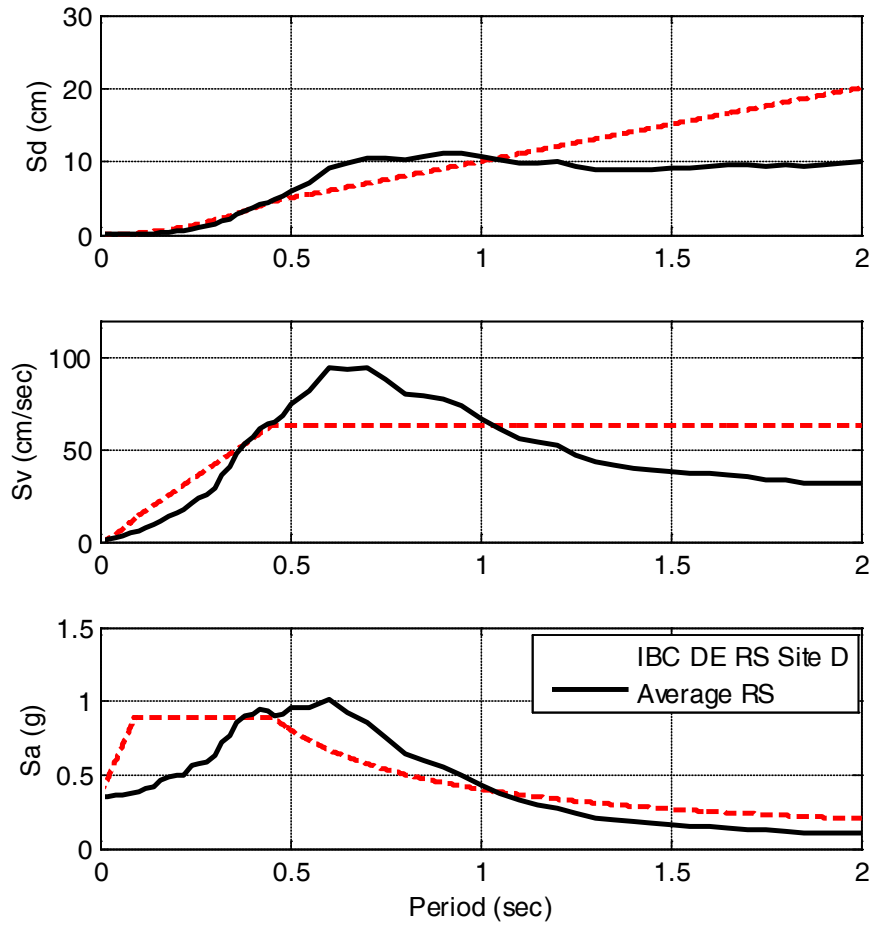


Figure 4.32 Average surface displacement, velocity and acceleration RS for the GC Site-Worst Case Scenario at IBC Design Earthquake (two-thirds of MCE) level hazard

## CHAPTER 6 – CONCLUSIONS AND SUGGESTED RESEARCH

### 6.1 Conclusions

A comprehensive analytical investigation of the effects of frozen soils including seasonally frozen soil and permafrost on the seismic site response has been conducted. Two sites, i.e. the C St-O'Malley Bridge site in Anchorage and the Goldstream Creek Bridge site in Fairbanks, were selected to represent typical sites with seasonally frozen soils and discontinuous permafrost, respectively. Two generic soil profiles were constructed based on the available geologic and geotechnical data for these two sites. A set of input ground motions has been selected from available strong-motion databases and scaled to generate an ensemble of seismic hazard-consistent input motions. One-dimensional equivalent linear analysis implemented in ProShake was used to analyze the seismic site response for three levels of seismic hazard, i.e. MCE, AASHTO Design Earthquake and IBC Design Earthquake. A series of parametric studies were conducted for assessing the sensitivity of the results to the uncertainties associated with shear wave velocity and thickness of seasonally frozen soil, permafrost table/thickness, and bedrock table. The strain levels induced in the soil profile were confirmed to be within the limit for equivalent linear approach to be effective.

Based on this systemic study, the following conclusions or recommendations can be made:

1. The effectiveness of seismic site response analyses of frozen soil sites by one-dimensional equivalent linear approach has been demonstrated by an example.
2. The effectiveness of the input motions selection and hazard-consistent scaling procedure has been confirmed.
3. The effects of seasonally frozen soil and permafrost are not particularly sensitive to the shear wave velocity of frozen soils.
4. Seasonally frozen soil has noticeable impact on the average spectral accelerations for periods shorter than 1.0 sec.
5. While peak ground acceleration, spectral accelerations at 0.2 and 1.0 sec all decrease with the increase in seasonally frozen soil thickness, spectral acceleration at 0.2 sec is more sensitive to the change in seasonally frozen soil thickness.
6. It is generally conservative to ignore the effects of seasonally frozen soils on seismic site response.
7. The average spectral acceleration, velocity and displacement response is substantially larger than that of site Class D when the permafrost table is located between -50 to -130 ft with the bedrock table at approximately -230 ft or shallower for periods between 0.5 and 1.0 sec.
8. The average spectral values reach the highest when the permafrost table is at -66 ft with the bedrock table at -216 ft. This is designated as the GC Site-Worst Case Scenario.

9. Compared with those suggested by design codes, the average values of spectral acceleration for periods in the range of 0.4 to 1.0 sec are up to 20% larger, those of spectral velocity for periods in the range of 0.4 to 1.0 sec are up to 50% larger, and those of spectral displacement for periods in the range of 0.5 to 1.0 sec are up to 40% larger for all three levels of seismic hazard in the GC Site-Worst Case Scenario.
10. The large amplification in the permafrost site was mainly caused by the unfrozen top soil layer. The permafrost layer itself does not amplify the bedrock motions; instead it attenuates high frequency components of the bedrock motions.
11. It is not always conservative to classify permafrost soil sites by using average shear wave velocity of the upper 30 m frozen or unfrozen soils and use code-defined site coefficients for seismic design. For permafrost sites similar to the GC Site-Worst Case Scenario, that is when the permafrost table is at -50 to -130 ft, and the bedrock table is at -230 ft or shallower, and the soil types are similar to the GC Site - Worst Case Scenario, the average response spectra obtained from this study could be used in seismic design. For other permafrost sites, particularly when soft soils and/or sensitive soils are present, site specific investigation should be conducted in a manner similar to the approach used in this study.
12. It is recommended that site exploration beyond the permafrost layer, e.g. drilling or seismic survey, be conducted to detect the bedrock table when other conditions are similar to the GC Site-Worst Case Scenario.

## **6.2 Suggested Research**

The main objective set forth for this project has been accomplished. In the course of conducting this project, the following topics for future research have been identified as worthy of future research:

1. A worst case scenario for permafrost sites has been identified by one-dimensional equivalent linear analysis. If a site similar to the worst case scenario permafrost site can be identified and instrumented with a downhole array, ground motion data can be collected by such instruments and can be used to further confirm the results.
2. It would add value to this study if a true nonlinear analysis (e.g. DEEPSOIL, OpenSEES, SUMDES) can be carried out for the worst case scenario to refine the results obtained from this project. This is particularly useful for the MCE level hazard due to its high nonlinearity.

## REFERENCES

- AASHTO LRFD Bridge Design Specifications, 4th Edition, Customary U.S. Units, 2007.
- Assimaki, D. and E. Kausel (2002). "An Equivalent Linear Algorithm with Frequency and Pressure-Dependent Moduli and Damping for the Seismic Analysis of Deep Sites," *Soil Dynamics and Earthquake Engrg.*, 22(3), 959-965
- Bielak, J., J. Xu and O. Ghattas (1999). "Earthquake ground motion and structure response in alluvial valleys," *Journal of Geotechnical & Geoenvironmental Engineering*, 125, 413-423.
- Bolt, B. A., and Gregor, N. J. 1993. "Synthesized Strong Ground Motions for the Seismic Condition Assessment of the Eastern Portion of the San Francisco Bay Bridge," *Report UCB/EERC-93/12*, University of California, Earthquake Engineering Research Center, Berkeley, CA.
- Boore, D.M. (1983). "Stochastic simulation of high-frequency ground motions based on seismological models of the radiated spectra," *Bull. Seis. Soc. Am.*, 73:1865-1894
- Building Seismic Safety Council (BSSC) (1997). *NEHRP Recommended Provisions for Seismic Regulations for New Buildings, Part 1 — Provisions*. 1997 Edition, Building Seismic Safety Council, Washington, D.C.: 337 pp
- Carballo, J. E., and Cornell, C. A., 2000. "Probabilistic Seismic Demand Analysis: Spectrum Matching and Design," Department of Civil and Environmental Engineering, Stanford University, *Report No. RMS-41*.
- Chopra, A.K. (2007). *Dynamics of Structures* (3<sup>rd</sup> Ed). Pearson Prentice Hall, Upper Saddle River, NJ.
- Combellick, R. A. (1999). "Simplified geologic map and cross sections of central and east Anchorage, Alaska: Alaska Division of Geological & Geophysical Surveys," *Preliminary Investigative Report 1999-1*. Department of Natural Resources, Fairbanks, Alaska.
- Czajkowski, R. L. and T. S. Vinson (1980). "Dynamic properties of frozen silt under cyclic loading," *J. Geotechnical Engineering Division*, 106:GT9, 963-980.
- Dalal, J.S., Seed, H.B., and Wu, D.L. (1976). "Site-Dependent Seismic Response Spectra for Soft Sites," *Journal of the Power Division*, 103(1), 15-25.
- Davis, N. T. (2001). *Permafrost: a guide to frozen ground in transition*. University of Alaska Press, Fairbanks, Alaska.
- Duhee, P. and Y. M. A. Hashash (2004). "Estimation of non-linear seismic effects for deep deposits of the Mississippi embayment," *MAE Center Report 04-06*. University of Illinois.
- EduPro Civil Systems, Inc. (1998). *ProShake: Ground Response Analysis Program version 1.1 User's Manual*. Redmond, Washington.

- Eckels, E.B. (1966). "The Alaska Earthquake, March 27, 1964: Lessons and Conclusions," U.S. Geological Survey Professional Paper 546, Superintendent of Documents, U.S. Government Printing Office, Washington, D.C.
- Ferrians, O.J., Jr. (1966). "Effects in the Copper River Basin Area," U.S. Geological Survey Professional Paper 543-E, Superintendent of Documents, U.S. Government Printing Office, Washington, D.C.
- Gasparini, D., and Vanmarcke, E. H. 1976. *SIMQKE: A Program for Artificial Motion Generation*, Department of Civil Engineering, Massachusetts Institute of Technology, Cambridge, MA.
- Golder Associates Inc. (2003). *Final report on structural foundation engineering, report C Street/O'Malley bridges No. 2081 and 2082*. Anchorage, Alaska.
- Harmsen, S. and A. Frankel (2001). "Geographic Deaggregation of Seismic Hazard in the United States," *Bull. Seism. Soc. Am.*, 91, 13–26.
- Hashash, Y. (2004). *DEEPSOIL version 2.5 Tutorial and User Manual*. University of Illinois at Urbana-Champaign, Illinois.
- Idriss, I. M. and Seed, H. Bolton (1968). "Seismic Response of Horizontal Soil Layers," *Journal of the Soil Mechanics and Foundations Division, ASCE*, Vol. 94, No. SM4, July.
- International Code Council (2000). *International Building Code*, 2000 Edition.
- Kanai, K. (1951). "Relation between the Nature of Surface Layer and the Amplitude of Earthquake Motions," *Bulletin*, Tokyo Earthquake Research Institute.
- Kausel, E. and D. Assimaki (2002). "Seismic Simulation Inelastic Soils via Frequency-Dependent Moduli and Damping," *J. of Engrg. Mech.*, ASCE, 128(1), 34-47.
- Kramer, S. L. (1996). *Geotechnical Earthquake Engineering*. Prentice Hall, Upper Saddle River, New Jersey.
- Kramer, S.L. and Paulsen, S.B. (2004). "Practical Use of Geotechnical Site Response Models," *Proceedings*, International Workshop on Uncertainties in Nonlinear Soil Properties and their Impact on Modeling Dynamic Soil Response, University of California, Berkeley, 10 pp.
- Lade, P.V., R.G. Updike, and D. Cole (1988). "Cyclic triaxial tests of the Bootlegger Cove Formation, Anchorage, Alaska," U.S. Geological Survey Bulletin-1825, 1-51.
- LeBlanc, A. M., R. Fortier, M. Allard, C. Cosma and S. Buteau (2004). "Seismic cone penetration test and seismic tomography in permafrost," *Can. Geotech. J.* 41, 769-813.
- Naeim, F., Alimoradi, A. and Pezeshk, S. (2004). "Selection and Scaling of Ground Motion Time Histories for Structural Design Using Genetic Algorithms," *Earthquake Spectra*, 20(2), 413–426.
- Péwé, Troy L. (1982). *Geologic Hazards of Fairbanks Area, Alaska*, Special Report No.15 (College, Alaska; Alaska Division of Geological and Geophysical Surveys) 109pp.

- Qi, J., W. Ma, C. Sun and L. Wang (2006). "Ground motion analysis in seasonally frozen regions," *Cold Regions Science and Technology*. 44, 111-120.
- Schnabel, P. B., J. Lysmer and H.B. Seed (1972). SHAKE: A Computer Program for Earthquake Response Analysis of Horizontally Layered Sites, *Report No. EERC 72-12*. Earthquake Engineering Research Center, University of California, Berkeley, Dec., 102p.
- Seed, H. Bolton and Idriss, I. M. (1970). "Soil Moduli and Damping Factors for Dynamic Response Analysis," Report No. UCB/EERC-70/10, Earthquake Engineering Research Center, University of California, Berkeley, December, 48p.
- Seed, H.B., Ugas, C. and Lysmer, J. (1976). "Site-dependent spectra for earthquake-resistant design," *Bulletin of the Seismological Society of America*. 1976; 66: 221-243.
- Seed, H. B., R. T. Wong, I. M. Idriss and K. Tokimatsu (1986). "Moduli and damping factors for analyses of cohesionless soils," *Journal of Geotechnical Engineering, ASCE*, 112, No. 11, 1016-1032.
- Singh, S., and N. C. Donovan (1977). "Seismic behavior of frozen-thawed profiles," presented at the October 17-21 *ASCE annual Convention, Exposition, and Continuing Education Program*, held at San Francisco, California.
- State of Alaska, Department of Highways (1974). *Log of test borings, Goldstream Creek at Ballaine Road*. Juneau, Alaska.
- Stevens, H. W. (1973). "Viscoelastic properties of frozen soils under vibratory loads," *North American Contribution to the Second International Conf. on Permafrost*, pp. 400-409. Yakutsk, U.S.S.R.
- Stewart, J.P. and Kwok, A.O.L (2008). "Nonlinear seismic ground response analysis: code usage Protocols and Verification against Vertical Array Data," *Geotechnical Earthquake Engineering and Soil Dynamics IV, Geotechnical Special Publication 181*, American Society of Civil Engineers.
- Sun, J. I., R. Golesorkhi and H. B. Seed (1988). Dynamic moduli and damping ratios for cohesive soils. *Report No. EERC-88/15*. Earthquake Engineering Research Center, University of California, Berkeley, California.
- Tsyтович, N. A. (1975). "The mechanics of frozen ground." *Translated by Scripta Technical Inc.*, New York, *Published by McGraw-Hill Book Co.*, New York.
- Vinson, T. S., R. Czajkowski and J. Li (1977). Dynamic properties of frozen cohesionless soils under cyclic triaxial loading conditions. *report No. MSU-CE-77-1*. Division of Engineering Research, Michigan State University, East Lansing, Michigan.
- Vinson, T.S. (1978). "Response of Frozen Ground to Dynamic Loadings," *Geotechnical Engineering for Cold Regions*, Eds. Andersland O.B. and Anderson, D.M., McGraw-Hill Book Company, Chap. 8, 405-458.

Wang, L., X. Ling, X. Xu and Q. Hu (2004). "Study on response spectrum characteristics of earthquake acceleration for roadbed on permafrost site," *Chinese Journal of Rock Mechanics and Engineering*, 23(8), 1330-1335.

Wesson, R.L, Frankel, A.D., Mueller, C.S. and Harmsen, S.C. (1999). "Probabilistic seismic hazard maps of Alaska," *Open-File Report 99-36*, U.S. Geological Survey.

Zhang, Y. (2009). *An Investigation on Cyclic Resistance and Dynamic Characteristics of Mabel Creek Silt. Ph.D. Dissertation*, University of Alaska Fairbanks. Nov.

Zhu, Y. and D. L. Carbee (1984). "Uniaxial compressive strength of frozen silt under constant deformation rates," *Cold Regions Science and Technology*, 9, 3-15.